

**INVESTIGATION INTO CHANGES OF THE BIOPHYSICAL PROPERTIES OF
BASEMENT MEMBRANES BY ATOMIC FORCE MICROSCOPY**

by

Joseph Eugene Candiello

B.S. Engineering Science and Mechanics, The Pennsylvania State University, 2003

Submitted to the Graduate Faculty of
Swanson School of Engineering in partial fulfillment
of the requirements for the degree of
Doctor of Philosophy

University of Pittsburgh

2009

UNIVERSITY OF PITTSBURGH
SWANSON SCHOOL OF ENGINEERING

This dissertation was presented

by

Joseph Eugene Candiello

It was defended on

October 27th, 2009

and approved by

Co-Director: Willi M. Halfter, PhD, Associate Professor, Department of Neurobiology

Michael S. Sacks, PhD, Professor, Department of Bioengineering

Steven D. Abramowitch, PhD, Assistant Professor, Department of Bioengineering

Dissertation Director: Sanjeev G. Shroff, PhD, Professor, Department of Bioengineering

Copyright © by Joseph Eugene Candiello

2009

INVESTIGATION INTO CHANGES OF THE BIOPHYSICAL PROPERTIES OF BASEMENT MEMBRANES BY ATOMIC FORCE MICROSCOPY

Joseph Eugene Candiello, PhD

University of Pittsburgh, 2009

Basement membranes (BMs) are sheets of extracellular matrix that separate epithelia from connective tissues and outline muscle fibers and the endothelial lining of blood vessels. A major function of basement membranes is to establish and maintain stable tissue borders. We introduce the inner limiting membrane (ILM), located at the retinal-vitreous junction, as a model system for studying the biophysical properties of BM. We also introduced atomic force microscopy techniques as important tools to investigate the ILM under physiologically relevant conditions. We were able to determine changes in both the thickness and elasticity of chick ILM during embryonic development. We also determined that BMs are much thicker in their native state than previously thought. Proteoglycans, specifically their heparan sulfate side-chains, were found to significantly contribute to ILM biophysical properties. The effects of aging on the composition, structure, and biophysical properties of the adult human ILM were investigated. A compositional shift in the ILM was associated with an increase in both the ILM thickness and elastic modulus during aging. The role of heparan sulfate molecules in the human ILM was determined to be similar to that of the chick ILM. The biophysical changes in mouse knockout models for congenital muscular dystrophy were also investigated. These models had protein knockouts that inhibit the proper formation of basement membranes. There were differences in the biophysical properties along with visually noted disruptions in the mouse inner limiting membranes due to improper formation of the BM. This study provided novel insight into the

biophysical importance of BMs and the ability to study changes associated with a variety of biological conditions that are relevant to proper biological function, in addition to setting a baseline for the biophysical properties of BMs.

TABLE OF CONTENTS

NOMENCLATURE.....	XIV
PREFACE.....	XV
1.0 INTRODUCTION.....	1
1.1 BASEMENT MEBRANES	1
1.1.1 Major basement membrane components and assembly.....	2
1.1.2 Evidence for importance of BM biomechanics	6
1.1.3 Basement membrane changes with aging	7
1.2 ATOMIC FORCE MICROSCOPY.....	9
1.2.1 Principles of operation.....	9
1.2.2 AFM as a tool for elasticity measurements.....	11
1.2.3 Calculation of elasticity	12
1.3 SPECIFIC AIMS OF STUDY	14
1.3.1 Objective #1: Biomechanical properties of basement membranes.....	15
1.3.2 Objective #2: Understanding the biophysical importance of BM proteoglycans.....	15
1.3.3 Objective #3: Compositional and biophysical properties of adult human ILM during aging.....	16

1.3.4	Objective #4: The biophysical properties of the mouse ILM in two knockout models for congenital muscular dystrophy.	16
2.0	BIOMECHANICAL PROPERTIES OF NATIVE BASEMENT MEMBRANES	17
2.1	INTRODUCTION	17
2.1.1	The inner limiting membrane as a model system for BM study.....	17
2.2	METHODS	18
2.2.1	Histology	18
2.2.2	ILM preparation.....	19
2.2.3	Western blot analysis.....	19
2.2.4	MS.....	20
2.2.5	AFM imaging and force indentation of ILM.....	21
2.2.6	Calculation of ILM elasticity	22
2.3	RESULTS	23
2.3.1	Evidence for role of BMs in vascular stability	23
2.3.2	Protein composition of the ILM.....	26
2.3.3	Histological characterization of the ILM.....	28
2.3.4	AFM imaging of the ILM.....	30
2.3.5	AFM measurement of ILM thickness	31
2.3.6	Elasticity of ILM	33
2.4	DISCUSSION	35
2.4.1	The ILM as a model system for measuring BM thickness and elasticity	35

2.4.2	Thickness of BMs	36
2.4.3	Elasticity of BMs	38
2.5	CONCLUSION	40
3.0	INVESTIGATION INTO BASEMENT MEMBRANE PROTEOGLYCAN....	42
3.1	INTRODUCTION	42
3.1.1	Proteoglycans.....	42
3.1.2	Basement membrane proteoglycans.....	42
3.2	METHODS.....	43
3.2.1	ILM sample preparation for SDS-PAGE and western blot.....	43
3.2.2	ILM flat mount preparation for AFM	44
3.2.3	AFM indention of chick ILM.....	45
3.2.4	ILM thickness.....	45
3.3	RESULTS	46
3.3.1	Chick ILM isolation and GAG removal	46
3.3.2	ILM elasticity	49
3.3.3	ILM thickness.....	50
3.4	DISCUSSION.....	50
3.5	CONCLUSION	52
4.0	AGE-DEPENDANT EFFECTS ON THE HUMAN INNER LIMITING MEMBRANE.....	53
4.1	INTRODUCTION	53
4.2	METHODS.....	55
4.2.1	Human eyes and antibodies.....	55

4.2.2	Histology	55
4.2.3	ILM preparation	56
4.2.4	Atomic force microscopy of the ILM	57
4.3	RESULTS	58
4.3.1	Protein composition of the fetal human ILM.....	58
4.3.2	Structure and composition of adult human ILM.....	63
4.3.3	Adult human ILM isolation and protein composition.....	64
4.3.4	The biophysical properties of adult human ILM.....	68
4.3.5	Removal of glycosaminoglycan side chains in adult human ILM	70
4.4	DISCUSSION	74
4.4.1	Age dependant changes in the ILM histology	74
4.4.2	Age dependant changes in the biophysical properties of the human ILM	76
4.5	CONCLUSION	77
5.0	BIOMECHANICAL CHANGES IN BASEMENT MEMBRANES FOR “POMGNT1” AND “LARGE” KNOCKOUT MOUSE MODEL	80
5.1	INTRODUCTION	80
5.1.1	Muscular dystrophy relating to basement membranes.....	80
5.1.2	Dystrophin associated protein complex	81
5.2	METHODS	82
5.2.1	AFM elasticity and thickness measurements	82
5.3	RESULTS	83
5.3.1	Mouse ILM elasticity	83

5.3.2	Mouse ILM thickness	86
5.4	DISCUSSION.....	87
5.5	CONCLUSION	88
6.0	OVERALL CONCLUSIONS AND FUTURE DIRECTIONS	90
6.1	OVERALL CONCLUSIONS	90
6.2	FUTURE DIRECTIONS.....	96
APPENDIX A		98
APPENDIX B		101
BIBLIOGRAPHY		109

LIST OF TABLES

Table 2-1: Elasticity of chick ILM.....	35
Table 3-1: ILM elasticity of ILM with GAG removal.....	49
Table 3-2: ILM thickness of ILM with GAG removal	50
Table 5-1: Elasticity of mouse ILM samples.....	86
Table 5-2. Knockout Mouse ILM Thickness.....	87

LIST OF FIGURES

Figure 1-1. The four major components of BM.....	4
Figure 1-2: Major basement membrane molecules interactions.....	5
Figure 1-3. Formation of basement membrane.....	6
Figure 1-4: AFM microscope schematic.....	10
Figure 1-5. AFM in imaging mode (left) and in force mapping mode (right).....	11
Figure 1-6: Representative force curves.....	12
Figure 2-1. Ocular hemorrhaging and retinal ectopias	25
Figure 2-2. Location and protein composition of the chick ILM.	27
Figure 2-3. Flat-mount preparations of ILMs from chick and mouse retina.	29
Figure 2-4. AFM images of flat-mount chick ILM.....	31
Figure 2-5: ILM thickness determined by AFM.....	32
Figure 2-6: Elasticity of the chick ILM..	34
Figure 2-7: Hydrated ILM thickness.....	38
Figure 3-1: Enzymatic removal of the GAG side chains from BM HSPG.....	48
Figure 4-1: Detection of BM proteins in the ILM of the fetal human eye.	60
Figure 4-2: Protein composition of human ILM.....	62
Figure 4-3: TEM micrographs of the vitreal surface of the retina.	64

Figure 4-4: Isolation of the inner limiting membrane (ILM) of the adult human retina..	66
Figure 4-5: Laminin and collagen IV content of adult human ILM.	68
Figure 4-6: Age related changes of the adult human ILM.	70
Figure 4-7: Proteoglycans role in adult human ILM.	72
Figure 5-1: Dystrophin associated protein complex	82
Figure 5-2: Biophysical properties of POMGnT1 knockout.	84
Figure 5-3: Biophysical properties of LARGE knockout.	85

NOMENCLATURE

BM	Basement Membrane
ILM	Inner limiting membrane
AFM	Atomic force microscopy
ECM	Extracellular matrix
E(#)	Embryonic day
P(#)	Postnatal day
PBS	Phosphate buffered solution
CNS	Central nervous system
TEM	Transmission electron microscopy
SEM	Scanning electron microscopy
PG	Proteoglycan
GAG	Glycosaminoglycan
HS	Heparan sulfate
HSPG	Heparan sulfate proteoglycan
BSA	Bovine Serum Albumin
MD	Muscular dystrophy
CMD	Congenital muscular dystrophy
BrM	Bruch's membrane

PREFACE

I would first like to thank and acknowledge my research advisors, Dr. Willi Halfter and Dr. Hai Lin, for the opportunity to learn the many facets of research. I appreciate all of the guidance I have received through you. I also would like thank Dr. Sanjeev Shroff for taking the duties involved with chairing my dissertation committee. Also, much appreciation goes to Dr. Michael Sacks and Dr. Steven Abramowitch for their time, help, and guidance as members of my committee. I would also like to thank the Bioengineering Department at the University of Pittsburgh for giving me the opportunity to study as a graduate student in such a great environment.

I especially would like to thank two people who I have shared labspace with. First, Kalpesh Upadhye, you are a great labmate and even better friend. It always helped that there was somebody to kick ideas back and forth between and share in the graduate experience with. Also, I would like to thank Andrew Feola for all of the time and effort put forth while he was an undergraduate student working in our lab. Working with you two has truly been an enjoyable experience that I am grateful for.

I have made many friendships during my time at the university, but two very important ones I was lucky enough to meet during my initial summer orientation. I would like to thank David Montag and Alicia Baumberger for providing many of the ups and none of the downs during my time here. Your friendship is greatly appreciated.

I absolutely could not be where I am today without my family. My parents have supported me in all of my endeavors throughout my life. I want to thank you for providing

guidance, but at the same time helping me to make own decisions in life. I would also like to thank my grandparents for all of their love and support. Two people who have always injected a bit of levity into life are my younger siblings; Jessica and Andy, you are two people who I can always count on for any reason.

1.0 INTRODUCTION

1.1 BASEMENT MEBRANES

Basement membranes (BM) are sheets of extra cellular matrix attached to the basal side of every epithelium, serving as a separation between the epithelial cells and the surrounding connective tissues [1]. These sheets not only provide attachment for these cells, they also create and maintain tissue borders and organ walls. BMs outline the muscle fibers and the endothelial lining of blood vessel, along with connecting the central nervous system with the meningeal cell layers. They also provide attachment sites for cells and influence cell proliferation, migration and differentiation, and can act as storage for enzymes, growth factors, and extra cellular proteins. While, there is variability in BM composition from tissue to tissue; the major components found in all BMs are collagen IV, nidogen, members of the laminin family, and proteoglycans [2, 3]. The laminins have a functional role in cell adhesion, while collagen IV provides mechanical stability to the tissue. Nidogen, which has binding sites for both collagen IV and laminins is thought to play the role of linker in BMs [4]. This study investigates the biophysical properties of a BM under a variety of biological circumstances.

1.1.1 Major basement membrane components and assembly

While basement membranes vary in composition from one tissue to another and during development there are major components that are part of all basement membranes. These include collagen IV, laminin, nidogen, and various heparan sulfate proteoglycans (agrin, perlecan, and collagen XVIII) [2, 3]. Structures of these BM components are found in Figure 1-1 [5]. ILM forming proteins have origins outside of the retinal cells that they ultimately attach to; traveling via the vitreous humor from the cells of the lens, ciliary body, and hyaloids vasculature. The major BM proteins are as follows:

Collagen IV: a non fibrillar collagen, forming the web-like mesh that provides structure and stability to BMs. There are six genetically distinct alpha chains ($\alpha 1$ - $\alpha 6$) that are arranged in triple-helical structures to form collagen trimers. These alpha chains contain a globular non-collagenous (NC) domain at the c-terminus end, and a long triple helical collagenous domain[6]. There are numerous kinks in the collagenous domain that allows for flexibility in the structure. Collagen IV protomers are secreted from cells as a heterotrimer formed by three a-chains with the NC1 domain of each chain forcing proper binding with appropriate alpha chains[7].

Laminin: large heterotrimeric proteins responsible for cell surface binding, which forms the base of the BM fiber network. Laminin is a pitchfork shaped protein comprised of an alpha, beta, and gamma chain. The C-terminus of each chain forms a triple-helical structure, or the “handle” of the pitchfork, while the N-terminal end of each chain form the three “prongs” of the pitchfork[8, 9]. The long tail of the laminin protein is the site of attachment to cell surface receptors, while the three shorter arms anchor the rest of the BM network assembly. There are 11 chains of the laminin protein family (a1-5, b1-3, and g1-3)[8]. Laminins are named for the

three chains making up the protein. For example Laminin 111, a prominent BM laminin, contains the $\alpha 1$, $\beta 1$, $\gamma 1$ chains.

Nidogen (Entactin): dumbbell shaped glycoprotein that binds to Collagen IV, perlecan, fibrinogen, fibronectin, and laminin. The protein core of which, is comprised of one G (globular) domain at the N-terminal (G1) and two G domains at the C-terminal end (G2, G3). The three G domains are separated by two rod shaped segments, the shorter being in between the G2 and G3 domain. NID1 and NID2 are the genes encoding the two types of nidogen, with both types being found in all basement membranes [5, 10, 11]. Nidogen's primary function is to bridge the laminin and collagen IV structural networks.

Heparan Sulfate Proteoglycans: There are three heparan sulfate proteoglycans found in basement membranes: agrin, perlecan, and collagen XVIII. Proteoglycans are heavily glycosolated proteins that contain a protein "core" structure bonded to long repeating carbohydrate side-chains called glycosaminoglycans (GAGs). In the case of BM proteoglycans, the GAG side chains are the linear polysaccharide, heparan sulfate[12].

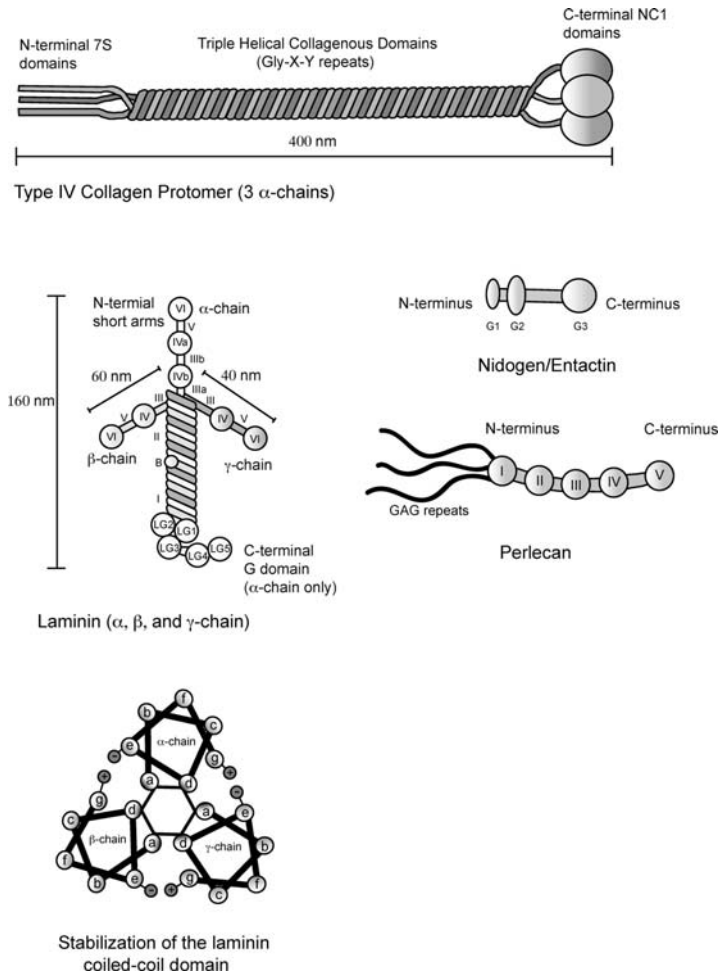


Figure 1-1. The four major components of BM [5].

While the laminin and collagen IV protomers are able to interact with their same type to form collagen IV and laminin networks, it has yet to be shown that they are able to interact directly with one another [13-15]. Other BM proteins, specifically nidogen, are responsible for facilitating the connecting of the laminin and collagen IV mesh to form the BM superstructure [3, 16]. These possible interactions between basement membranes proteins are shown in Figure 1-2 [17]. The arrows indicate the available interactions between proteins. Note nidogen's ability to bind to laminin, collagen IV, and BM proteoglycans. These complex interactions are

necessary for the proper formation of basement membranes. Yellow arrows indicate a components ability to interact directly (self polymerize) with other like molecules.

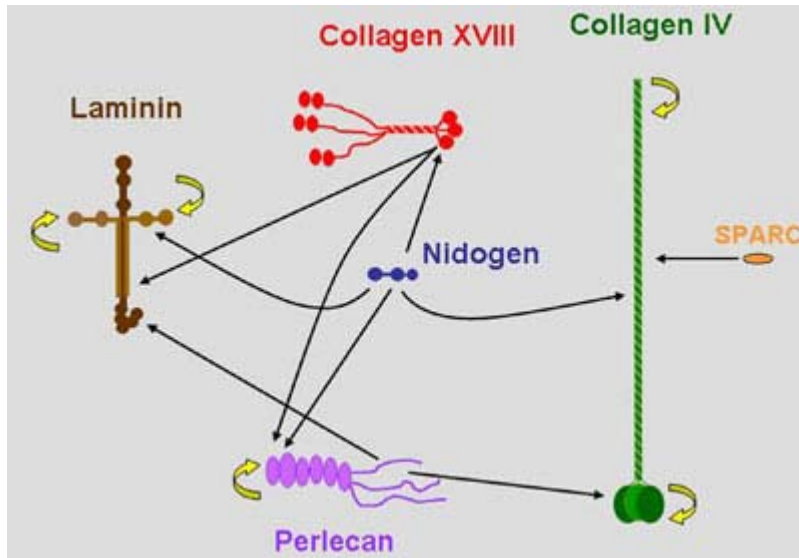


Figure 1-2: Major basement membrane molecules interactions[17].

As shown in Figure 2-3[18], Basement membrane assembly begins with laminin binding to cell surface receptors, such as integrin or dystroglycan complex. Laminin binds to these surface receptors via the long tail of the α chain [18, 19]. Without proper functioning laminin α chain or cell surface receptors it is impossible to form properly functioning basement membranes. The shorter arms of the laminin molecule bind with each other to one another to form the initial BM structure. A collagen type IV fibrillar mesh attaches to the laminin polymer network with nidogen serving as the bridge. The formation and linking of the laminin and collagen IV network is the major structure of BMs [1, 5]. While laminin and collagen IV networks self assemble and are integrated into BM formation, linkers such as nidogen and perlecan integrate as single molecules to stabilize the BM ultrastructure.

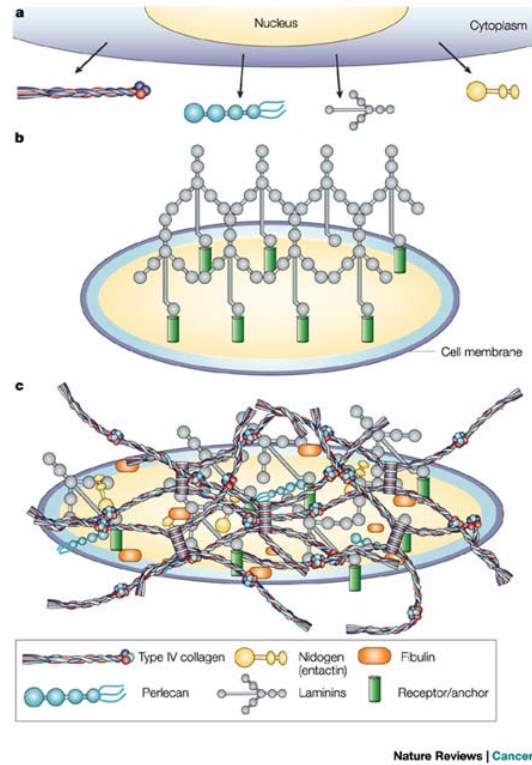


Figure 1-3. Formation of basement membrane [18].

1.1.2 Evidence for importance of BM biomechanics

While basement membranes perform a variety of necessary functions, there is ample evidence to suggest that the biophysical and biomechanical properties of basement membranes are vital components of proper development. Various mutations or deletions of specific BM proteins lead directly to early embryonic death, usually resulting from disruptions in the vascular system or defects in the placenta of the amnion [13, 20-24]. There are also nonlethal mutations of BM proteins that result in early onset muscular dystrophy, along with kidney and skin defects [25-28]. Mutant mice with BM defects often display vascular problems, such as ocular and cortical hemorrhaging and disruptions at the pial surface of the brain and vitro-retinal border of

the eyes. These vascular disruptions, observed in mice with targeted deletions or mutations of perlecan, nidogen, and collagen IV, primarily occurred in the brain and eye. In both cases the blood vessels rely primarily on the BM for vessel wall stability, as the vasculature is not surrounded by other dense ECM. Breaks in the vasculature were not present during initial vasculature development, but rather when blood pressure rises during mid-embryogenesis [4, 21, 29, 30]. Mutations in mouse BM protein receptors (integrin β 1, and dystroglycan) exhibit breaks in the retinal and pial BMs along with neural ectopias [31-33]. Enzymatic disruption of the ILM and pial BM also exhibited blood vessel rupture in chick embryos, demonstrating that the resulting vasculature breaks were not the result of a specific missing protein, but due to the weakening of the BM itself [34-36]. These vascular breaks and retinal and cortical ectopias lend to the idea that the mechanical resistance provided by BMs are critical in strengthening of the endothelial wall of the vasculature and creating a stable border between the central nervous system and the surrounding connective tissue. Previous to this work there was little information into the biophysical properties of BMs.

1.1.3 Basement membrane changes with aging

There is evidence that the protein composition and the thickness of BM change during aging. A recent study has shown that in embryonic chick ILM the dominant proteins are nidogen and laminin, comprising approximately 60% of BM proteins [37]. This is different from the ‘textbook’ model of BM, in which BMs were thought to be comprised of equal parts of collagen IV and laminin. This indicates that the protein makeup of BMs may not be the same during embryonic development as in adults. In human cerebral microvessels, for example, an increase

in BM collagen IV content was linked to an increase in the thickness of the BM. This progressive thickening and compositional change coincided with a decrease in microvessel function and blood flow regulation, thought to be due to a ‘choking’ of vessels and decrease of functional vessel numbers [38]. In the vasculature of the inner ear, age related thickening of the stria vascularis BM has been associated with impairment in circulation and degeneration of the vasculature [39]. A study involving Brown Norway rats showed that a thickening of the seminiferous tubules in the testes was linked to age-related factors, and not irregular protein expression. This age-related thickening of the tubule BM was associated with the degeneration of the tubules and decrease in sperm production [40]. An increase in human BM thickness of the glomerulus and tubules of the kidneys has also been associated with the disease pathogenesis of diabetes mellitus [41, 42]. The Bruch’s membrane, a basement membrane separating the retinal pigment epithelium and vasculature of the eye, has shown an increase in thickness associated with the onset of exudative age-related macular degeneration. Data from work attempting to investigate the biomechanical properties of this ocular extra cellular membrane can be found in Appendix B. It is evident that there are significant changes to the composition and the thickness of various BMs that are directly related to the detriment of proper biological function of organs and the vasculature. There, however, is no information on what biophysical/biomechanical changes in the BM that may coincide with these compositional and age-related variances.

1.2 ATOMIC FORCE MICROSCOPY

In this study the Atomic Force Microscope (AFM) was the primary tool used to measure the structural and biophysical properties of basement membranes. The uniqueness of this tool allowed for the study of these very thin structures under physiological conditions.

1.2.1 Principles of operation

The AFM uses a very sharp stylus or tip mounted at the end of a flexible cantilever (Figure 1-4) to probe and map the morphology of the sample surface. AFM images consist of a series of parallel line contours acquired by scanning the surface of a specimen using the sharp tip with an extremely small (nanonewtons) tracking force. As the tip is scanned across the specimen, the net interaction force between the molecules on the sample surface and tip apex deflects the cantilevered-tip. The tip-deflection is sensed by detecting the angular deflection of a laser beam reflected off the cantilever, which is converted to electrical signals by photodetectors (Figure 1-4). An electronic feedback loop keeps the cantilever deflection and the tracking force constant by moving the sample up and down as the tip traces over the contours of the surface.

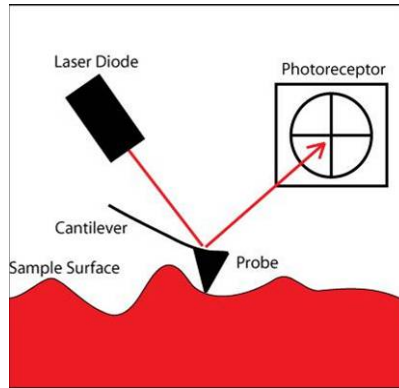


Figure 1-4: AFM microscope schematic

An image is obtained by plotting the vertical motion (z) of the tip and hence the sample height (z) as a function of specimen lateral position (XY). By choosing a very soft cantilever (low spring constant k), the imaging force can be in the range of interatomic forces (about 10^{-9} Newton), thus the name “atomic force” microscopy. Precise lateral and vertical position of the sample with respect to the probe is controlled by a computer-driven piezoceramic scanning stage. Depending on the design, the scanner may move the sample relative to a stationary probe or scan the probe over a stationary sample. The state of the art AFM used in our study (Asylum Research Inc.) uses a Z-scanner to control the vertical position of the probe (stationary in the XY plane) and a XY scanning stage to control the sample horizontal position.

There are two commonly used imaging modes to acquire sample topography with AFM: contact (static) mode and tapping (dynamic or intermittent contact) mode. In the contact mode imaging, the electronic feedback loop keeps the cantilever deflection and hence the tracking force constant during the raster-scanning of a sample. In the tapping mode, the cantilever beam is oscillated near its resonant frequency and interaction between tip and sample will alter the oscillation amplitude. The feedback loop maintains constant oscillating amplitude by keeping a

constant interaction force (which translates to a fixed distance) between the tip and sample and the raster-scanned probe traces out the surface height contour of the sample.

1.2.2 AFM as a tool for elasticity measurements

In the imaging modes, the AFM tip is raster scanned over the surface of the sample, which gives the surface topography of the sample (The left panel of Figure 1-5 shows the principle of AFM imaging of a cell). AFM can also be used to study the mechanical characteristics of soft samples at nanometer resolutions, including single cells [43, 44]. In the force mapping (also referred as force-volume) mode, the AFM feedback loop is turned off and the tip is lifted up from the sample surface and is then advanced towards the sample, which exerts a predetermined force on the sample and produces a small indentation ($\sim 10\text{s}-100\text{s nm}$) on sample.

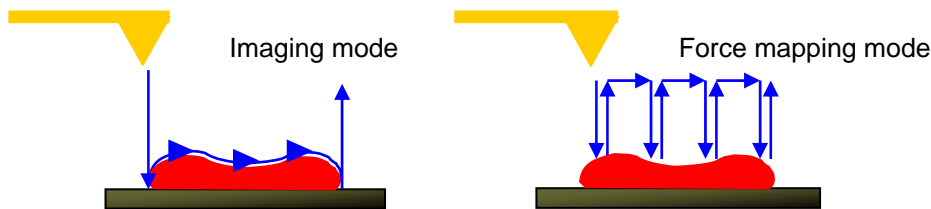


Figure 1-5. AFM in imaging mode (left) and in force mapping mode (right).

When the cantilevered AFM tip is pushed against the sample surface, the repulsion force deflects the cantilever. This interaction between the tip and the sample is commonly represented by the force curve (Figure 1-6). The degree of cantilever deflection is dependent on the stiffness of the sample. For a soft sample, the tip penetrates deeper into the sample and thus the cantilever deflection is less (Figure 1-6, dotted line) compared to that of a hard impenetrable surface (Figure 1-6, solid line).

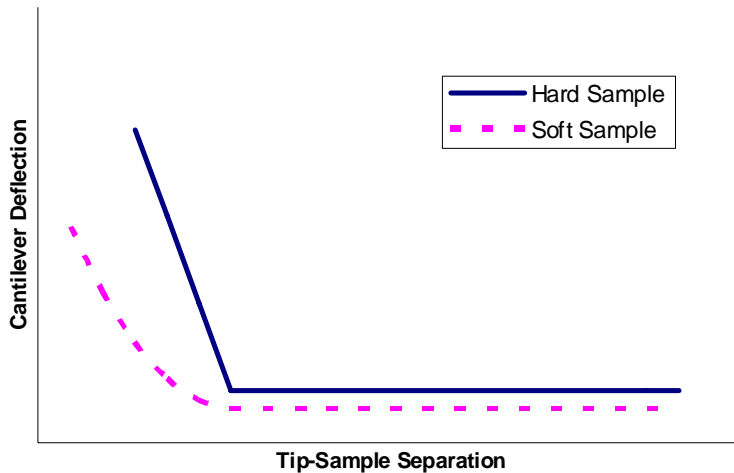


Figure 1-6: Representative force curves as AFM tip approach the sample (from right to left): cantilever is deflected as tip contacts the sample; a soft sample (dashed line) deflects the cantilever less than a hard sample (solid line).

The indentation depth of the AFM tip pushing into the sample can be determined by comparing force curves on the soft tissue with force-curves on a hard glass substrate. The elastic or Young's modulus of the tissue can be calculated based on these force curves using the Hertzian or Sneddon models [43-45]. This force mapping process can be repeated after moving the tip laterally to the next measuring point thus creating a *force-volume* plot over the whole scan area. The mapping can achieve a spatial resolution of < 10 nm.

1.2.3 Calculation of elasticity

After collecting a large number of force indentation curves at different sample locations, the relationship between the depth of tip indentation and the applied force at each point can be derived from the individual force curves (Figure 1-6), though the task of processing large

number of curves (e.g. 1024 curves for a 32x32 map) is still tedious and technically challenging. The Young's modulus of the sample (E) can be calculated using the Hertzian/Sneddon model:

Equation 1

$$F = \frac{2E \tan \alpha}{\pi(1 - \nu^2)} \delta^2;$$

where F is the applied force, δ is the depth of tip indentation into the sample (see Figure 1-7), α is the half angle of the AFM tip, E is the Young's modulus, and ν is the Poisson's ratio. The Hertz model assumes absolute elastic behavior and material homogeneity, which is not exactly true for biological materials. Also, the Hertzian model is good for indentations of 5-10% of sample thickness, where the underlying substrate does not affect the sample properties.

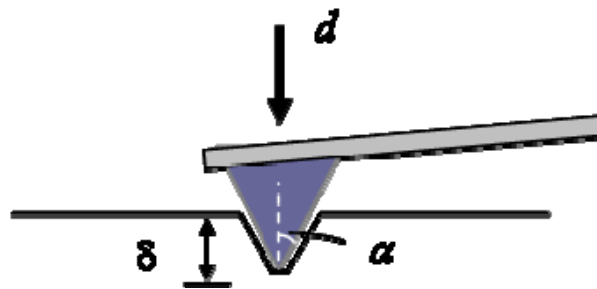


Figure 1-7: AFM tip indenting an elastic sample

1.3 SPECIFIC AIMS OF STUDY

BM's are thin sheets of extracellular matrix that have a structural role for the development and maintenance of all multicellular organisms. Despite the fact that the biomechanical importance of BM's is obvious by the vascular ruptures in mice with mutations of BM proteins, actual measurements of the biomechanical strength of BM's are not available. Technical problems were the lack of a suitable BM model and a method to probe the very thin and delicate ECM sheets. The focus of this study was to provide fundamental insights into the biophysical properties of basement membranes. In order to accomplish this, the embryonic chick and adult human ILM was identified as a suitable and representative BM that could be isolated and prepared without altering its physiological status. In addition AFM was introduced as a suitable technique for measuring the fine biophysical characteristics of these thin and delicate structures. *Using the ILM as a model BM and AFM as a measuring technique, the linear story of BM development from embryonic development through aging was investigated. This includes not only changes in the biophysical properties that occur during this timeline, but also an investigation into a developmental step that is essential for BM assembly: the initial laminin/cell surface receptor interaction.* While a structural function for the majority of BM proteins has been proposed, a previously unknown structural function of a prominent BM component, proteoglycans, was discovered by our measurements. These results tell a story of the timeline for the structural functions of BM's, from initial laminin binding through late stage age-related

changes that may have functional implications in a variety of physiological abnormalities. This is the first investigation of the BM and its biophysical properties under physiological conditions.

1.3.1 Objective #1: Biomechanical properties of basement membranes.

Objective #1: Develop a method to investigate the biomechanical properties of basement membranes, by (1) finding a suitable BM that is both accessible and typical of BM structure and by (2) applying AFM as a tool capable of investigating biomechanics of small structures under physiological conditions.

Hypothesis: AFM force indentation technique will be able to detect biomechanical properties of embryonic chick and adult human inner limiting membranes. This BM will be isolated and demonstrated to contain basic BM protein structure.

1.3.2 Objective #2: Understanding the biophysical importance of BM proteoglycans

Objective#2: Determine the previously unknown structural function of BM proteoglycans by investigating the changes in biophysical properties after removing the heparan sulfate glycosaminoglycan side chains from the ILM proteoglycans in embryonic chick and adult human basement membranes.

Hypothesis: The negatively charged GAG side chains of basement membrane proteoglycans are structurally relevant in sequestering water to BM, and removal of GAGs will result in changes in BM biophysical properties. This hypothesis is based on PG function in other extra-cellular matrices and our data demonstrating that BM undergo significant shrinking due to dehydration by EM preparation protocols.

1.3.3 Objective #3: Compositional and biophysical properties of adult human ILM during aging.

Objective #3: Investigate the relationship between compositional changes in the human ILM and the coinciding physiologically relevant changes in the biophysical properties of the human ILM during aging.

Hypothesis: Human BMs have been shown to both increase in thickness and collagen IV content during aging. We expect relevant coinciding changes in the biomechanical properties of the adult human ILM due to age-related thickening and compositional shifts.

1.3.4 Objective #4: The biophysical properties of the mouse ILM in two knockout models for congenital muscular dystrophy.

Objective #4: Knockout of two glucotransferases responsible for the glycosylation of a BM cell surface receptor causes ruptures of ILM in mice. The biophysical properties of the mouse ILM for these two models will be investigated.

Hypothesis: The ruptures of the knockout model mouse ILM are due to improper BM formation, as properly functioning laminin molecules and BM cell surface receptors are necessary for ILM formation. There will be a difference in the thickness and biomechanical properties in the mouse ILM from wild type that may be responsible for ILM rupture.

2.0 BIOMECHANICAL PROPERTIES OF NATIVE BASEMENT MEMBRANES

2.1 INTRODUCTION

2.1.1 The inner limiting membrane as a model system for BM study

As stated, there is a significant amount of evidence that the biophysical and biomechanical properties of BMs are important for proper development of a variety of biological systems; however there was a lack of information into these properties as they relate to BMs due to the difficulty in isolating a homogeneous sample of BM. The information in this chapter was the introductory study into basement membrane biomechanical properties and was published in the FEBS Journal in 2007 under the title *Biomechanical properties of native basement membranes* (Candiello, et al) [46].

We introduce here the retinal basement membrane, also referred as inner limiting membrane (ILM), as a model system to study the biophysical properties of BMs. Initially, we show that the mechanical strength of the ILM and the BMs of the ocular vasculature is essential for normal eye development, and thus provides a biological context and a justification for the present study. Subsequently, we show that the ILM resembles, in terms of ultrastructure and biochemical composition, a typical BM. Furthermore, we demonstrate that our ILM isolation procedure results in a preparation that is free of cellular contaminants and free of nonbasement

membrane proteins. Finally, atomic force microscopy (AFM) measurements reveal that native BMs are much thicker than previously referenced in the available literature and that mature BMs have a surprisingly high mechanical strength. We also show that BMs undergo significant morphological and biochemical changes during development.

2.2 METHODS

2.2.1 Histology

To demonstrate the importance of BMs in the stability of blood vessels and the maintenance of smooth muscle tissue border in brain and retina, the status of BMs in mice with a targeted deletion of a 50 amino acid long segment in the laminin α 1 chain was investigated[23]. The eyes of E18 mice were fixed in 2.5% glutaraldehyde overnight and embedded in EPONTM (Hexion Specialty Chemicals, Columbus, OH, USA) according to standard procedures. Eyes from embryos that were homozygous or heterozygous for the mutation were compared by light and electron microscopy in terms of BM continuity, hemorrhages, blood vessel rupture and retinal ectopias. Maintenance and killing of mice were carried out under approved protocols and in accordance with NIH and the European Community guidelines for animal care.

2.2.2 ILM preparation

For preparing BM flat-mounts for AFM, retinae from E4 to E15 chick embryos and from P1 and adult mice were dissected and spread on membrane filters (Millipore, Bedford, MA, USA). The filter/retinal sandwiches were placed, vitreal surface down, on poly lysine-coated (Sigma, St Louis, MO, USA) glass slides (Superfrost/plus, Fisher Scientific, Pittsburgh, PA, USA). After a 5 min attachment period, the filters with the retinae were lifted off from the slides, a procedure that splits the retina at the vitreal surface and leaves large segments of the retinal BMs on the glass slides [47]. To remove adherent endfeet of the ventricular cells from the BM sheets, the BMs were incubated with 2% Triton-X-100 for 30 min and washed several times in NaCl/Pi [47]. The preparations were always kept under NaCl/Pi. To assist visualization of the transparent and barely visible BM flat-mounts, some chick preparations were stained with a monoclonal antibody to nidogen-1 (mAb 1G12) [48], for 1 h, followed by a Cy3-labeled goat anti-mouse IgG (Jackson ImmunoResearch, West Grove, PA, USA). For mouse ILM preparations, the flat-mounts were labeled with an antibody to mouse laminin-1 (Invitrogen, Carlsbad, CA, USA). For thickness measurements, the preparations were scratched with 100 μ L pipette tips.

2.2.3 Western blot analysis

For western blot analysis, chick ILMs were isolated in bulk as previously described [49], pelleted by centrifugation, and dissolved in 8 M urea and SDS sample buffer. The proteins were resolved by PAGE, transferred to nitrocellulose, and the blots were labeled with antibodies to laminin-1 (mAb 3H11)[49], nidogen-1 (mAb 1G12)[48], agrin (mAb 6D2) [50], collagen 18

(mAb 6C4) [51], perlecan (mAb 5C9)[52], collagen 9 (mAb 2B9) [53]and NCAM (mAb 9H2)[50]. The monoclonal antibodies are available from the Developmental Studies Hybridoma Bank (University of Iowa, IA, USA). A rabbit antiserum against LG4-5 of laminin alpha 1 (E3 fragment, code no. 992+) was kindly provided by Dr Takako Sasaki (Max Planck Institute of Biochemistry, Munich, Germany). The collagen 4 bands were detected by running the PAGE under nonreducing conditions and using a polyclonal antiserum (Rockland, Gilbertsville, PA, USA) for the western blots. The labeled proteins were detected by alkaline phosphatase-labeled goat anti-mouse and goat anti-rabbit IgG (Jackson ImmunoResearch) with Nitro Blue tetrazolium and 5-bromo-4-chloroindol-2-yl phosphate as chromogenes (Roche, Indianapolis, IN, USA).

2.2.4 MS

BM proteins were resolved by PAGE and reverse Zinc stained. Eluted proteins from the stained bands were buffered in 100 mM ammonium bicarbonate, denatured by heating to 65 °C for 15 min after addition of 2% SDS, reduced with 2.5 mM tris(2-carboxyethyl)phosphine, alkylated with 3.75 mM indole-3-acetic acid, followed by digestion with porcine trypsin (Promega, Madison, WI, USA). LC-MS experiments were performed on a Surveyor nanoflow HPLC system interfaced with an ion trap mass spectrometer (LCQ Deca, Thermo Electron Corp., San Jose, CA, USA). Data were acquired using the triple play method and analyzed with Mascot Daemon, version 2.1.0 (Matrix Science, Boston, MA, USA) with the settings: 400–4000 mass range, scan grouping 1, precursor charge state set to Auto, peptide error tolerance 1.5 Da, fragment error tolerance 0.8 Da, one missed cleavage, NCBI no. database (version 16 May 2006;

3284262 sequences, 112594017 residues), and variable modifications were carbamidomethylation of cysteine and oxidation of methionine.

2.2.5 AFM imaging and force indentation of ILM

All AFM imaging and force indentation experiments were carried out using an MFP-3D Atomic Force Microscope (Asylum Research, Santa Barbara, CA, USA), which was placed on top of an Olympus IX-71 fluorescence microscope (Olympus, Tokyo, Japan). Standard commercially available, 100- μm long Si_3N_4 cantilevers, with integrated pyramidal tips (Veeco, Inc, Santa Barbara, CA, USA) and a nominal spring constant, k , of 0.6 N/m) were used. The spring constant of each cantilever was measured by the thermal fluctuation method [49] before each experiment. For a few selected indentation experiments, we also attached glass spherical beads of 7 μm diameter to the tips, which did not alter the cantilever spring constants. The topography of the ILM samples were imaged in intermittent contact mode (AC, or tapping mode) with a scan rate of approximately 1 line/s), in NaCl/Pi at room temperature. The tissues were kept under NaCl / Pi solution throughout the experiments. The elasticity of the ILM was measured by nano-indentation with an AFM tip [54, 55]. A 20 μm x 20 μm or 10 μm x 10 μm area of the ILM retinal surface was first imaged with AFM, and indentions were made over a 10 x 10 grid points evenly distributed over the imaged area. The automated indentation was carried out using the cFVol software program (Chad Ray, Duke University, Durham, NC, USA), at a rate of one load/unload cycle per second. The speed of the AFM tip indenting the tissue was between 2.0 and 10.0 $\mu\text{m/s}$). Out of the 100 total indentations on each sample, 20 were randomly

chosen for quantitative analysis. To reduce the viscoelastic contributions, the apparent Young's modulus of the tissue at each indentation point was calculated from only the retraction (unloading) portion of force-indentation curve using the Sneddon model [43, 54].

2.2.6 Calculation of ILM elasticity

The Sneddon model [56] was used to evaluate tissue elasticity from the force-indentation measurements. Calculations were made for both a conical indenter and a spherical indenter. We used the conical geometric model for the sharp AFM tips and the spherical model for the attached spherical glass bead. In the case of a conical indenter, the relationship between the applied load/force f and the indentation δ can be expressed as:

Equation 2

$$f = \frac{2}{\pi} \cot \alpha \frac{E}{1-\nu^2} \delta^2$$

where E is the Young's modulus, ν is the poisson's ratio, α is the half vertical angle of the AFM tip ($\alpha = 35$ degrees). The relationship between f and δ for a spherical indenter can be expressed as:

Equation 3

$$f = \frac{4}{3} \frac{E}{1-\nu^2} \sqrt{R} \delta^{\frac{3}{2}}$$

where R is the radius of the spherical indenter. The indentation δ can be calculated from the AFM cantilever piezo position z and cantilever deflection d : $\delta = (z-z_0)-d$, where z_0 is the initial indentation contact point. The z - d relationship for conical and spherical indenters can be similarly expressed, respectively, as:

Equation 4

$$z = z_0 + d + \sqrt{\frac{\pi kd(1 - \nu^2)}{2E \cot \alpha}}$$

and:

Equation 5

$$z = z_0 + d + \sqrt[3]{\frac{3kd(1 - \nu^2)}{4ER^{\frac{1}{2}}}}$$

where k is the cantilever spring constant. Values of the apparent Young's modulus, E, were obtained from the force-indentation data by curve fitting the experimentally capture z-d curves with Eqns (2-3) and (2-4) using E and the initial contact point z_0 as fitting parameters[54]. The curve fitting was limited to the initial contact region of the z-d curve, which corresponds to a region of small loading force ($f = 6-8$ nN) and small indentations ($d = 40-50$ nm). The poisson's ratio was assumed to be $\nu = 0.47$, a value measured on lens capsule, another retinal basal lamina[57].

2.3 RESULTS

2.3.1 Evidence for role of BMs in vascular stability

Histological data from mice with several different mutations of BM proteins strongly suggest that the mechanical stability of BMs is important in: (a) establishing a defined tissue border between the CNS and its surrounding meningeal layers; (b) stabilizing blood vessels in the eye and CNS; and (c) preventing muscle fibers from undergoing terminal damage [4, 21, 27-

30]. To emphasize the importance of BM stability for blood vessels and the integrity of the vitreo-retinal border, mutant mice with a targeted deletion of the nidogen binding site in the laminin γ 1 chain were investigated. BMs in these mutant mice lack nidogen [4, 23, 29], which leads to random ruptures in many of the BMs and to the death of the homozygous mutant mice at late embryogenesis due to kidney agenesis and lung dysplasia [4, 23, 29]. Phenotypic analysis showed that all embryonic day (E)18 mutant mice had massive hemorrhages in their eyes (Figure 2-1 A,B).

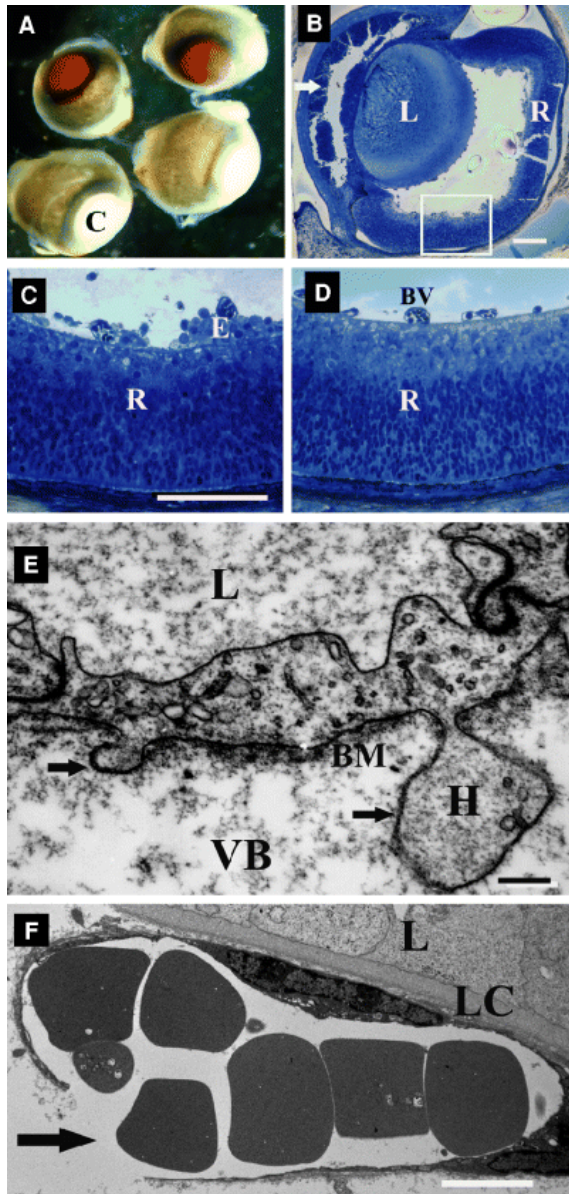


Figure 2-1. Ocular hemorrhaging and retinal ectopias in mice with a mutation in the laminin $\gamma 1$ chain (A). The red eyes of E18 homozygous mutant mice indicate massive intraocular bleedings, but none in the normally colored eyes from the heterozygous control (C) embryos. A cross-section through a mutant eye (B) shows blood vessel rupture in the anterior chamber of the eye as indicated by the aggregated red blood cells next to the cornea (arrow). R, retina; L, lens. A high power view (C) of the mutant retina (B, box) shows ectopias of retinal cells (E) through ruptures in the retinal BM. The smooth vitreal surface of a retina (R) from a control mouse is shown in (D) for comparison. BV, hyaloid blood vessel. TEM micrographs (E,F) of the hyaloid vasculature in the vitreous body (VB) and around the lens (L) of the mutant mice showed herniation (H) of endothelial cells through breaks (E, arrows) in the vascular BM (BM) or ruptures of the entire vessel wall (F, arrow). LC, lens capsule. Bar, (B) 150 μm ; (C,D) 100 μm ; (E) 100 nm; (F) 10 μm .

Ultrastructural studies of the ocular vasculature revealed herniation of endothelial cells through disruptions in the endothelial BMs (Figure 2-1E) and breaks of entire vessel walls (Fig. 2-1F). Ectopic cells along the vitreo-retinal border due to gaps in the retinal BM (Figure. 2-1C) was another hallmark in all eyes of mutant mice. In heterozygous control mice, the retinal border was smooth and continuous (Figure 2-1D), and endothelial herniation or breaks in the ocular vasculature were never observed. As described previously [29], excessive hemorrhages and neuronal ectopias were also observed in the cortex of mutant mice. The retinal and cortical ectopias confirmed that BMs are required in maintaining smooth and stable tissue borders along the CNS and in preventing cortical and ocular hemorrhages. The frequent retinal ectopias also show that the stability of the retinal BM is important for retinal histogenesis. The data illustrate why biophysical measurements of BMs are biologically relevant and provide a justification for the AFM measurements presented below.

2.3.2 Protein composition of the ILM

Force and thickness measurements of BMs were performed with chick and mouse ILMs. The ILM is located at the vitreal surface of the retina and separates the retina from the vitreous body (Figure 2-2A). The ILM is one of three BMs of the eye, which include the lens capsule, the BM of the pigment epithelium and the ILM (Figure 2-2A).

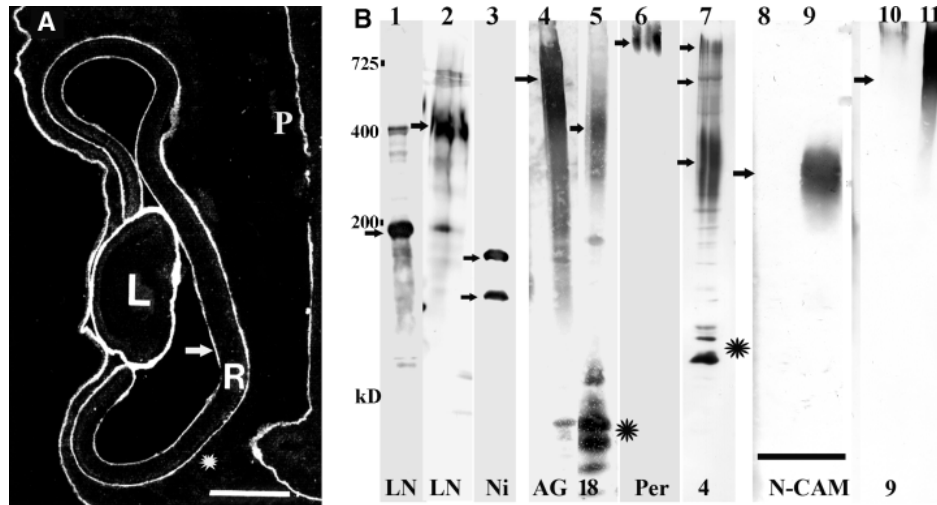


Figure 2-2. Location (A) and protein composition (B) of the chick ILM. (A) Fluorescent micrograph of a cross-section of an E4 chick eye stained for laminin-1 shows all BMs of the developing eye, including the lens capsule (L), the BM of the pigment epithelium (star) and the ILM (arrow). The pial BM (P) of the adjacent diencephalon is labeled as well. Western blots (B) show that the ILM is comprised of the following proteins: laminin-1 (LN) with bands at 200 and 400 kDa (lane 1). The band at 400 kDa is also labeled with an antibody to the C-terminal globular domains of laminin-1, and thus represents the α chain of laminin-1 (lane 2). Nidogen-1 (Ni) appeared as two bands, both of which were confirmed to be nidogen-1 by MS (lane 3). The smear at 600, 400 and 700 kDa in lanes 4, 5 and 6 represents the proteoglycans agrin (AG), collagen 18 (18) and perlecan (Per). The multiple bands of lane 7 represent monomeric and oligomeric forms of collagen 4. Degradation bands of collagen 18 and 4 are indicated by stars (lanes 5 and 7). N-CAM, a cell membrane protein that is abundant in the retina (lane 9), was not detectable in the ILM (lane 8). Likewise, collagen 9 (9), which is very abundant in the vitreous (lanes 11), is only present in traces in the ILM matrix (lanes 10). The specific bands for each of the proteins are indicated by arrows. The samples for the collagen 4 and collagen 9 were run under nonreducing conditions. Bar = 200 μ m.

Western blot analysis showed that the ILM is comprised of extracellular matrix proteins that are found in other BMs as well, namely laminin-1 (Figure 2-2B, lanes 1 and 2), nidogen-1 (Figure 2-2B, lane 3), three BM proteoglycans, agrin (Figure. 2-2B, lane 4), collagen 18 (Figure 2-2B, lane 5) and perlecan (Figure 2-2B, lane 6) and collagen 4 (Figure 2-2B, lane 7). Two bands were observed for nidogen. Peptide mass finger printing confirmed that both bands (Figure 2-2B, lane 3) were nidogen- 1: the full-length protein and a truncated version. Laminin was detected by the very prominent 200 kDa β 1 and γ 1 chains, and its identity as laminin-1 was established by

detecting the laminin α 1 chain using a α 1 chain-specific antibody (Figure 2B, lane 2). The western blotting data were confirmed by capillary liquid chromatography (LC) electrospray ionisation MS/MS that identified the peptide SDFMSVLSNIEYILIK (AA 1938–42 of the bovine laminin α 1; GI 57164373) of the laminin α 1 chain in trypsin-digests of ILM preparations. The three proteoglycans, agrin, collagen 18 and perlecan appeared in the blots as smears of 600, 400 and 800 kDa (Figure 2-2B, lanes 4, 5 and 6, respectively). The smears resulted from the microheterogeneity of the glycosaminoglycan carbohydrate side chains. Collagen 4 appeared in multiple bands that represented the monomeric and several cross-linked oligomeric versions. To determine potential contamination of the ILM preparations, the blots were assayed for neural cell adhesion molecule (NCAM) and collagen 9. As shown in Figure 2-2, NCAM and collagen 9 are very abundant in retinal membranes and the vitreous (Figure 2-2, lanes 9 and 11, respectively). Both proteins were barely detectable in the ILM preparations (Figure 2-2, lanes 8 and 10).

2.3.3 Histological characterization of the ILM

ILM flat-mount preparations from chick embryos, neonatal and adult mice were obtained by mechanically splitting the retina [47]. The ILM flat-mounts were firmly attached to glass slides (Figure 2-3C,G). They were immunoreactive for laminin-1 (Figure 2-3C,G), nidogen-1, perlecan, agrin and collagen 18, as expected from the strong labeling of the ILM for these proteins in tissue sections of chick and mouse retina (Figure 2-3A,F).

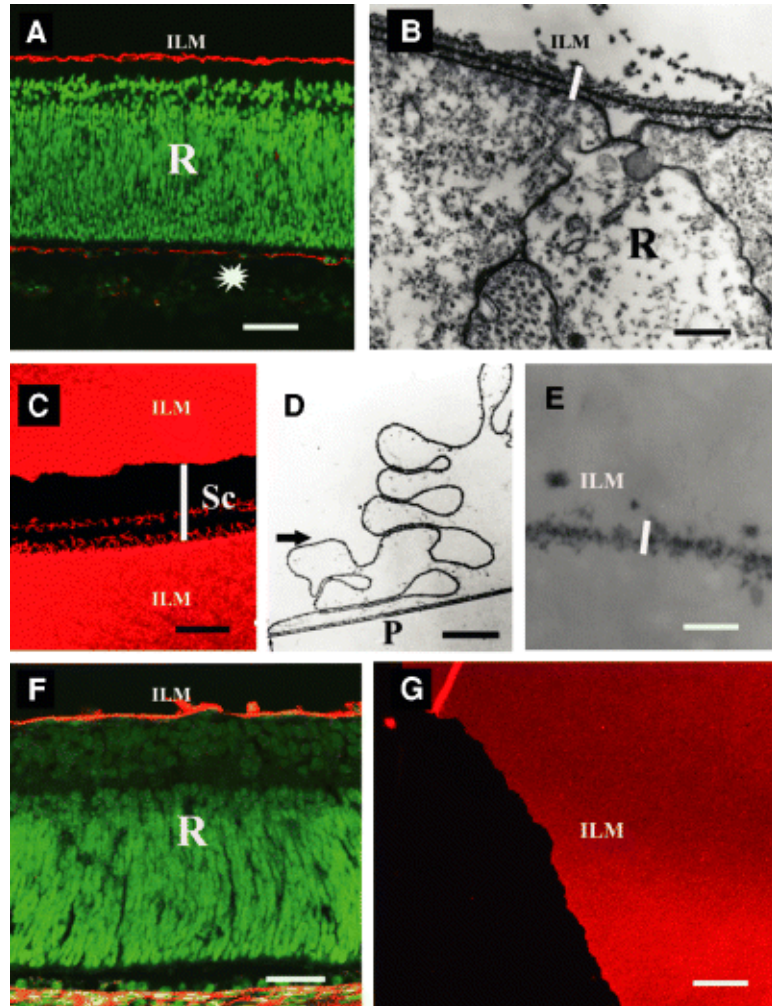


Figure 2-3. Flat-mount preparations of ILMs from chick and mouse retina. Large segments of chick (C) and mouse (G) ILM were prepared on glass slides by mechanically splitting the retina. The isolated ILM preparations were strongly labeled for laminin-1 (red in C,G), identical to the strong labeling (red) of the ILM in cross-sections of chick (A) and mouse (F) retina (R). The white star in (A) is next to the BM of the pigment epithelium. The sections were also stained with the nuclear counter-stain Sytox-Green (Molecular Probes, Eugene, OR, USA). The preparation shown in (C) was scratched (white bar and Sc, scratch) for thickness measurements with the AFM. TEM micrographs show that the ILM preparations are clean BM sheets: a low power micrograph (D) shows a thin sheet of ECM on the plastic support (P) that loops multiple times at the margin. A high power view (E) from the area indicated in panel D (arrow) showed the ILM as a 60 nm thin sheet, similar in thickness and appearance as ILM in retinal cross-sections (B). The measured thicknesses are indicated by the white bars. Bar, (A,F) 50 μm ; (B,E) 100 nm; (C,G) 25 μm ; (D) 2.5 μm .

Ultrastructural studies at low (Figure 2-3D) and high power (Figure 2-3E) showed that the ILM preparations were 50–70 nm thin sheets of extracellular matrix (Figure. 2-3D,E), free of cellular contaminants (Figure 2-3D). The isolated ILMs were similar in their ultrastructural morphology as ILMs in situ (Figure 2-3B). The low power transmission electron microscopy (TEM) images also showed that the ILM preparations formed extensive loops at their margins (Figure 2-3D), which were also detected in AFM thickness measurements.

2.3.4 AFM imaging of the ILM

Flat-mount preparations of chick ILM were imaged with AFM in intermittent-contact mode under NaCl/Pi. At low magnification, the retinal side of ILM was relatively smooth and did not exhibit detailed structural features. Figure 2-4A,C shows representative AFM images of E4 and E9 ILM imaged at 40 μm x 40 μm . When the ILM was imaged at 2 μm x 2 μm with higher imaging force (low amplitude set point in intermittent-contact mode), the images revealed a fibrillar structure (Figure 2-4B,D). These fibrillar networks are likely formed by collagen 4 fibrils. The individual fibrils in the E9 ILM appeared to be thicker (Figure 2-4D) than the E4 ILM (Figure 2-4B), suggesting modification of the BM during development.

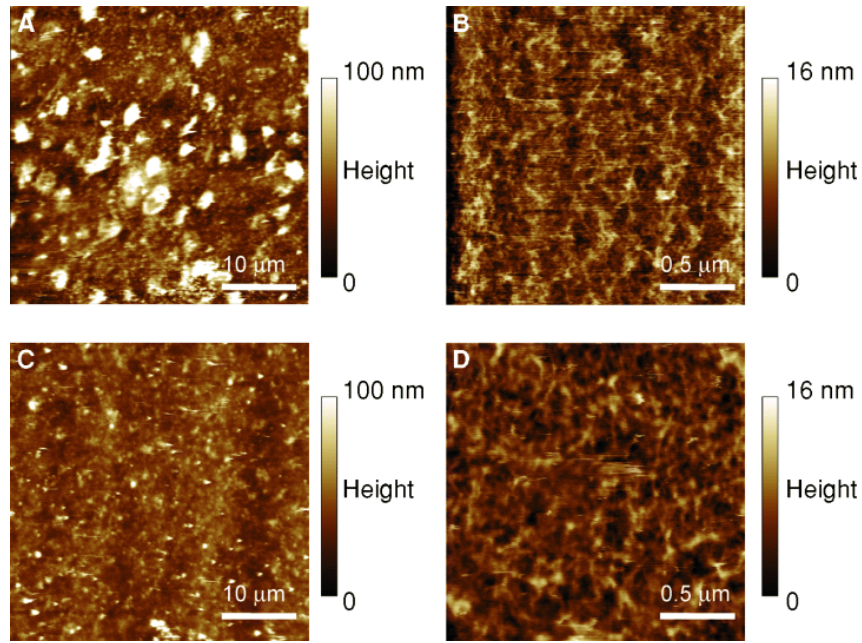


Figure 2-4. AFM images of flat-mount chick E4 (A and B) and E9 (C,D) ILM samples. At $40\ \mu\text{m} \times 40\ \mu\text{m}$ (A,C), the retinal side did not exhibit distinct features. Zooming into a $2\ \mu\text{m} \times 2\ \mu\text{m}$ region (B,D), the fibrillar network of the ILM could be seen. The fibrils in E9 ILM (B) appeared to be thicker than that of E4 (D).

2.3.5 AFM measurement of ILM thickness

The thickness of ILM was obtained from AFM images of the sharp edges of ILM where the underlining glass substrate was exposed. To obtain sharp ILM/ glass edges, scratches in the ILM were made using plastic pipette tips (Figure 2-3C). Figure 2-5A shows a height mode AFM image of a scratched edge of an E9 chick ILM with the exposed glass surface on the left, and the ILM on the right. Figure 2-5B shows the ILM height profile as indicated by the dashed line in Figure 2-5A along with the height profile of an E4 ILM. At the scratching edge, the ILM height was elevated due to scratch induced folding and accumulation of the scratched ILM debris.

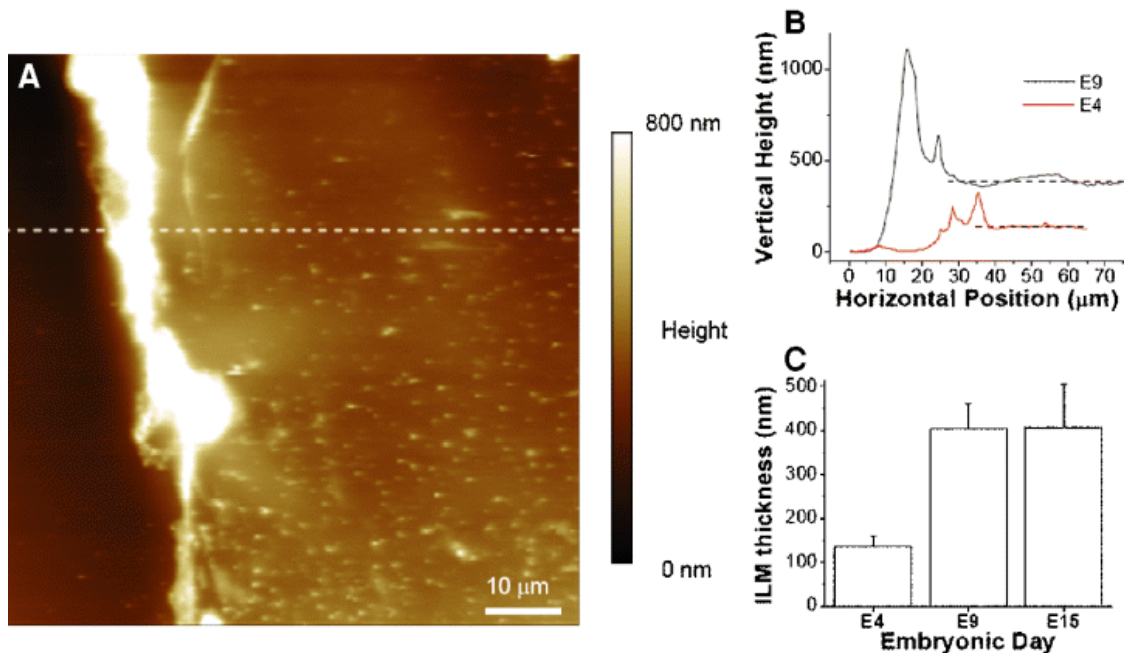


Figure 2-5: (A) Showing a height mode image of an E9 ILM near a scratched edge. The area on the left of the image is the glass substrate, whereas the area on the right is the ILM surface. A dashed line in (A) shows the location of a cross section profile, which is plotted as the black trace in (B), and is used to determine the thickness of the E9 ILM. The height profile of an E4 ILM sample (red trace) is also plotted in (B). (C) Summarizing the measured ILM thicknesses from four ILM samples for each of the E4, E9 and E16 development stages (ten measurements per sample). There is a significant increase in ILM thickness from E4 to E9, but not between E9 and E15. Data in (C) are presented as the mean \pm SD.

The thickness of the ILM was measured from the flat segment of the height profile (dashed lines) with the glass surface serving as the zero reference. The ILM thickness measurements were made for ILM preparations from four chick retinæ at development stages of E4, E9 and E15. For each ILM, ten height measurements were made from different crosssections. The measured thicknesses from each ILM sample are summarized in Table 2-1. The thickness (mean \pm SD) of the E4 chick ILM was 137 ± 22 nm ($n = 40$) and the thickness of E9 chick ILM was 402 ± 59 nm ($n = 40$; Fig. 2-5C). There was a three-fold change of ILM thickness ($P < 0.01$) during development between embryonic day 4 and embryonic day 9. The

ILM thickness for E15 retina was 406 ± 99 ($n = 40$); thus, ILM thickness did not change significantly between E9 and E15 (Figure 2-5C).

2.3.6 Elasticity of ILM

The Young's modulus of chick embryonic ILM was measured by AFM tip indentation using pyramidal tips (see Experimental procedures). The apparent Young's moduli of ILM samples from four different eyes were each measured for E4, E9 and E15 chick embryos. On each sample, 20 elasticity measurements were made from randomly chosen points each separated by 1–5 μm . Figure 2-6A shows representative experimental curves of AFM loading force versus z-piezo position for E4 (black solid line), E9 (blue solid line) and E15 (pink solid line) ILM. The dotted line is a fitted curve to the E4 ILM data using E (Young's modulus) and the initial contact point z_0 as fitting parameters.

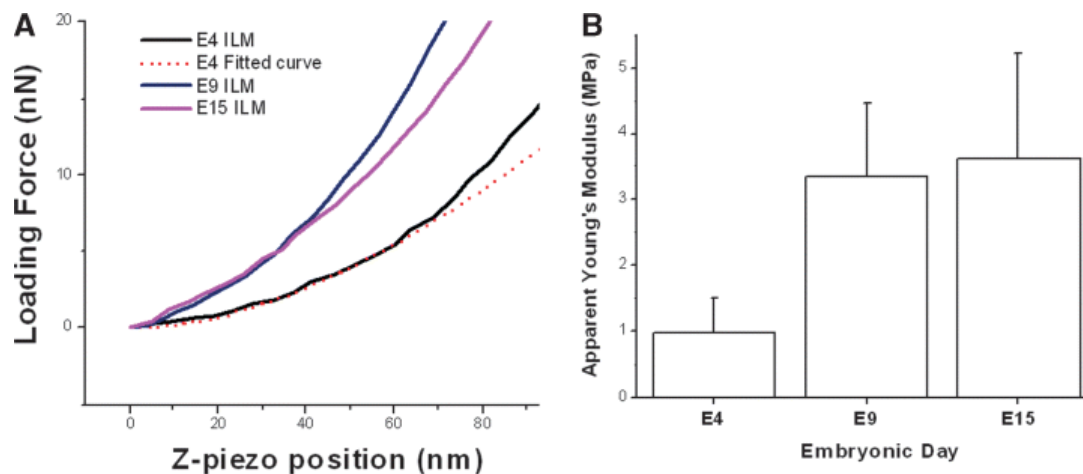


Figure 2-6: Elasticity of the chick ILM. (A) Representative AFM force-displacement curves for indentation experiments on ILMs from E4 (black), E9 (blue) and E15 (pink) chick retinæ. The dotted line is a fitted curve to the E4 experiment data using the Sneddon model. (B) Summarizing the average apparent Young's modulus of chick ILM at E4, E9 and E15 (mean \pm SD), the error bars represent standard deviations. Four ILM tissues for each development stage were studied; 20 measurements from each ILM sample were analyzed. There was a significant increase in the apparent Young's modulus between E4 and E9, but not from E9 to E15.

The apparent Young's modulus for the chick ILM of E4, E9 and E15 embryos is summarized in Table 2-1 and Figure 2-6B. The apparent Young's modulus of chick ILM was 0.95 ± 0.54 MPa at E4, 3.34 ± 1.11 MPa at E9 and 3.57 ± 1.58 at E15. There was a significant increase in the ILM stiffness (Young's modulus) from E4 to E9 ($P < 0.01$), but no significant change of ILM elasticity was observed from E9 to E15 ($P > 0.05$; Figure 2-6B). We also measured the elasticity of ILMs from postnatal day (P)1 mice and adult mice. The elastic (Young's) modulus of the neonatal mouse ILM was 3.81 ± 1.07 MPa (mean \pm SD, three different ILM tissues, 16 measurements on each tissue). The apparent Young's modulus of the adult mouse ILM was 4.07 ± 2.25 MPa. There was no significant difference between the apparent

Young's moduli of P1 and adult mouse ILM. The ILM elasticity is very similar for the neonatal mouse and the late embryonic chick (3.81 ± 1.07 MPa versus 3.57 ± 1.58 MPa).

Table 2-1: Elasticity of chick ILM

Apparent Young's Modulus (MPa)			
Sample #	E4	E9	E15
1	0.94 ± 0.35	3.28 ± 0.87	4.37 ± 1.74
2	0.79 ± 0.58	3.46 ± 1.00	2.73 ± 1.50
3	0.92 ± 0.39	3.54 ± 1.02	3.48 ± 1.36
4	1.19 ± 0.66	3.09 ± 1.43	3.84 ± 1.30
Average of 4 Samples	0.95 ± 0.54	3.34 ± 1.11	3.57 ± 1.58

2.4 DISCUSSION

2.4.1 The ILM as a model system for measuring BM thickness and elasticity

To investigate the mechanical stability of BMs, we chose the chick and mouse ILM as a model system. The ILM is located at the vitreo-retinal border, and it has the typical three-layered ultra structure of BMs that includes the two laminae lucida interna and externa, and the electron-dense lamina densa. Western blot analysis and MS showed that the ILM consists of extracellular matrix proteins that are also found in other BMs. These included laminin-1, nidogen-1, collagen 4 and the proteoglycans agrin, perlecan and collagen 18, consistent with previous studies [48, 58]. Our histological analysis of a mutant mouse showed that the ILM is important to confine retinal cells because breaks in the ILM lead to ectopic retinal cells in the vitreous cavity (Figure. 2-1). Thus, the mechanical stability provided by the ILM is critical for proper organogenesis of the eye. Likewise, endothelial herniation and frequent breaks of ocular and cortical blood vessels

in this mutant mouse (Figure. 2-1) confirm that the mechanical stability of BMs is one the essential functions of BMs in situ. To date, the mechanical properties of few BMs have been characterized, in large part, due to difficulty of isolating the delicate and thin BMs and the lack of tools to make mechanical measurements on such submicron thin membranes. A unique advantage of using the ILM over other BMs is that it is readily separable from the vitreous body, whereas most other BMs are tightly connected to interstitial connective tissue. Another unique advantage is that the ILM can be prepared as large flat-mount preparations on solid surfaces, such as glass or plastic, allowing reliable thickness measurements. It is also of note that the ILM isolation method uses firmly mounted retina as a source; thus, the preparation procedure avoids the chance for folding, stretching or compression of the BM. Taken together, the ILM is a BM that shares all typical features of most BMs and provides a series of unique experimental advantages making it particularly suitable for biomechanical measurements by AFM.

2.4.2 Thickness of BMs

AFM measurements showed that the chick ILM increases in thickness three-fold from 137 nm to 402 nm between E4 and E9. However, attempts to measure the thickness of mouse ILM were not successful because the retinal surface of rat ILM was very uneven and the measurements varied greatly, most likely due to the firmly attached hyaloid blood vessels to the mouse ILM. Since the chick eye lacks a hyaloid vasculature, this was not a problem for chick preparations. Based on TEM images of retinal cross sections, the thickness ILM from embryonic chick eyes has previously been estimated to be 50–70 nm [59] (Figure 2-3B). Similar values (40–120 nm) also have been reported for most other BMs investigated using TEM, such as BMs from muscle, blood vessels, the pia, lung and skin. These BM thickness measurements are currently

considered as textbook values for basal membranes [60]. However, sample preparation for TEM requires dehydration, which will lead to shrinkage of the BMs. Shrinkage following dehydration is probably much greater for BMs than for other tissue structures because at least three highly hydrated proteoglycans are major BM constituents. To confirm our result that the hydrated BM thickness is significantly greater than the previous TEM measurements, we measured the thicknesses of two freshly isolated chick E8 ILM under hydrated condition and then made measurements on the same ILMs after tissues were dehydrated following standard TEM drying procedures. The drying process reduced the thicknesses of these ILM from 356 ± 25 nm and 404 ± 14 nm to 48 ± 7 nm and 52 ± 9 nm, a reduction of approximately 87% (Figure 2-7). Therefore, we have shown that the thickness of ILMs had been greatly underestimated in previous TEM studies. This underestimation most likely applies to other BMs as well.

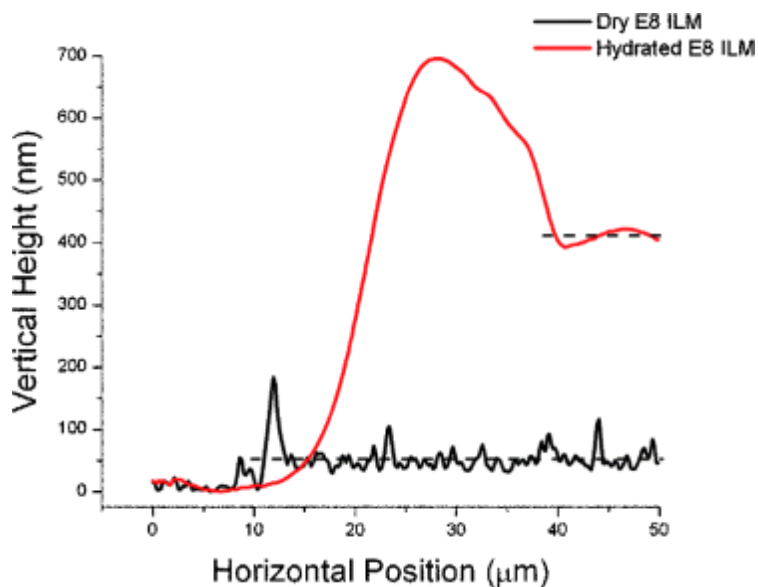


Figure 2-7: The cross section profiles of an E8 chick ILM under native, hydrated state (red line) and after dehydration (black line). The ILM thicknesses were measured from the elevation of the top membrane surface (dashed lines). In this E8 chick ILM, the drying process reduced the ILM thickness from 404 ± 14 nm to 52 ± 9 nm (mean \pm SD; ten measurements), which is a reduction of 87%.

2.4.3 Elasticity of BMs

Although many connective tissues, such as cartilages and BM, consist of similar extracellular matrix (ECM) molecules, including various collagens and proteoglycans, their mechanical properties vary significantly due to the different composition and crosslinks between the ECM molecules. For example, the Young's moduli of cartilages have been measured in the range 0.95–7.7 Mpa, depending on the location of the cartilage and there are even variations of stiffness at different regions of the same cartilage [61-66]. A recent AFM indentation study of the highly flexible tectorial membrane in the cochlea reported a Young's modulus in the range 37–135 kPa, with large spatial variations within the membrane [67]. At present, very little data

exists on the biomechanical properties of the conventional, thin BMs. The most extensively studied BM is the lens capsule, which can be readily separated from the lens cortex and is the thickest BM in the body (approximately 5–10 μm for the anterior capsule and 20–30 μm for the posterior capsule in humans) [68]. Under low strains, which correspond to our AFM experimental conditions, the Young's modulus of lens capsules has been reported to be approximately 0.6 MPa for rat, 0.82 MPa for cat, and between 0.3 and 2.4 MPa in humans [69–72]. The apparent Young's modulus of the Bruch's membrane was approximately 1 MPa, measured on cryosections of Bruch's membrane by AFM indentation [73]. The Bruch's membrane is another ocular BM (approximately 2 μm thick) located between the retinal pigment epithelium and the choroid and is composed of predominantly collagen 4 and elastin. The present study showed that the changes in the thickness and the bulk size of the chick ILM from E4 to E9 were accompanied by internal structural modification during development. The apparent Young's modulus of ILM, an intrinsic measurement of the material elasticity independent of the membrane thickness, increased from 0.95 ± 0.54 MPa at E4 to 3.34 ± 1.11 MPa at E9 (Table 2-1), although there was little change between E9 and E15 (3.34 ± 1.11 MPa versus 3.57 ± 1.58 MPa). These ILM elasticity measurements were made using sharp pyramidal tips (with a tip diameter of approximately 20 nm). We also made measurements using spherical tips (diameter 7 μm) to confirm our results. In a previous AFM study of articular cartilage elasticity, the measured elasticity could differ up to 100-fold depending on whether a sharp tip or a larger spherical tip was used, reflecting different tissue properties at nanometer and micrometer scales [65]. We did not detect significant discrepancy between measurements made using sharp pyramidal tips versus larger spherical tips. For E4 ILM, using the spherical tip, the apparent Young's modulus was 0.93 ± 0.19 MPa (mean \pm SD, two tissues and 16 measurements each),

which was very similar to results obtained using sharp pyramidal tips. The large increase of the apparent Young's modulus of ILM from E4 to E9 suggests significant remodeling of internal ILM structure during this development period. Higher resolution AFM images of the ILM surface show clear differences in the ILM fibrillar network at E4 and E9 (Figure 2-4B,D), consistent with structure modifications such as higher degrees of cross-link between collagen fibrils. Inhibition of crosslinking in collagen has been shown to significantly reduce the stiffness of aorta [74]. The biomechanical properties of ECM also depend on the variation in collagen and proteoglycan content [75]. Increases in both the membrane thickness and stiffness (Young's modulus) would enhance BM strength to resist stress induced during the growth of the eye. The change in stiffness is biologically useful because the embryos and its organs expand most dramatically during early stages of development and a more elastic BM is required, whereas at later stages mechanical stability of organs becomes more important.

2.5 CONCLUSION

In our study, we provided the first investigation into the biophysical properties of basement membranes. In order to accomplish this, we had to address two fundamental difficulties in studying such thin structures. The first is finding a suitable BM that is representative of typical BM composition and structure. The second is applying a tool for studying the biomechanics on a small scale, while keeping the tissue in as much of a native state as possible.

We introduced the inner limiting membrane of the vitreo-retinal border of the eye. It was demonstrated that the ILM contains typical BM composition and structure. We showed that the

ILM has mechanical importance to proper retinal development, and also were able to successfully isolate and prepare the ILM for study. Atomic force microscopy techniques were applied to the flat-mounted ILM samples. We were able to develop techniques and gather information of developmental changes in the both the Young's modulus and thickness for the embryonic chick ILM at varying time points during embryonic development. There was a notable increase in both chick ILM thickness and elastic modulus during early embryonic development that was not present during the later stages of development. We also provided insight into the real thickness of BM, as previous methods for determining BM thickness, such as EM techniques, involved processes that severely dehydrated the samples. This is an important detail in understanding the biological significance of BMs.

This study provided the first insight into the biomechanical properties of native basement membranes and developed techniques that can be applied to garner additional information about BMs under varying conditions.

3.0 INVESTIGATION INTO BASEMENT MEMBRANE PROTEOGLYCANS

3.1 INTRODUCTION

3.1.1 Proteoglycans

In general terms, proteoglycans are glycoproteins comprised of a central protein core that has one or more glycosaminoglycan (GAG) side chains. These GAG side chains are negatively-charged, long linear carbohydrates that are made of repeating disaccharide units. GAGs vary by the type of monomers that form the disaccharide unit. These differing types include chondroitin sulfate, heparin, heparan sulfate, and keratin sulfate. In ECM, such as cartilage, it has been demonstrated that GAGs store large amounts of water [76]. The BM proteoglycans relevant to this study are heparan sulfate proteoglycans.

3.1.2 Basement membrane proteoglycans

Heparan sulfate proteoglycans (HSPGs) are major constituents of basement membranes. There are three major HSPGs found in BMs: perlecan, agrin, and collagen XVIII [2, 3, 77]. These proteoglycans consist of a protein core attached to two or more long linear disaccharide, heparan sulfate GAG side chains. BM HSPGs are involved in biological processes such as

angiogenesis and managing growth factor activity [78]. They are able to inhibit and promote angiogenic signaling through the HS GAG side chains ability to gather growth factors close to cell surface receptors, where they can become biologically active. This may also act as an inhibitor; for example as the side-chains bind to growth factors, they may be unable to diffuse over larger distances[12]. While HSPGs biological function in signaling has been investigated, there is no direct information present in what structural importance they may have in terms of biomechanics. Targeted deletion of the HSPG perlecan in mice has led to exencephaly along with heart and vascular problems [25, 26, 79]. A mouse model for the targeted deletion of perlecan GAG side chains have resulted in postnatal lens degeneration [80]. These results suggest that the GAG side chains of BM HSPGs have implications in proper BM structural function. This study provides the first investigation into whether proteoglycans, specifically their HS GAG side chains' ability to hold water is a major influence on BM biophysical properties and structure.

3.2 METHODS

3.2.1 ILM sample preparation for SDS-PAGE and western blot

Embryonic day 8 (E8) chick ILM were dissected from the eye, and incubated in 2% Triton-X-100 in water overnight followed by incubation in 1% deoxycholate. The BMs, visible under dark field microscopy, were transferred a minimum of four times in Triton/deoxycholate before undergoing multiple washes in PBS. For SDS PAGE, 150-200 chick ILM were used.

The BM was digested for 1h with heparan sulfate lyase (*Flavobacterium heparinum*) and chondroitin ABC lyase (*Protease vulgaris*) (Seikagaku Corporation, Japan). Both the BMs and the digest supernatant were analyzed to compare protein loss due to enzymatic degradation. Coomassie staining was used for the SDS-PAGE runs. After resolving BM proteins by SDS-PAGE and transferring to nitrocellulose, both the supernatant and BM were labeled with antibodies to laminin-1. Additionally Western blots labeled for laminin-1 and agrin (a BM HSPG) for both control and enzymatically degraded samples were done to examine the specificity of the enzymatic degradation by heparanitinase and chondroitinase.

3.2.2 ILM flat mount preparation for AFM

Chick ILM flat-mounts were prepared for AFM study as described earlier; briefly, retinae from E8/9 chick embryos were dissected and spread on membrane filters (Millipore, Bedford, MA, USA). The filter/retinal sandwiches were placed, vitreal surface down, on poly lysine-coated (Sigma, St Louis, MO, USA) glass slides (Superfrost/plus, Fisher Scientific, Pittsburgh, PA, USA). After waiting 5 minutes for attachment, the filters with the retinae were lifted off from the slides, leaving large segments of the retinal BMs on the glass slides [47]. The BMs were incubated with a 2% Triton-X-100 solution for 30 minutes to remove the endfeet of the ventricular cells from the BM surface. The BM on the glass slide then underwent multiple washes under PBS solution, keeping the ILM hydrated at all times. The ILM of one eye of an embryo was treated with a heparitinase 1mU and chondroitinase 1mU for 2 hours, and the other eye with only BSA for the same time period as a control. Each sample was washed a minimum of 5 times and labeled for laminin to visualize the transparent BMs on the slide.

3.2.3 AFM indentation of chick ILM

As described previously, an MFP-3D Atomic Force Microscope (Asylum Research, Santa Barbara, CA, USA), mounted on top of an Olympus IX-71 fluorescence microscope (Olympus, Tokyo, Japan) was used for all AFM imaging and force indentation experiments. Standard commercially available, 100- μm long Si_3N_4 cantilevers, with integrated pyramidal tips (Veeco, Inc, Santa Barbara, CA, USA) and a nominal spring constant, k , of 0.6 N/m) were used for all experiments. The tissues were kept under NaCl/Pi solution throughout the experiments. The elasticity of the ILM samples were measured by nano-indentation with an AFM tip. The automated indentation was carried out using the cFV01 software program (Chad Ray, Duke University, Durham, NC, USA), at a rate of one load/unload cycle per second. The speed of the AFM tip indenting the tissue was between 2.0 and 10.0 $\mu\text{m/s}$. The Sneddon model, as previously described in chapter 1 was used to calculate the apparent Young's modulus for each of the E8 chick ILM samples.

3.2.4 ILM thickness

For thickness measurements, the topography of the ILM sample edge/glass substrate interface was imaged in intermittent contact mode (AC, or tapping mode), at room temperature. The thickness of the chick ILM was determined by analyzing these AFM topography images taken at the edge of the tissue sample, with the underlying glass substrate used as a zero reference. The change in height between the flat ILM surface and the glass substrate was

determined to be the thickness of the ILM sample. The thickness was calculated on chick ILM samples both before and after treatment to remove the GAG side chains from the HSPGs contained in the ILM. Samples from 4 different E8 chick ILM embryos were measured for both the control and heparitinase/chondroitinase treated ILM.

3.3 RESULTS

3.3.1 Chick ILM isolation and GAG removal

In order to investigate the function of proteoglycans in relation to ILM biophysical properties it was necessary to remove the long, negatively charged carbohydrate side chains (GAG) from the protein core of the proteoglycans. In cartilage, these side chains are responsible for storing large quantities of water in the ECM, which plays an important role in the biophysical properties of the matrix. It was important to determine that the treatment to remove the GAG side chains from the ILM proteoglycans did not result in a loss of constituent protein mass or change the ultrastructure of the ILM, but did successfully cleave the GAGs from the HSPG. Transmission electron microscopy (TEM) demonstrated that there was not a visible difference in the thickness or structure of the control (Figure 3-1D) and the treated (Figure 3-1E) samples, showing that there was not a significant change in structure or protein loss. Furthermore, SDS Page (Figure 3-1F) and Western blot (Figure 3-1G) results show that there was not a major loss of ILM proteins due to heparitinase/chondroitinase treatment, as seen by the lack of proteins present in the supernatant after the enzyme treatment. Western blots also demonstrated that the enzymes successfully removed the GAG side chains from the BM proteoglycan agrin (Figure 3-

1H, α -Ag), but did not lead to a change in molecular weight of laminin (F3-1H, α -Ln). These findings showed that the enzymes were indeed removing the GAG side chains from the PGs and not contributing to a general proteolysis of other BM proteins.

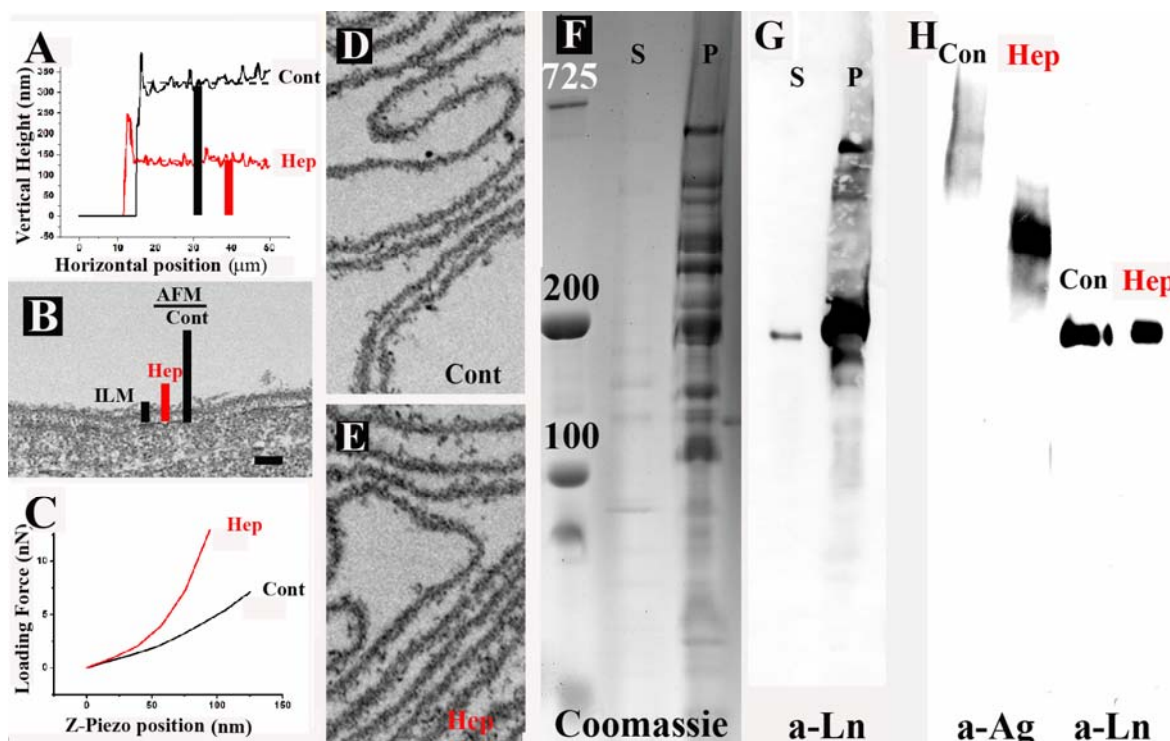


Figure 3-1: Enzymatic removal of the GAG side chains from BM HSPGs leads to a reduction in the thickness and an increase in the stiffness of the ILM. (A) AFM scans from a control (Cont, black line) and a heparitinase-chondroitinase-treated ILM (Hep, red) from the same E9 chick embryo showed that the removal of the GAG chains resulted in a 55% reduction of the ILM thickness from 327 ± 26 to 143 ± 22 nm. The treatment also resulted in an 80% increase in the stiffness of the BM from 3.21 ± 1.02 MPa in control to 5.81 ± 1.41 MPa in the enzyme-treated sample. Representative AFM force-displacement curves for stiffness measurement experiments are shown in (C). A TEM micrograph of the ILM of an E9 chick retina in situ is shown in (B). The short black bar indicates the thickness of the dehydrated ILM of the TEM micrograph. The longer black line indicates the thickness of the hydrated ILM as measured by AFM, while the red bar shows the thickness of the hydrated ILM measured by AFM after removal of the GAG side chains. TEM shows that the enzyme treatment did not alter the ultra-structure and thickness the dehydrated ILM samples (D, E). (F) Further, the enzyme treatment did not solubilize major quantities of BM proteins as shown by comparing the supernatant (S) and the BM pellet after Coomassie staining (P) or in western blots stained for laminin (G). Further, the enzyme incubation resulted in the loss of the GAG chains of agrin (a-Ag; H), indicated by the loss in molecular mass and an increase in staining intensity in the western blot; but, the enzymes did not lead to non-specific proteolysis of BM proteins as shown in a western blot with the same samples but stained for laminin (a-Ln; H). The blots compare untreated control (Con) and enzyme-treated samples (Hep) of the same protein concentration. Bars in C: 100 nm, in G, H: 500 nm. (Figure from submitted paper Balasubramani 2009, [37])

3.3.2 ILM elasticity

The Young's modulus of chick embryonic ILM was measured by AFM tip indentation using pyramidal tips as described previously. The apparent Young's moduli of ILM samples from five different eyes were each measured for both the control and GAG-removed E8 chick ILM samples. On each sample, 20 elasticity measurements were made from randomly chosen points each separated by 1–5 μm . Figure 3-1B shows representative experimental curves of AFM loading force versus z-piezo position for both the control (black) and treated (red) ILM samples. The apparent Young's modulus for all of the samples of both the treated and untreated samples is shown in Table 3-2. The apparent Young's modulus of the untreated E8 chick ILM (3.21 ± 1.02 MPa) was comparable to results from previous studies[46]. Removal of the GAG side chains led to an 80% increase in the stiffness for the treated chick ILMs (5.81 ± 1.41 MPa).

Table 3-1: The apparent Young's modulus from each chick ILM were taken for both the control and heparinase treated ILM. The data is presented as mean \pm SD.

Apparent Young's Modulus (MPa)		
Sample Number	Control	Experimental
1	2.87 ± 1.31	4.83 ± 1.63
2	3.16 ± 1.01	6.18 ± 1.88
3	3.73 ± 0.83	5.48 ± 2.12
4	3.25 ± 0.97	6.73 ± 1.23
5	3.06 ± 1.11	5.81 ± 1.72
Average of 5 Samples	3.21 ± 1.02	5.81 ± 1.41

3.3.3 ILM thickness

Thickness measurements were made on 4 samples for E8 ILM flat mount preparations of both the native and treated ILMs. For each ILM, n=20 thickness measurements were taken. The measured thicknesses from each ILM sample are summarized in Table 3-2. The average thickness of the native samples ($327 \pm 26\text{nm}$) was comparable to previously found results for the chick ILM[46]. The samples that had been treated for GAG removal, however, underwent a 55% reduction in thickness ($143 \pm 22\text{nm}$). Once again, histological and immunohistochemical results have shown that this is not due to a loss of protein mass, but rather is a consequence of GAG side chain removal.

Table 3-2: ILM thickness of ILM with GAG removal

ILM thickness (nm)		
Sample Number	Control	Experimental
1	314 ± 36	117 ± 27
2	362 ± 18	136 ± 27
3	346 ± 22	189 ± 15
4	284 ± 25	129 ± 21
Average of 4 Samples	327 ± 26	143 ± 22

3.4 DISCUSSION

Although the function of HSPG's role in growth-factor signaling pathways and other non-structural functions have been studied extensively [78], there has been a lack of information into the role of HSPGs in regards to basement membrane structural properties. Deletion of either

the HSPG itself or the GAG side chains leads to developmental deficiencies. For example, the deletion of perlecan in mice has shown a variety of defects, such as exencephaly, along with heart and vascular problems [21, 22]. Deletions of just the heparan sulfate side chains of perlecan in mice have adversely affected the lens capsule integrity, leading to postnatal lens degeneration and microphthalmia [80].

In our study, we investigated whether there is evidence that BM proteoglycans play a role in the biophysical properties of the ILM, such as HSPG water binding in cartilage. We used the AFM to measure the thickness and elasticity of the embryonic chick ILM before and after removal of GAG side chains by enzymatic treatment with heparitinase/chondroitinase. It was determined through TEM, western blot, and SDS page that there was no loss of protein mass or change in the ultrastructure due to GAG side chain removal. Non-specific protein degradation by the enzymes also did not occur.

There was a significant decrease (55%) in the thickness of the chick ILM after GAG side chain removal. It is important to note that TEM showed no change in the thickness of the ILM, and as previously demonstrated (Chapter 2) the TEM images are representative of the ILM after undergoing fixation/preparation steps that dehydrate the sample. The change in thickness is most likely then related to the loss of the water that was held by the GAG sidechains in the HSPG.

There was also a significant increase (80%) in the apparent Young's modulus after removal of the GAG side chains. This is possibly explained by an increase in the concentration of protein fibers with the loss of water from the GAG removal. By losing a significant amount water and changing the thickness of the BM, but not losing any of the proteins that form the ILM meshwork there is an increase in the amount of fibers present in a given volume. When the

AFM probe contacts the ILM surface it now is ‘pushing’ against more fibers than in the native state, causing an increase in the AFM probed stiffness of the sample.

These results demonstrate that water is an abundant molecule present in BMs, and the presence of HSPG GAG side chains is important in a BMs ability to retain hydration level. This ability is important in determining the biophysical properties of basement membranes, as a loss of water coincides with a decrease in BM thickness and increase in stiffness.

3.5 CONCLUSION

In this study we were able to use previously developed techniques to investigate the biophysical significance of a major constituent of basement membranes. Previously, there was no information into the structural importance of the heparan sulfate proteoglycans present in all BMs: agrin, perlecan, and collagen XVIII. In order to accomplish this, we first successfully cleaved the glycosaminoglycan side chains from the BM HSPGs. We demonstrated that the heparitinase/chondroitinase treatment did not result in a loss of BM protein mass, and directly removed the GAG side chains without indiscriminately degrading other proteins.

We used AFM techniques to detect changes in the thickness and elastic properties of the E8 chick ILM. There was a noted decrease in the ILM thickness coinciding with an increase in the ILM stiffness due to a loss of ILM hydration levels. This study provided novel insight into the previously unknown contribution of HSPGs into the biomechanical properties of basement membranes.

4.0 AGE-DEPENDANT EFFECTS ON THE HUMAN INNER LIMITING MEMBRANE

4.1 INTRODUCTION

As described in the introduction, there is ample evidence to BM being fluid in both thickness and composition during development and aging. There was no information on the coinciding biomechanical changes of BM during aging. This study, currently submitted for publication under the title *Age-dependant changes in the structure, composition and biophysical properties of the inner limiting membrane of the human eye* (Candiello, et al) provides the first information on the biophysical properties of a human BM, providing a baseline for future investigation into human BM properties.

The inner limiting membrane (ILM) is a basement membrane (BM) that is located at the border between the retinal neuroepithelium and the vitreous body (VB). It is considered the BM of the retina, yet in situ hybridization studies in chick and mice have shown that its protein constituents originate primarily from the ciliary body, the lens or the optic disc and not from the retina [81-84]. The function of the retina in ILM assembly is to provide the cellular receptors that are necessary for the deposition of the BM proteins on the retinal surface [31, 85, 86]. Analysis of mice, zebra fish and humans with mutations or deletions of BM proteins [4, 87-89] or their receptors [31, 86] have shown that the ILM is essential in retinal histogenesis by primarily

establishing a substrate for the neuroepithelial endfeet processes to attach to. In cases of a defective ILM, the vitreal processes are retracted, and the histogenesis of the retinal cell layers is greatly disrupted, eventually resulting in retinal dysplasia, retinal ectopia and a massive loss of ganglion cells and optic axons [4, 86-89]. An identical phenotype was obtained in chick embryos after enzymatic removal of the ILM [34, 36].

Another function of the ILM is connecting the retina with the extracellular matrix of the vitreous. The tight connection of ILM and vitreous is most evident in cases of retinal detachment where the contracting vitreal matrix pulls the retina from the retinal pigment epithelium via focal adhesions to the ILM [90-93]. Retinal detachment occurs during posterior vitreal detachment following age-related vitreal liquefaction and at younger age in cases of congenital high myopia [26, 79]. Further, a tight connection of the ILM to an epiretinal membrane may also lead to retinal detachment in proliferative diabetic retinopathy. A means to halt traction-induced retinal detachments is the peeling of the ILM in combination with vitrectomy. ILM removal has no deleterious consequences for the retina, demonstrating that the importance the ILM for the retina lies predominantly in early embryonic development. The present study investigates age dependent changes in the structure, composition and biophysical qualities of the human ILM.

4.2 METHODS

4.2.1 Human eyes and antibodies

Adult Human eyes were obtained from CORE, the “Center of Organ Recovery and Education” of the University of Pittsburgh. Fetal human eyes were obtained from the Brain and Tissue Bank for Developmental Disorders of the University of Maryland (Baltimore, MD). The internal review board of the University of Pittsburgh approved the use of human eyes under IRB protocol number #0312072. Polyclonal antisera to collagen IV, laminin-1, $\alpha 2$ macroglobulin and transferrin were obtained from Rockland Immunochemicals (Gilbertsville, PA), and Invitrogen (Carlsbad, CA). Antibodies to the BM proteoglycans human perlecan, collagen XVIII, and agrin were obtained from Drs Renato Iozzo (Thomas Jefferson University), and Alexander Marneros (Department of Cell Biology, Harvard Medical School). The polyclonal rabbit anti-human agrin antiserum was raised against a fusion protein from the N-terminal part of human agrin [94]. SytoxGreen was used as a nuclear counter stain (Molecular Probes, Eugene, OR).

4.2.2 Histology

Fetal eyes or adult retinal samples were fixed in 4% paraformaldehyde and processed (insert process). The resulting sections were mounted in 90% glycerol and examined with an epifluorescence or a confocal microscope (Flowview, Olympus). Transmission Electron microscope samples were prepared from the dorso-central region of the retina and fixed in a 2.5% glutaraldehyde/2.5% paraformaldehyde solution overnight. The samples were then

osmicated and embedded in EPON as per standard TEM preparation procedures. Thin sections were examined via JEOL electron microscope. TEM measurements of the ILM thickness were taken on 19 pairs of human donor eyes at 20,000x magnification. A minimum of 20 ILM measurements were taken at random from two retinal samples taken for each eye. An average thickness was calculated for the pairs of eyes from each age grouping. Donors had died from the following: stroke (3), myocardial infarction (6), kidney failure (2), accident (1), and cancer (1). None of the donor eyes came from patients who were diabetic.

In situ hybridization on sections of 10 and 20 week fetal human eyes were performed as previously described [84]. The cDNA for human nidogen 1 (PUNB) was 5.8kb long; the cDNA for human α 1 collagen IV (P13) was 1.75kb long.

4.2.3 ILM preparation

Human ILM flat mount preparations were prepared by immersing the adult human retina overnight in 2% Triton-X-100 in water. Using a Pasteur pipette under a dark-field illuminated dissecting microscope the detergent-insoluble ILMs were moved into a new Triton-X-100 and 1% deoxycholate solution. This process was repeated 3 more successive times in the same manner. The washed ILM samples were pelleted by centrifugation at 10,000 rpm. The resulting pellets were incubated with 100 μ L of 0.1 μ U/ μ l heparitinase and 100 μ L of 0.1 μ U/ μ l chondroitinase (Seikagako Corporation, Japan) for 1 h to facilitate ILM solubilization for SDS PAGE. A 10x SDS sample buffer and solid urea is added to concentrations of 1x and 8M. After boiling for 5 minutes, the samples were centrifuged and loaded into 3.5%-15% SDS gradient gels.

The vitreous body was taken from dissected fetal and adult human eyes, homogenized and cleared by centrifugation. Identical volumes of VB homogenate were loaded into Western blots as the concentrations of individual ECM proteins and the total protein concentration of the VB changes with age. The Western blots were probed for laminin-1, perlecan, collagen IV, $\alpha 2$ macroglobulin, and transferrin using the listed polyclonal antibodies. The lens capsules of the human eyes were isolated by manual dissection.

4.2.4 Atomic force microscopy of the ILM

For AFM investigation, both ILM and lens capsule flat mounts were made. Glass slides were prepared by coating them with 10 μ g/ml polylysine (P-1524; Sigma) and washing them 3 times successively with PBS. The area of the slide coated with polylysine was circled with a PAP-Pen (Research Products International, Mt. Prospect, Il) to create a hydrophobic barrier to contain the droplet of PBS carrying the BM sample. Segments of ILM or lens capsule (see previous section) were transferred into the PBS droplet on the slide and the entire slides were centrifuged at 1000 rpm for 5 minutes to attach the ILMs to the polylysine coated slides. Once the BMs were adhered to the slides, they were washed 3 times with PBS. Some of the ILM flat-mount preparations were immuno-stained for laminin or collagen IV for better visualization of the BMs. Other ILM preparations were treated with 500 μ l or 0.1 μ U/ μ l of both heparitinase and chondroitinase (Seikagaku) and 1mg/ml BSA in PBS for 2 h at 37°C to investigate the GAG importance in human ILM thickness and elasticity. Control samples from the same eyes were incubated with only the 1mg/ml BSA in PBS for the same time period. Both the experimental and control samples were washed at least 5 times with PBS before AFM probing.

All of the imaging and force indentation experiments were done using an MFP-3D AFM (Asylum Research, Santa Barbara, CA) mounted on top of the Olympus IX-71 fluorescence microscope (Olympus, Tokyo, Japan). For all experiments 100 mm long silicon-nitride triangular cantilevers with pyramidal tips were used (Veeco, Inc, Santa Barbara, CA) that had nominal spring constant of ~ 0.8 N/m. The spring constant was individually calculated for each cantilever prior to experimentation using the thermal fluctuation method [95]. The images of the ILM used for thickness measurements were done in the intermittent contact mode (AC, tapping) and the elasticity was determined by the force-indentation method as previously described [46]. For the thickness and elasticity measurements, 10 ILM and 3 lens capsules were probed. For thickness characterization, 25 image cross sections were measured at 4 different locations on each sample. Measurements of the elastic properties were taken at 100 random locations on each sample. For the heparitinase experiments, 3 samples of the enzyme-treated ILM and 3 samples of the control were probed. To investigate the thicknesses, 25 thickness measurements were taken at 4 randomly selected locations. Elastic properties were again measured at 100 random locations.

4.3 RESULTS

4.3.1 Protein composition of the fetal human ILM

The ILM, as shown in Figure 4-1A, is located at the vitreal/retinal border. The ILM is one of 4 BMs found in the eye, along with, the lens capsule, the BM of the pigment epithelium, and the intravitreal hyaloids vessels BMs. Immunocytochemistry using antibodies against

specific basement proteins in human fetal eyes showed strong labeling of the ILM and other ocular BMs. Collagen IV (Figure 4-1A), laminin-1 (Figure 4-1B), nidogen-1 (Figure 4-1D), and the proteoglycans: perlecan (Figure 4-1E), agrin (Figure 4-1G), and collagen XVIII (Figure 4-1F) were present in the ILM and other ocular BMs. TEM of both 10 and 20 week fetal human eyes show typical ultrastructure of a BM under electron microscopy (Figure 4-1C). The ILM has a thickness of around 70nm (n=6) and shows the inner and outer lamina rara and central lamina densa.

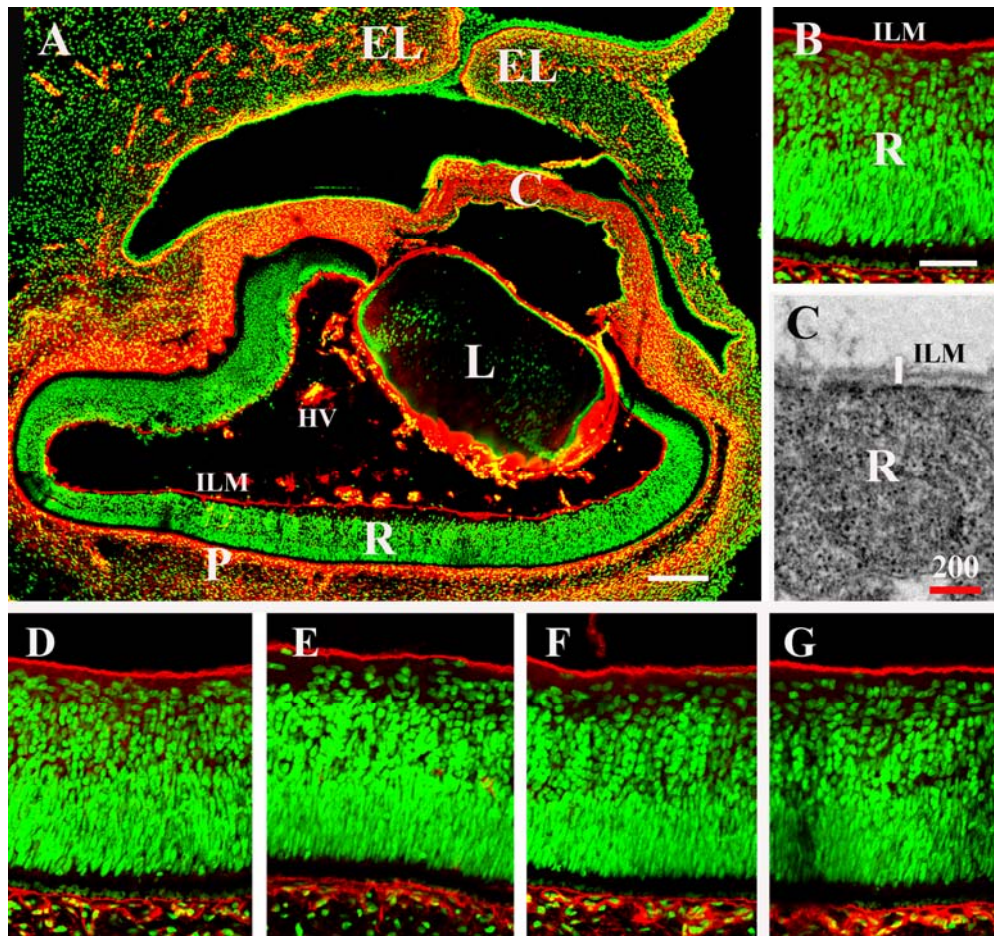


Figure 4-1: Detection of BM proteins in the ILM of the fetal human eye. The low power overview of an 10-week fetal human stained for collagen IV (red) shows the BM of the lens (L), the hyaloids vessels in the vitreous (HV), the pigment epithelium (P), the ILM, and the vascular BMs in the eye lids (EL). The corneal stroma (C) is also labeled. High power micrographs of the 10 week fetal retina show strong labeling of the ILM and the BM of the pigment epithelium and the choroid for laminin-1 (B), nidogen (D), perlecan (E) and collagen XVIII (F), and agrin (G). The immuno-stained sections were counter-stained with Sytox Green (green; A, B, D-G). A TEM micrograph showing the vitreal portion of a 20 week fetal retina with the ILM is shown in (C). Bars: a: 150 μ m; B, D-G: 35 μ m.

The site of synthesis of the ILM proteins in 10 and 20-week fetal human eye was determined by in situ hybridization to localize the mRNA expressions for $\alpha 1$ collagen IV and nidogen 1. While the ILM proteins are located in the BM along the vitreo-retinal surface (Figure 4-2A), collagen IV and nidogen 1 mRNAs were expressed by the lens epithelial cells and by the endothelial cells of the hyaloids vessels (Figure 4-2B, C). There was also a weaker expression of nidogen-1 by the epithelial cells of the future ciliary body (star in Figure 4-2C). There was no expression of collagen IV and nidogen mRNA in the neural retina, and there was no labeling of any eye tissues after incubating the sections with a sense probe to collagen IV (Figure 4-2D).

Since ILM forming proteins have origins outside of the retinal cells, the proteins would have to originate from the lens, ciliary body, and hyaloids vasculature and enter the vitreous to have access to the retinal surface. This was confirmed by Western blots of the 20-week old vitreous demonstrating the presence of laminin-1, perlecan, and collagen IV in the vitreous body of the human fetal eyes (Figure 4-2E). In contrast, western blots showed laminin-1 and collagen IV concentration was greatly reduced and perlecan was no longer detectable in the adult vitreous (Figure 4-2E). As a control, both fetal and adult vitreous samples were probed for transferrin and $\alpha 2$ macroglobulin, two proteins originating from the ciliary body that have previously been detected in the vitreous [96, 97]. These proteins were detected, via western blot, in the fetal and adult human vitreous in either similar (transferrin) or increased ($\alpha 2$ macroglobulin) (Figure 4-2E) concentrations. This data is consistent with previous data showing laminin, collagen IV, and collagen XVIII in human fetal vitreous, but not in the adult human vitreous [96, 97].

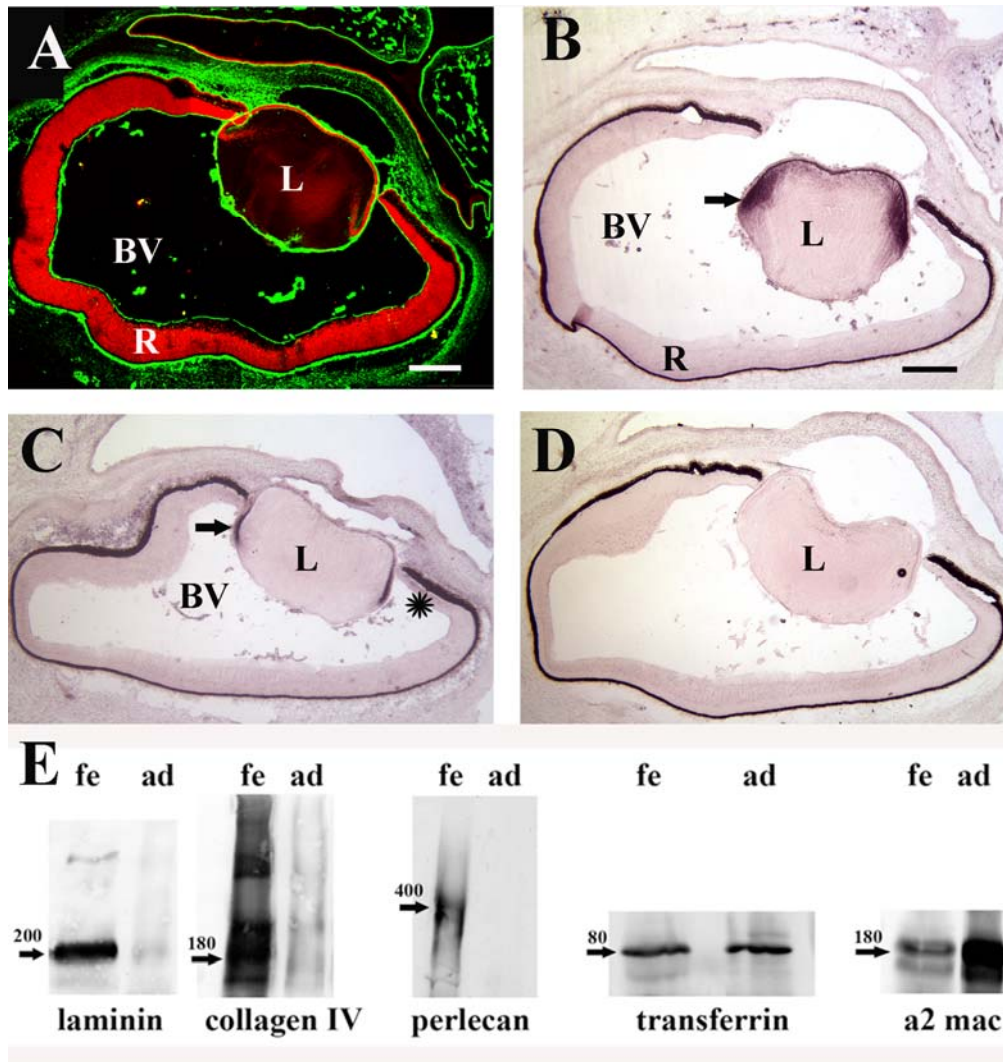


Figure 4-2: Immuno-localization of collagen IV (A) and in situ hybridization for the detection of collagen IV $\alpha 1$ mRNA (blue; B) and nidogen mRNA (C) in a 10 week fetal human eye. The sections in panel (A) was stained with a polyclonal antiserum to collagen IV (green) and counter-stained for Pax6 (red). Adjacent sections were processed for in situ hybridization to localize the mRNA expressions of collagen IV $\alpha 1$ (blue; B) and nidogen1 (blue; C). A sections treated with the sense probe for collagen IV is shown in panel D. The mRNA for collagen IV $\alpha 1$ and nidogen-1 was located in the epithelium of the lens (L; arrow) and the hyaloids blood vessels (BV). There was little expression of nidogen also in the future ciliary epithelium (star in C), but there was no expression of collagen IV and nidogen mRNA in the neural retina (R). Western blots (E) demonstrated that laminin, collagen IV and perlecan were detected in the 20-week fetal vitreous (fe) but not in the adult vitreous (ad), indicating a developmentally regulated synthesis of the ILM proteins in the eye. Transferrin and $\alpha 2$ macroglobulin are present in similar concentrations in fetal and adult vitreous. The specific bands of the monomeric proteins and their molecular weights are indicated by arrows. Bars: A-D: 150 μ m.

4.3.2 Structure and composition of adult human ILM

Thin sections of fetal and adult human ILM were investigated via TEM to look at age-related structural changes. The ILM at week 20 of fetal development is shown to be 70nm and very even (Figure 4-3A). With increased age the ILM loses its layered ultrastructure as shown in the 22 year old sample (Figure 4-3B). At 22 years old the ILM thickness is around 250 nm, but is still uniform. At age 86, the ILM thickness had increased to over 1000nm (Figure 4-3 C-E). In addition to thickening, the ILM has also become irregular from age 50 onwards. The vitreal side of the ILM has remained smooth, but the retinal surface as developed long protruding extensions into the retina (Figure 4-3F). These protrusions become more pronounced with increasing age. Figure (Figure 4-3C-E) shows the age-dependant increase in thickness and increase in extension length of the ILM at the retinal surface.

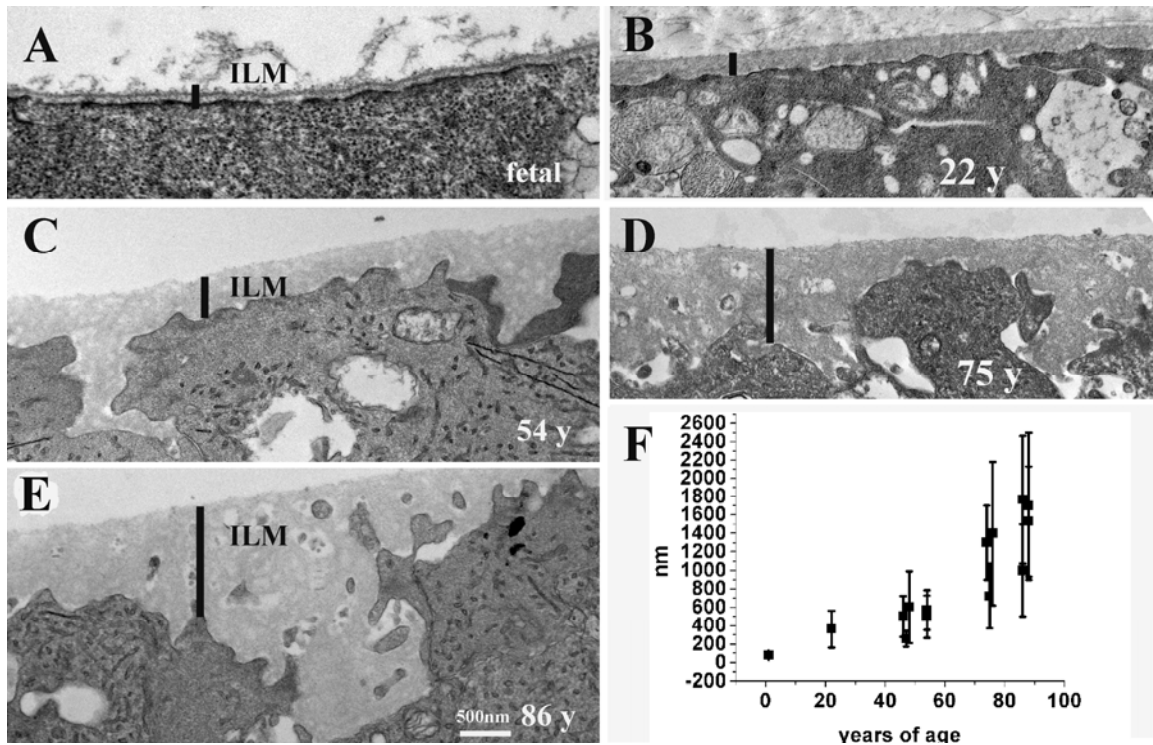


Figure 4-3: TEM micrographs of the vitreal surface of the retina showing the ILMs from a 16-week fetal (A) and from 22, 54, 75 and 86 year-old adult human retinas (B-E). The ILM from the fetal eye has the typical morphology of a BM: it is 70nm-thick with a typical lamina densa (A). Between 22 and 86 years of age, the ILM dramatically increases in thickness, becomes highly irregular at the retinal surface and is no longer structured with a distinct lamina densa. The graph in panel (F) shows the age-dependent increase in thickness. Note the ever-increasing variation of ILM thickness, expressed by the large standard deviations. Each postnatal data point of the represents one pair of eyes, the measurements of fetal eyes is based on 6 pairs of eyes between 10 and 20 weeks of age. The black bars in (A) to (E) indicate the thickness of the ILM.

4.3.3 Adult human ILM isolation and protein composition

To analyze the protein composition and to probe the biomechanical qualities of the adult human ILM we devised a method to isolate the ILM from adult human retina. The procedure takes advantage of the fact that BMs are insoluble in detergent [98, 99]: following the dissolution of the retinal cells in Triton-X-100 and deoxycholate the ILMs were collected from the detergent

solution under a dissecting microscope using dark field illumination (Figure 4-4A, insert). TEM micrographs (Figure 4-4A) showed that the isolated ILMs were clean sheets of extracellular matrix, free of cellular debris and organelles. Further, the vitreal surface of the sheets was smooth and even whereas the retinal surface had a very irregular appearance, identical to the retinal surface of the ILM seen in situ (Figure 4-4B). The ILM sheets were readily differentiated from the vascular BMs that were also isolated from the detergent extracted human retina (Figure. 4-4C). To further prove the purity of the isolated ILM preparations, mice were immunized with the BMs, and the antisera from the mice were tested by immunocytochemistry on sections of human retina. As shown in Figure 4-4D, the antisera only labeled the ILM and vascular BMs, identical to the labeling obtained by using anti-collagen IV or anti-laminin antibodies (Figure. 4-4E).

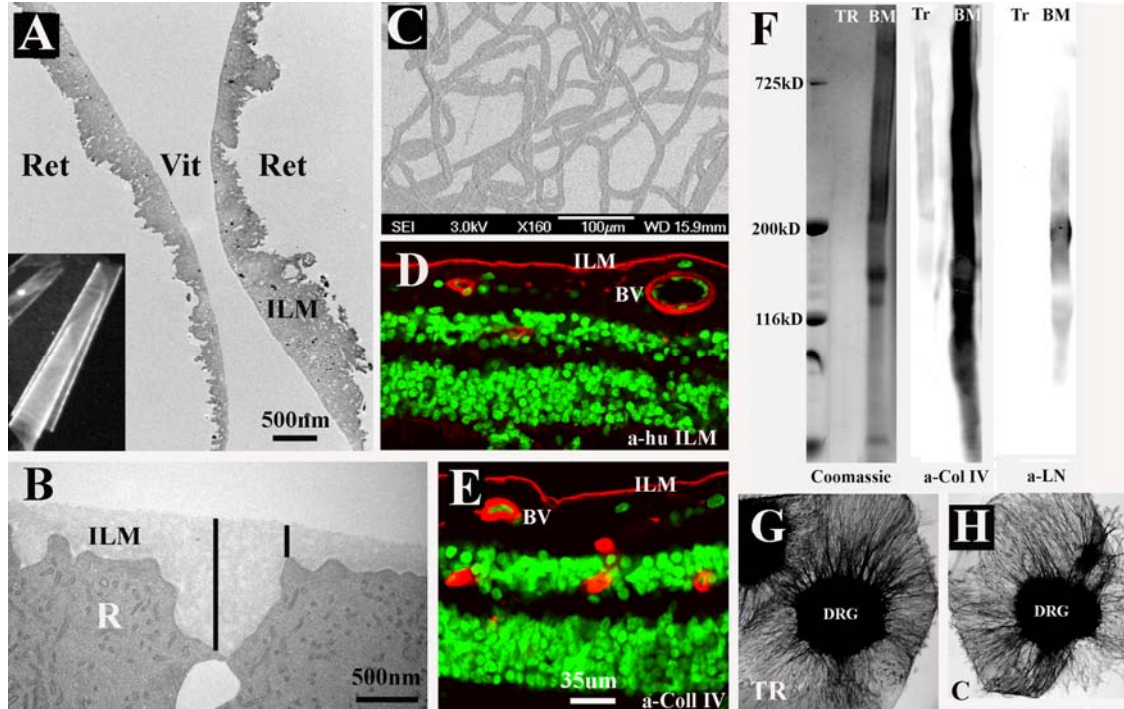


Figure 4-4: Isolation of the inner limiting membrane (ILM) of the adult human retina. TEM micrograph (A) shows an isolated and folded human ILM with a smooth vitreal (Vit) and an irregular retinal surfaces (RET). The insert shows a rolled-up human ILM as seen under a dissecting microscope using dark field illumination. The isolated ILMs (A) are structurally very similar as ILMs in situ (B). The bars in (B) indicate the alterations in the thickness of the ILM. The morphology of vascular BMs from human retina, as shown by scanning electron microscopy, are shown in (C) for comparison. An antiserum from a mouse immunized with purified human ILMs exclusively labeled the ILM and the BMs of the blood vessels (BV) in sections of human retina (D). The staining pattern was similar to that obtained by staining with anti-collagen IV (E). Detergent treatment of BMs does not lead to major loss of protein: human lens capsule BMs were extracted with Triton-X-100/deoxycholate overnight and the Triton supernatant (Tr) and the insoluble BM (BM) were probed by SDS PAGE and western blotting. Coomassie staining showed very little protein in the detergent supernatant, but large quantity of protein in the detergent-insoluble BM pellet. Western blots stained for laminin and collagen IV confirmed that detergent did not solubilize these proteins from the BM. Explants from chick dorsal root ganglia (DRG) were explanted on human lens capsule that were treated with Triton-X-100/deoxycholate overnight (G) or on control, non-treated lens capsules (H). Axon outgrowth was equally well on both substrates showing that detergent does not lead to a denaturation of the BM. The sections in (D) and (E) were counter stained with SytoxGreen. Bar: E: 35 μ m.

To determine whether the isolation of ILMs with Triton-X-100 and deoxycholate leads to a loss of protein or to a denaturation of the BM we used the identical detergent treatment on human lens capsules that was isolated by dissection alone. To this end, we assayed for proteins that were extracted from the lens capsule by detergent. In Coomassie stained SDS gels, we found that very little protein was extracted from the lens capsule by the detergents (Figure 4-4F), while the dominant portion of the protein stayed with the BM pellet. Western blots probing for collagen IV and laminin confirmed that the BM proteins were undetectable in the detergent supernatant (Figure 4-4F). When the lens capsule were tested for its substrate properties for axon outgrowth from embryonic chick dorsal root ganglia and retinal explants it was found that the axons and Schwann cells grew equally well on the detergent-treated lens capsule (Figure 4-4G) as on the non-treated control lens capsules (Figure 4-4H) showing that the cell adhesive and neurite-outgrowth-promotive activity of the BM was not affected by Triton/deoxycholate treatment. Previous immunocytochemistry has shown that the adult human ILM is comprised of laminin 1, nidogen 1, collagen IV, agrin and collagen XVIII [58, 59, 100], ECM proteins that have been detected in the fetal ILM as well (Figure 4-1A). To determine to what percentile collagen IV and laminin 1 contribute to the ILM we determined the concentration of both proteins in adult human ILM by western blotting (Figure 4-5). Reference samples of purified collagen IV and laminin were used to establish calibration curves. Densitometry and extrapolation from the calibration curves showed that the concentration of laminin γ 1 was 7.5% of the total ILM protein. The concentration of collagen IV was 57% of the total ILM protein (Figure 4-5) showing that collagen IV is the dominant protein of the adult human ILM.

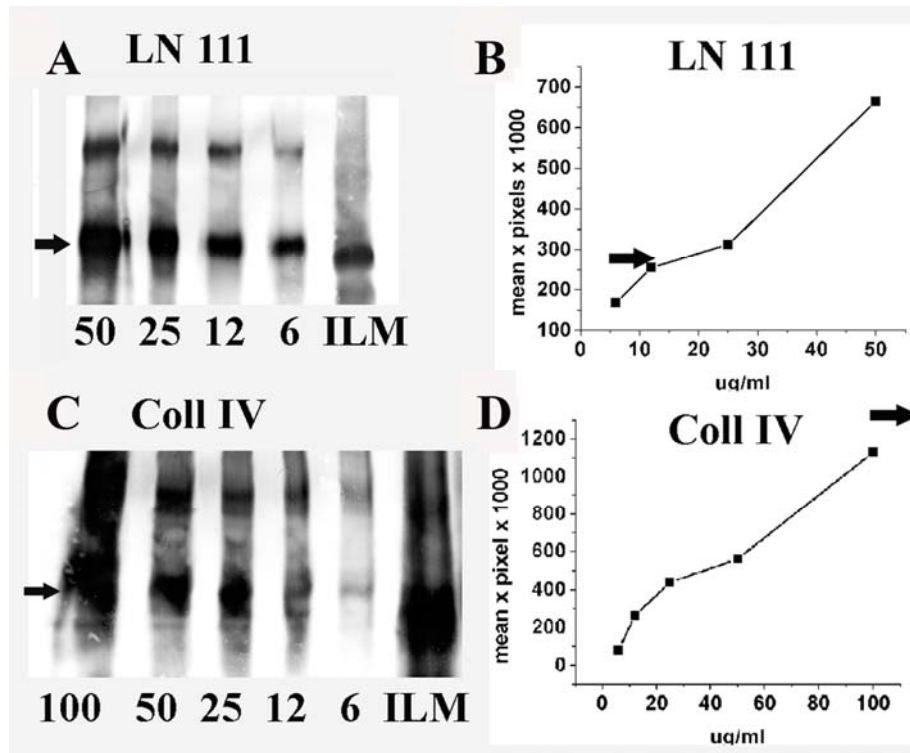


Figure 4-5: Western blots stained for laminin (A) and collagen IV (C) to determine the concentration of both proteins in human ILM. The ILM samples were run out on SDS PAGE in parallel with either Laminin or collagen IV references to establish calibration curves from which the concentrations of laminin and collagen IV in human ILM was extrapolated. The calibration curves (B, D) were established by densitometry of the laminin and collagen proteins bands indicated by arrows. The laminin concentration of the 88-year old human ILM was estimated at 15 μ g/ml, which equals 7.5% at a total ILM protein concentration of 200 μ g/ml. The concentration of collagen IV was estimated for the same sample at 115 μ g/ml, with equals 57% of the total ILM protein.

4.3.4 The biophysical properties of adult human ILM

To investigate the biomechanical qualities of the adult human ILM, segments of human ILM were mounted on glass slides (Figure 4-6A, B) and probed by atomic force microscopy (AFM). It is important pointing out that the measurements by AFM were taken while the ILM was submerged in PBS, thus the preparations were fully hydrated. Force indentation by the AFM probe has previously been used to determine the elasticity of cells [43-45, 101, 102], and AFM

has been successfully used to determine the thickness of the native ILM from chick embryos [46]. Two parameters were determined: thickness and elasticity. Both data sets were sorted according to the age of the donor eye. Measurements by AFM showed that the thickness of the ILM increases with advancing age (Figure 4-6C). Further, the hydrated ILMs were by average four-times thicker than the dehydrated ILMs processed for TEM. The variation in thickness, as measured by AFM, increased with advancing age, similar as for the thickness measurements by TEM. The apparent Young's modulus, measuring the elasticity of the human ILM independent of thickness, was between 1.5 to 5 MPa, and the graph in Figure 4-6D shows that the apparent Young's modulus increased with advancing age. The apparent Young's modulus of elasticity was also determined for human lens capsule using the same AFM probing technique as for the ILM. The primary goal of these experiments was to find out how the AFM measurements of the lens capsule compare with elasticity measurements of lens capsule probed by conventional hydrostatic measurements [103-105]. The apparent Young's modulus of human lens capsule, as measured by AFM, was 3.92, 2.70 and 4.37MPa for 3 lens capsules. The values are similar as the data obtained by hydrostatic measurements [103-105]. Further, the Young's modulus of the human lens capsule was in the same range as for human adult ILM and embryonic chick ILMs, despite the fact that the lens capsule is a bout 10-times thicker than the human and 100 times thicker than the embryonic chick ILMs, demonstrating that the Young's modulus is a measure for the biomechanical property of BMs and independent of the thickness. Finally, the fact that the lens capsules had never been in contact with detergent yet resulted in a similar Young's modulus as the detergent-treated human and chick ILMs showed that Triton/deoxycholate treatment of BMs does not affect their biomechanical quality.

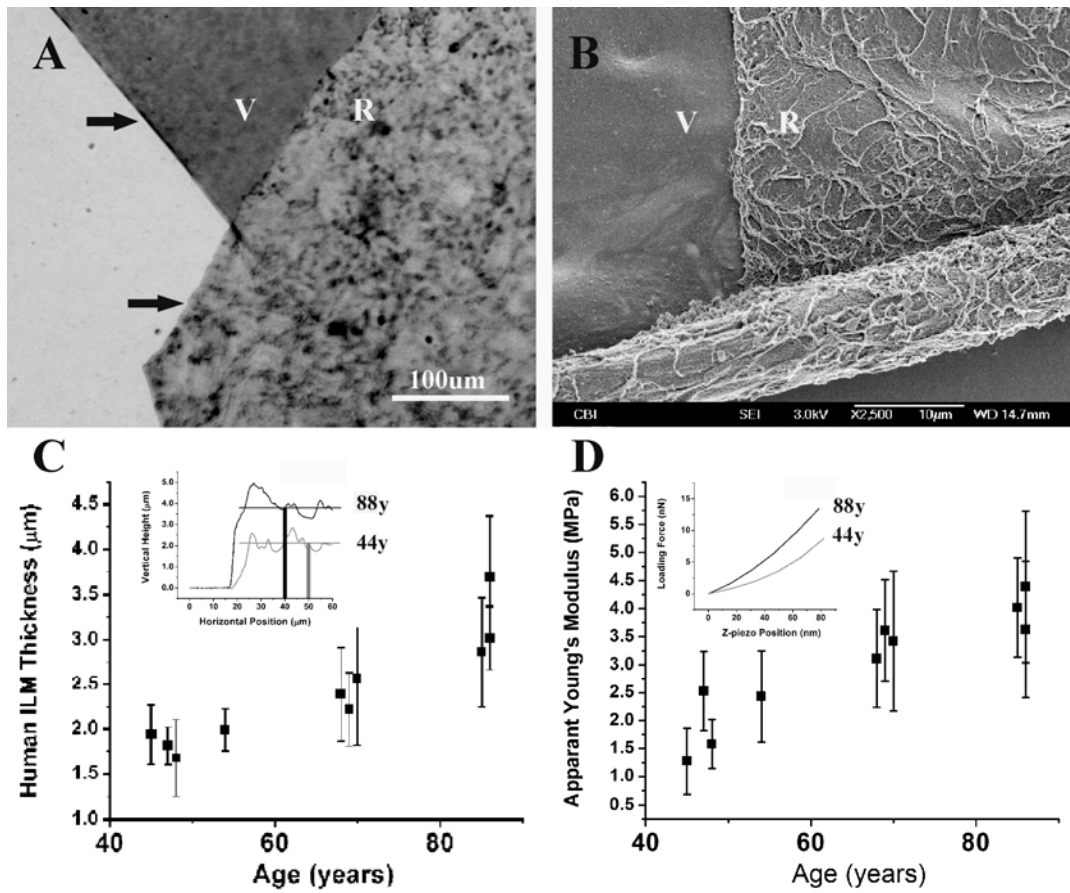


Figure 4-6: Adult human ILM segments immobilized onto cover slips and stained for collagen IV (A) or processed for SEM (B). The ILMs in (A, B) were folded showing the smooth vitreal surface (V), and the irregular retinal surface (R). The arrows in (A) indicate single-layered segments of the ILM, where AFM thickness and elasticity scans were done. The smooth vitreal (V) and the irregular retina surface (R) are particularly well demonstrated in the SEM micrograph in panel (B). AFM thickness measurements of the human ILM according to age is shown in (C). Actual AFM measurements of a 44 and an 88year-old ILM is shown in the insert: the bars show the average thickness of each of the samples, the baseline is the glass slide on the left of the scan. The age-dependent increase in Young's modulus of elasticity is shown in (D). Actual AFM elasticity scans of a 44 and 86 year-old ILM are shown in the insert.

4.3.5 Removal of glycosaminoglycan side chains in adult human ILM

The four-fold difference in the thickness of the hydrated ILM, as measured by AFM, vs. the dehydrated ILM, as measured by TEM (Figure 4-7A), indicated that some ILM components

bind large quantities of water to the matrix and thereby influences thickness and possibly other properties. The most likely candidates for binding high amounts of water to the BM matrix are the GAG side chains of the proteoglycans. As shown in Figure 4-1 and as reported earlier [96], the human ILM includes 3 proteoglycans, namely perlecan, agrin and collagen XVIII. To test whether the removal of the GAG side chains has an effect on the biomechanical properties of BMs human ILM flat mounts were treated with heparitinase/chondroitinase, and the enzyme treated ILM samples were compared with nontreated control samples. AFM measurements showed that the removal of the GAG side chains resulted in a major reduction in ILM thickness that ranged between 30 and 50% depending on the age of the eye from which the ILM was obtained (Figure 4-7B). Further, the Young's modulus of ILMs increased by at least 30% after GAG removal (Figure 4-7C), showing a loss of ILM elasticity after the GAG side chains had been removed. The decrease in thickness and the increase in the Young's modulus after GAG removal were less with advancing age (Figure 4-7B, C).

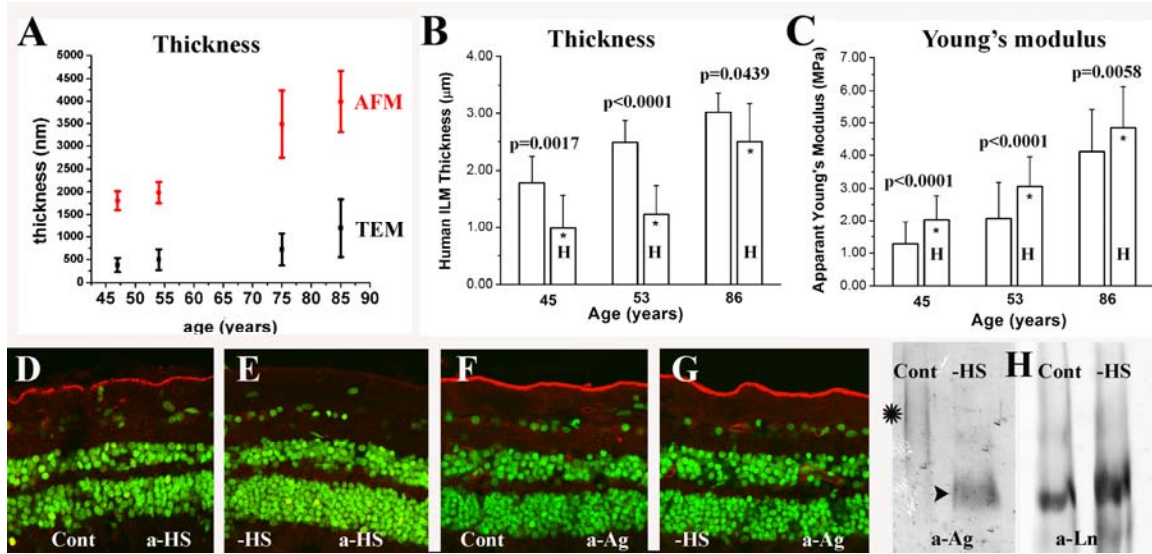


Figure 4-7: ILM thickness measured by AFM and TEM. Thickness measurements of the hydrated ILM by AFM (red) resulted in values that were four times higher than thickness measurements based on TEM of the dehydrated samples (black; A). The AFM and TEM samples for each age group are from the same retina. As shown by AFM, when the GAG side chains of the BM proteoglycans are removed by heparitinase/chondroitinase the ILMs shrank by 30 to 50% (B). Elasticity measurements showed that the enzyme treatment leads to a 20-30% increase in the Young's modulus (C). The reduction in ILM thickness and the increase in stiffness after heparitinase treatment is less at older age. The p-values between control and heparitinase-treated (H) ILM samples are indicated. The selectivity of the heparitinase-treatment was confirmed by immunocytochemistry. Staining human control sections (Cont) with an antibody against the HS carbohydrate epitope (a-HS) labeled the ILM (red; D). When the sections had been incubated with heparitinase (-HS), the HS-labeling was undetectable (E). When sections were stained for the agrin core protein, staining of the non-treated (F) and the enzyme-treated sections (G) was indistinguishable showing that the enzyme did not degrade the core proteins of the proteoglycans. The selective removal of the HS chains was also confirmed by western blots (H). Control ILM sample (Cont) labeled for agrin (a-Ag) showed the typical smear of the agrin proteoglycan at 400kD (star), whereas in the enzyme treated ILM sample (-HS) the agrin immunoreactivity had shifted to a narrow band at 200kD (arrow head). When blots with the same samples were labeled with an antibody to laminin (a-Ln) the same 200kD laminin bands appeared in control and enzyme-treated samples showing that the enzymes did not lead to proteolysis of the peptide chains. The sections in (D) to (G) were counterstained with Sytox Green.

The selectivity of the enzyme treatment was confirmed by staining retinal sections from human eyes for heparan sulfate side chains of the proteoglycans (HS) or for the core proteins of one of the proteoglycans, namely agrin. In control sections, an antibody directed to HS-side chains labeled the ILM and the BM of the retinal blood vessels (Figure 4-7D). After heparitinase-treatment, the HS staining was no longer detectable (Figure 4-7E). When ILMs were labeled for the agrin core protein, the ILM labeling of the non-treated control (Figure 4-7F) and the enzyme-treated retinal sections (Figure 4-7G) was indistinguishable. The data showed that heparitinase-treatment led to the removal of the GAG side chains of the proteoglycans, but did not lead to the degradation of their protein cores. Further confirmation came from western blots: ILM samples were treated without and with heparitinase/chondroitinase. The western blots with these samples were labeled for agrin (a-Ag) and laminin (a-Ln). In control samples, agrin appeared as a long smear of 400kD, typical for the highly glycosylated proteoglycans (Figure 4-7H; cont). In samples treated with enzyme, the agrin immunoreactivity appeared as a relatively narrow band at 200kD, the predicted molecular weight of the agrin core protein (Figure 4-7H; -HS). When blots with the same samples were labeled for laminin, the same prominent 200kD band of laminin γ 1 appeared in the control and the enzyme-treated samples. The data combined demonstrate that the heparitinase/chondroitinase treatment leads to the removal of the GAG side chains from the BM proteoglycans, but does not lead to a generic proteolysis of BM proteins.

4.4 DISCUSSION

4.4.1 Age dependant changes in the ILM histology

The ILM from fetal human eyes is a 70nm thick, sub-structured ECM sheet that resembles a standard BM. As shown by immunocytochemistry, the fetal human ILM is comprised of laminin 1, collagen IV, nidogen 1, perlecan, agrin and collagen XVIII [58, 59, 100], the typical proteins that are found in other BMs as well [2, 3]. A recent mass spectrometry analysis of the ILM from chick embryos showed that the ILM consists of 26 proteins and polypeptides with a multitude of laminin, nidogen and collagen IV family members [37]. Further, semi-quantitative measurements showed that laminins and nidogens are the dominant components of the embryonic chick ILM, whereas collagen IVs is only a minor constituent [37]. A similar extended list of proteins and a similar stoichiometry of ILM constituents as in chick has also to be expected for the fetal human ILM. The adult human ILM is structurally very different from the fetal ILM: it is much thicker than the fetal ILM and no longer sub-structured with a central lamina densa. Rather, the adult human ILM is an amorphous and irregular layer of ECM with long intrusions into the retinal tissue [106-108]. The thickness and the extensions of the ILM increase in size with advancing age, both of which were reliable indicators to estimate the age of the donor eye.

The current data are consistent with earlier publications showing that the humans and monkeys ILMs increase in thickness with advancing age [106-108]. The enlarged and irregular structure of the ILM as seen in older humans and monkeys is not detectable in the eyes of the relatively short-lived mice, rats and rabbits demonstrating that it takes decades of life for the thickening and the indentation of the ILM to become apparent.

Earlier studies in chick and mice have demonstrated that the dominant sites for the intraocular synthesis of ILM proteins are the lens, the ciliary body and the intraocular vasculature [81-84]. Except for agrin, the retina does not contribute in the synthesis of ILM proteins in chick; rather, the retina provides the cellular binding proteins for ILM assembly [31, 86]. The in situ hybridization data for the fetal human eyes indicated a similar situation in the human eyes. The finding of high concentration of all ILM proteins in the vitreous is consistent with the extra-retinal synthesis of ILM proteins. This and previous studies have demonstrated that the concentration of ILM proteins in the vitreous is very high during embryogenesis and very low in the adult. The previous, more detailed time course study in chick and human eyes demonstrated that the ILM protein concentrations in the vitreous sharply decline after hatching in chick and within 2 years after birth in humans [59, 100]. The data combined indicate that the ILM in the chick and human eyes is assembled during embryonic, fetal and early post-natal life with very little turnover in the adult. Yet, the continuous increase in ILM thickness indicates that a slow-rate of ILM protein synthesis does occur in the adult human eye. We speculate that proteins already assembled into BMs have a very long half-life and that the continued growth in ILM thickness is both due to a slow rate of ILM protein synthesis and an even slower decay of the existing BM constituents. Indeed, the turnover of some collagens in vitreous and cartilage have been determined between 11 and 100 years [109-112]. We also speculate that the early down-regulation of the ILM synthesis is necessary, since a high rate of synthesis of ILM proteins throughout life with a slow degradation rate would eventually lead to a very thick extracellular matrix sheet that would interfere with the transparency of the eye. It is of note that soluble proteins in the vitreous, such as transferrin and α_2 macroglobulin that are also synthesized by the ciliary body [96, 97] are not down-regulated in the adult eye, thus, it appears

that only the slowly metabolized ECM proteins of the eye have a developmentally regulated synthesis.

There are no data of the abundance of laminin and collagen IV in the fetal human eye, but extrapolating from the chick embryonic ILM, where laminin and nidogens are the dominant proteins and collagen IV is only a minor component, we expect a similar composition for the fetal human ILM. Since the adult human ILM consists of over 50% of collagen IV it appears that the human ILM undergoes a compositional change from a laminin to a collagen IV dominated BM. We also propose that the shift in the composition of the ILM is due to the fact that the protease-resistant collagens have a much slower turnover rate than the proteinase-sensitive laminins and nidogens.

4.4.2 Age dependant changes in the biophysical properties of the human ILM

Probing the adult human ILM by AFM we found that the native ILM is much thicker than previously measured by TEM. Sample preparation for TEM requires dehydration which leads to tissue shrinkage. Shrinkage due to dehydration is for average tissues in the range between 10-20% and does not explain the 30-50% shrinkage that we observed for the ILM. Our AFM thickness measurements indicated that BMs contain a much greater amount of water than other tissues and that the water in BMs is tightly bound by some of the ILM constituents. The GAG chains of cartilage proteoglycans are well known to bind large quantities of water and determine the elastic qualities of cartilage. They are, therefore, the prime candidates for the water binding constituents in BMs. Indeed, the ILM underwent a major contraction that was accompanied by an increase in the stiffness when the GAG chains were enzymatically removed. The data are in perfect agreement with studies in embryonic chick ILM, where the removal of the GAG side

chains by heparitinase/chondroitinase leads to a 50% reduction in ILM thickness and a four-fold increase in ILM stiffness [37]. In the chick study, we showed that the heparitinase/chondroitinase did not solubilize ILM proteins and did not change the ultrastructure of the ILM as seen by TEM. Further, consistent with the data for human ILM, the glycosidases removed the GAG side chains but did not lead to a generic proteolysis of BM proteins. Based on these findings, we propose that the proteoglycans in BMs are essential for the hydration status of BM and thereby determine BM swelling, thickness and elasticity. The data also demonstrate that water is the most prominent component of BMs. Our finding that the adult human ILM loses elasticity with age and the finding that the shrinkage of the ILM after GAG removal is less at older age indicates that the water content of the aged BM is less than in younger ILMs, possibly due to a reduced concentration of proteoglycans or fewer or shortened GAG side chains in older BMs. The reduced elasticity with age would indicate that older BMs are more brittle and may break easier due to loss of elasticity.

4.5 CONCLUSION

In our study, we investigated age-related changes to the structure, composition, and biophysical properties of basement membranes. Analysis of the human fetal eye demonstrated that ILM proteins are secreted by the epithelium of the lens capsule and the hyaloids vasculature of the eye into the vitreous, and did not originate in the retina. Western blots, showed that these BM proteins were present in the vitreous of human fetal eyes, but not (or in very small quantities) in the vitreous of adult eyes. This suggests that the ILM is primarily formed early during early developmental stages. TEM images however demonstrated that the human ILM

does not remain the same throughout a person's lifespan. The thickness of the ILM was shown to not only dramatically increase in thickness, but also at later ages develops a much more irregular structure, protruding into the retina. This indicates that while primary ILM synthesis occurs during early development, there is some slow synthesis of BM proteins which occurs during a person's lifespan. We demonstrated that adult human ILM is constituted of over 50% collagen IV, which means the ILM composition probably shifts from a laminin dominant composition to a collagen IV dominant one during aging. This may be due to slow protein synthesis of collagen IV with an even slower degradation rate.

We successfully isolated and studied the biophysical changes in the human ILM using atomic force microscopy under physiological conditions. Results again demonstrated that there was an increase in the thickness of the adult human ILM, as also seen in the TEM images. Once again, the ILM was significantly thicker when studied by AFM due to the ILM being fully hydrated. There was also an increase in the apparent Young's modulus of the human ILM during aging. This increase in elasticity is possibly due to the shift in protein composition of the ILM during aging to a collagen IV dominated structure. In real terms the ILM becomes stiffer, or less elastic. This may have biological implications into problems primarily thought to be associated only with thickening of BMs. Removal of GAG side chains by enzymatic degradation once again showed the functional importance of PGs in human BM. We successfully demonstrated that the enzymatic process only removed the GAG side chains of the HSPGs, leaving the protein core in tact. AFM was then used to investigate the biophysical changes in the treated ILM. There was a decrease in ILM thickness and increase in IM elasticity associated with the removal of the GAG side chains, and resulting decrease in its ability to sequester water.

In addition to providing the first insight into the composition, structure, and biophysical properties of basement membranes during aging, this study provides a baseline for studying BM changes associated with biological complications, such as BM role in the pathogenesis of diabetes in the glomerular BM of the kidneys.

5.0 BIOMECHANICAL CHANGES IN BASEMENT MEMBRANES FOR “POMGNT1” AND “LARGE” KNOCKOUT MOUSE MODEL

5.1 INTRODUCTION

5.1.1 Muscular dystrophy relating to basement membranes

Muscular dystrophy (MD) is a collection of genetic disorders that amongst other complications involve the progressive weakening of skeletal muscle, defects in muscle proteins, and decay of muscle cells and tissue. MD problems are associated with a variety of locations in the body such as the skeletal muscle, heart, nervous system, eyes, and other organs[113]. While there are specific diseases that are always recognized as MD (Congenital, Duchennes, Becker’s Limb-girdle, etc), there are many more diseases that also contain MD associated complications[114]. For the purposes of this preliminary investigation, the focus will be on the forms of MD that are related to complications of the laminin/dystroglycan-associated-proteins necessary for the proper development and attachment of BMs to their related endothelium.

These include Duchenne’s MD, which is the most common form of MD, affecting males during childhood development leaving most unable to walk by age 12. This type of MD is linked to a mutation in the gene encoding the protein dystrophin, which provides stability to the dystroglycan complex (see below). This cell membrane-related protein complex is involved in

attachment of the cells to the surrounding BM and ECM. Becker's MD is a less severe form related to DMD, as it is characterized by the production of a truncated form of dystrophin[113].

Congenital MD refers to MDs that are present at birth and progress during a person's lifespan. Some forms of CMD affect the genes that code for structural proteins of the BM, such as Laminin- α 2-deficient CMD[113]. Other forms of CMD have mutations in the genes that encode the glycotransferases that are responsible for the glycosylation of dystroglycan. These include Walker-Warburg syndrome (POMT1 and POMT2)[86], Fukuyama CMD (FKTN), muscle-eye-brain disease (POMGNT1), and CMD related pachygyria (LARGE)[113]. Fundamentally, all of these CMD forms result in problems with the interaction between the laminin of the BM and their attachment site, the dystroglycan complex of the cell membrane.

5.1.2 Dystrophin associated protein complex

The dystrophin associated protein complex is a membrane-spanning group of proteins that form a bridge involved in attaching BM via laminin to the attached cell's actin/cytoskeleton network, via dystroglycan (Figure 5-1) [115]. Dystrophin is an intracellular protein which binds to actin and the dystroglycan β subunit. Dystroglycan, a glycoprotein consisting of 2 subunits, bridges the intracellular dystrophin to the proteins of the extracellular matrix. The β subunit of dystroglycan is the transmembrane portion of the dystroglycan complex that binds to dystrophin. The α subunit of dystroglycan forms an attachment to the laminin α chain of the BM[116]. Glycosylation of dystroglycan is dependant on glycotransferases to covalently bind the sugar chains to form a functioning dystroglycan complex [117, 118]. POMGnT1 and LARGE are two such glycotransferases that are part of the pathway leading to sugars being added to

dystroglycan. Failure to properly glycosylate the dystroglycan alpha chain results in incomplete BM formation.

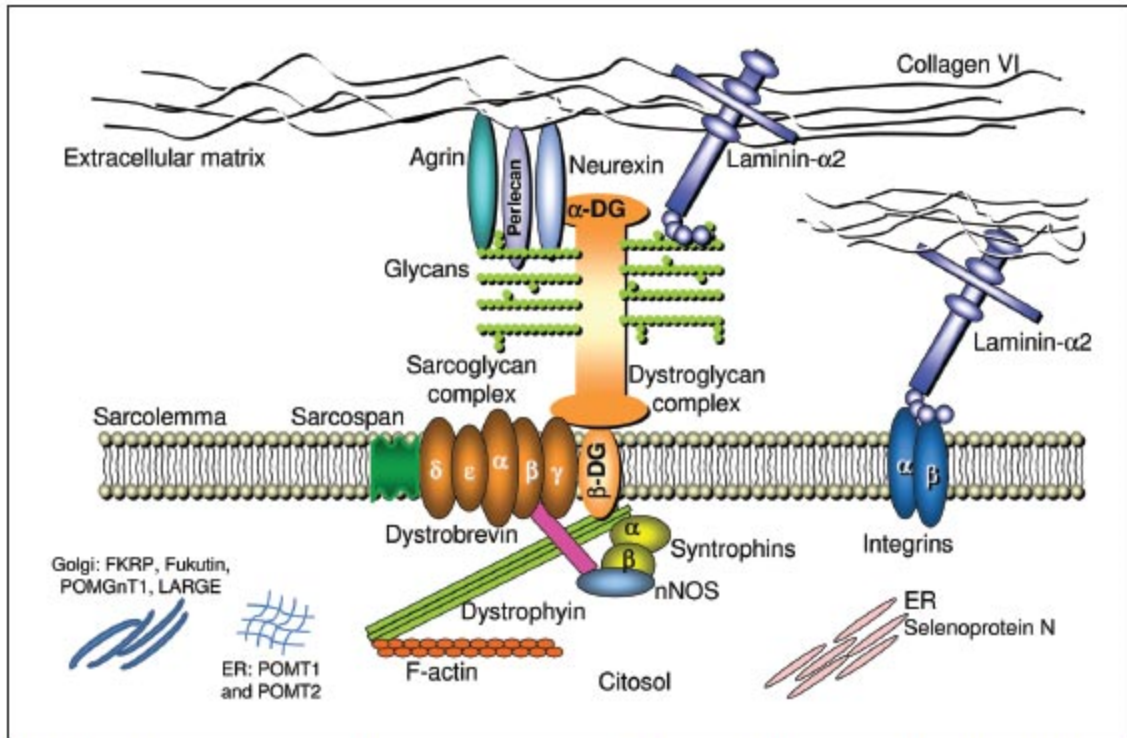


Figure 5-1 Dystrophin associated protein complex [115].

5.2 METHODS

5.2.1 AFM elasticity and thickness measurements

Flat mount P2 mouse ILM wildtype, LARGE knockout, and POMGnT1 knockout samples were provided by Dr. Huaiyu Hu (Upstate Medical University, Dept of Neuroscience and Physiology). All AFM force indentation experiments were carried out as previously

described. Samples from 5 mice from each of the three groups (Wild Type, LARGE KO, POMGnT1 KO) were measured by nano-indentation with an AFM tip. The apparent Young's modulus of the tissue at each indentation point was calculated from the force-indentation curve using the Sneddon model. ILM thickness measurements ($n = 20$) were also made on all three samples.

5.3 RESULTS

5.3.1 Mouse ILM elasticity

Images taken of the flat mount preparations for both LARGE (Figure 5-3A) and POMGnT1 (Figure 5-2A) knockout models mouse ILM exhibited disruptions where retinal cells protruded into the vitreous during development. The Young's modulus of mouse postnatal day 2 ILM was measured by AFM tip indentation using pyramidal tips (see Experimental procedures). The apparent Young's moduli of ILM samples from four different eyes were each measured for wild type, POMGnT1 knockout, and LARGE knockout. On each sample, 20 elasticity measurements were made from randomly chosen points each separated by 1–5 μm . Figure 5-2D shows representative experimental curves of AFM loading force versus z-piezo position for wild type (black) and POMGnT1 knockout (red). Figure 5-3D shows representative experimental curves of AFM loading force versus z-piezo position for wild type (black) and LARGE knockout (red).

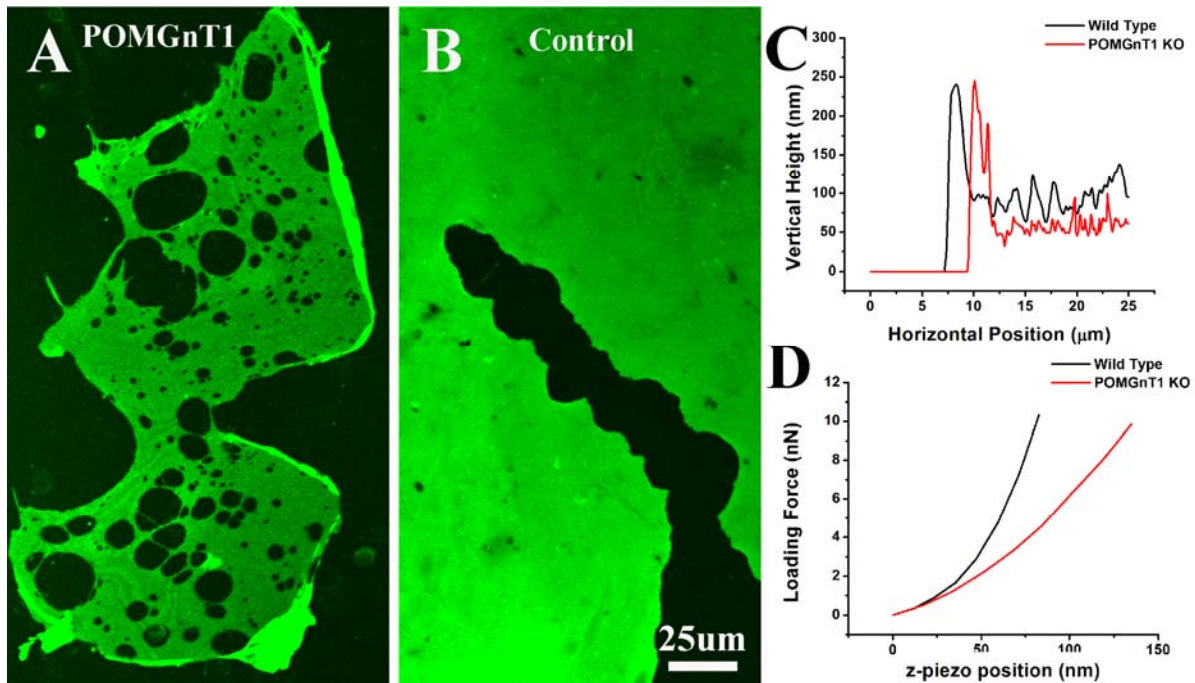


Figure 5-2: Biophysical properties of POMGnT1 knockout. Flat mount ILM samples for (A) POMGnT1 knockout mice and (B) wild type mice were compared. Visually the POMGnT1 knockout ILM had numerous disruptions where cells from the retina had broken into the vitreous during development. The wild type ILM was in tact and had no visual disruptions present (disruption in (B) is from pipette tip scratch used to expose substrate for thickness measurements). Cross section profiles (C) for the wild type (black) and POMGnT1 KO (red) were used to determine the thickness of the ILM by using the glass substrate as a zero reference point. Representative force curves (D) for wild type (black) and POMGnT1 KO (red) were used to calculate the apparent Young's modulus of elasticity. The wild type shows a steeper force-indentation curve, which relates to a higher elastic modulus.

The apparent Young's modulus for the mouse ILM of wildtype, POMGnT1, and LARGE is summarized in Table 5-1 and Figure 5-3E. The apparent Young's modulus of mouse ILM was 4.08 ± 1.19 MPa for wild type, 2.82 ± 1.22 MPa for POMGnT1 knockout and 1.68 ± 0.73 for LARGE knockout. There was a significant decrease in the ILM stiffness (Young's modulus) between the wild type and both knockout models ($P < 0.05$).

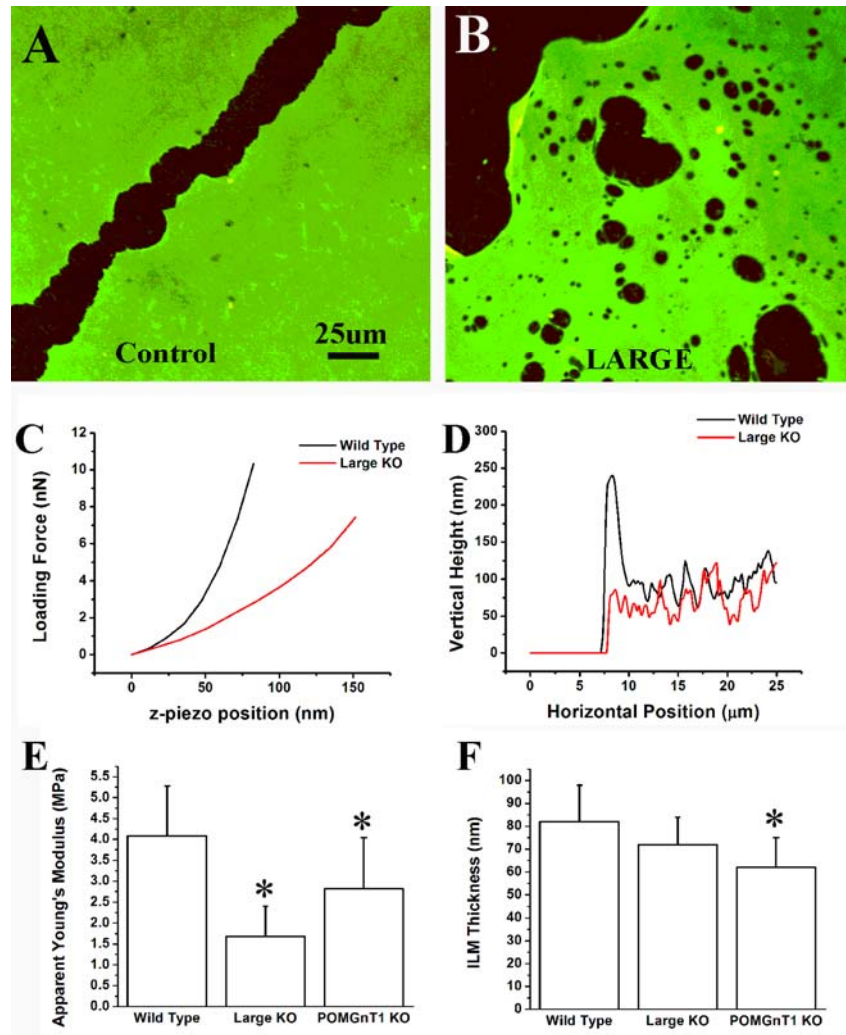


Figure 5-3: Biophysical properties of LARGE knockout. Flat mount ILM samples for (A) wild type mice were compared and (B) LARGE knockout mice. Visually the LARGE knockout ILM had disruptions where cells from the retina had broken into the vitreous during development. The wild type ILM was in tact and had no visual disruptions present. Representative force curves (C) for wild type (black) and LARGE KO (red) were used to calculate the apparent Young's modulus of elasticity. Cross section profiles (D) for the wild type (black) and LARGE KO (red) were used to determine the thickness of the ILM by using the glass substrate as a zero reference point. There was a significant difference in the elastic modulus (E) between the wild type and both knockout models. Only the POMGnT1 knockout ILM was significantly thinner (F) than the wild type ILM (* mark significant differences, $p < 0.05$)

Table 5-1: Elasticity of mouse ILM samples

Apparent Young's Modulus (MPa)			
Sample #	Wild Type	Large KO	POMGnT1 KO
1	4.11 ± 0.90	1.66 ± 0.56	2.83 ± 0.95
2	4.01 ± 1.02	1.90 ± 0.93	2.75 ± 1.02
3	3.76 ± 1.14	1.69 ± 0.49	3.10 ± 0.84
4	4.46 ± 1.41	1.46 ± 0.54	2.59 ± 0.79
Average of 4 Samples	4.08 ± 1.19	1.68 ± 0.73	2.82 ± 1.22

5.3.2 Mouse ILM thickness

The thickness of ILM was obtained from AFM images of the sharp edges of ILM where the underlining glass substrate was exposed. To obtain sharp ILM/ glass edges, scratches in the ILM were made using plastic pipette tips (Figure 5-2A,B and Figure 5-3A,B). Figure 5-2D shows the ILM height profile for the wild type and POMGnT1 knockout model. Figure 5-3D shows the ILM height profile for the wild type and LARGE knockout model.

The thickness of the ILM was measured from the flat segment of the height profile with the glass surface serving as the zero reference. The ILM thickness measurements were made for ILM preparations from four P2 mouse retinæ for wild type, LARGE knockout, and POMGnT1 knockout models. For each ILM, 20 height measurements were made from different crosssections. The measured thicknesses from each ILM sample are summarized in Table 5-2 and in Figure 5-3F. The thickness (mean ± SD) of the wild type was 82 ± 16 nm and the thickness of LARGE knockout mouse ILM was 73 ± 12 nm. The thickness of the POMGnT1 knockout was 62 ± 13 nm. There was a statistical difference ($p < 0.05$) between the wild type and POMGnT1 KO, but not between the wild type and LARGE KO.

Table 5-2. Knockout Mouse ILM Thickness

Thickness of ILM (nm)			
Sample #	Wild Type	Large KO	POMGnT1 KO
1	73 ± 12	71 ± 14	65 ± 8
2	81 ± 16	74 ± 11	58 ± 11
3	94 ± 15	69 ± 9	70 ± 16
4	78 ± 19	75 ± 12	56 ± 13
Average of 4 Samples	82 ± 16	73 ± 12	62 ± 13

5.4 DISCUSSION

A common phenotype of various forms of congenital muscular dystrophy is a disruption between the Laminin of the BM and the dystroglycan complex cell adhesion site. In CMD related such as Walker-Warburg Syndrome (WWS) there are a variety of cortical and ocular disruptions along with typical CMD complications, which are usually lethal [86]. Dystroglycan deletion in mice has exhibited WWS pathogenesis. While the disease pathogenesis is clinically defined by physical disruptions in ocular BMs there was no information into the biophysical differences between normal and CMD model tissues. Postnatal day 2 knockout mice models for CMD had targeted deletions of the genes encoding for LARGE and POMGnT1, two cellular glucotransferases responsible for glycosylation of the dystroglycan complex. The dystroglycan complex is a primary binding site for the laminin BM protein, and critical for proper BM development. It has been noted that in mice with a mutation of the LARGE protein saw a decrease in CMD progression by reintroducing LARGE artificially into the mice [119].

The knockout models for both mice showed visual disruptions in the ILM in P2 mice. This swiss-cheese like ILM was visually different from the in-tact smooth control ILM preparations. Investigation by AFM probing showed that while there was a minimal decrease in the thickness of the mouse ILM knockout models there was a significant decrease in the elastic modulus. This resulting decrease in elasticity may be due to downstream effects from a significant decrease in laminin attachment sites. It is postulated, that by reducing the number of laminin attachment sites, there would be a significant loss in the amount of collagen IV and general ILM structure formation. This loss of BM structural components would result in a decrease of the apparent Young's modulus and overall BM stability. This is the first investigatory study into the biophysical complications resulting from a disruption of BM's ability to form properly in CMD like knockout models.

5.5 CONCLUSION

This is the initial study into the biophysical properties of BM that are associated with complications of congenital muscular dystrophy "like" phenotypes. Mouse postnatal day 2 ILM samples from wild type, LARGE knockout, and POMGnT1 knockout models were indented by AFM to determine the apparent Young's modulus. Also AFM thickness measurements were taken for each group. With the knockout of genes encoding the glucotransferases necessary for proper interaction between the proteins of the BM and the associated cell layer, there was a decrease in the apparent Young's modulus of the knockout mouse ILM. This is probably due to the decrease in laminin molecule attachment sites that are important for initializing proper BM formation. Surprisingly there was not as noticeable a decrease in the thickness of the ILM in

knockout models. With this being an initial investigatory study into the biophysical properties of CMD model basement membranes, future work would entail comparing these biophysical results to a deeper study of the histology to determine a possible difference in ILM protein composition or laminin binding efficiency to the cells of the retina.

6.0 OVERALL CONCLUSIONS AND FUTURE DIRECTIONS

6.1 OVERALL CONCLUSIONS

The overall goals of this study were to first develop methods to study the biophysical and biomechanical properties of basement membranes and investigate changes in BM composition, structure, and biophysical properties due to a variety of biological conditions. We investigate the BM properties over a complete timeline, from the importance of the initial laminin binding to the cell surface receptor (chapter 5), through embryonic development (chapter 2), and changes that occur during aging (chapter 4) that may have implications in a variety of biological complications. The two fundamental obstacles were finding an adequate sample that could be isolated from surrounding tissues and applying AFM techniques to obtain measurements for BM elasticity and thickness.

The study presented in Chapter 2 had a primary focus of investigating the inner limiting membrane as a model for studying basement membranes. The ILM proved to be isolatable, contained typical ultrastructure and BM protein composition, and its biophysical properties were able to be measured via atomic force microscopy techniques. In addition, the importance of mechanical stability of the ILM was demonstrated during embryonic development as mutations in the ILM resulted in ectopic retinal cells in the vitreous cavity. There is a possibility that the breach of the mutant ILM might be due to simply malformed ILM and not a physical weakening,

however BM blood vessel rupture in the eye during embryonic periods of increasing blood pressure infer that the failure of improperly formed BM are a result of a weakening of BM structural integrity, and not just improper protein structure. This study also demonstrated that the thickness and elasticity of the ILM increase during early embryonic development (E4 to E9), but does not increase further during later stages of development (E9 to E15). It is conceivable that a thinner, more elastic BM during early embryonic development is advantageous during the periods of rapid embryonic expansion, but during late stage development, when more stable and defined tissue border and organ formation is necessary, a thicker and stiffer BM is more suitable. Of particular interest in this study, is that the thickness of the ILM was, to our surprise, much thicker than the “textbook” values we expected. We determined that this 87% decrease in thickness seen via electron microscopy was due to the fixation and dehydration steps necessary for standard EM protocol. This high water content seemed to make sense, as three major components of basement membranes are heavily hydrated proteoglycans, but further experiments were required to confirm this hypothesis.

The idea that the ILM is hydrated like a sponge by the water-binding proteoglycans was further investigated in chapter 3 of the project. It has been demonstrated in other extra-cellular matrices, such as cartilage, that the “swell” of water in the tissue directly contributes to the biomechanical properties of the material. Based on this knowledge, we tested whether the hydration of basement membranes is similarly tied to the heparan sulfate proteoglycans, and further that the HSPG role in hydrating the BM directly affects the overall biophysical properties of the BM. We removed the heparan sulfate GAG side chains from chick and human ILMs by enzymatic degradation using heparitinase and chondroitinase. The enzymes cleave the HS side chains into smaller carbohydrate segments that are no longer associated with the BM and that are

no longer osmotically active. Electron microscopy and western blotting showed that the enzyme treatment did not change either the ultrastructure or the protein composition of the ILMs. Utilizing previously established AFM techniques there was noted both a 55% decrease in the thickness of the ILM, and an 80% increase in the stiffness. The maximum indentation depth was kept at less than 10% of the total sample thickness to avoid artifact from the hard glass support of the BMs. This and the finding that we found increases in elasticity coinciding with increases in thickness and vice versa means that thickness and elasticity changes are a result of changes in the BM composition or structure, in this case removal of GAG side chains from BM proteoglycans, and not artifacts resulting from the underlying hard glass surface. We propose that when the ILM loses bound water after GAG removal, the same protein fibers take up a smaller space, the BM sponge collapses to a smaller volume. In this scenario the higher density of fibers within the BM would lead to a higher resistive force against the indenting AFM cantilever. It was also noted that while there was a large reduction of thickness in the GAG removed ILM, we still did not reach 87% reduction in thickness found by EM protocol dehydration. This would infer that either there is some transient amounts of fluid retained in the membrane unrelated to GAG side chains, or that the enzymatic treatment broke up most, but not all of the proteoglycan side chains. Our results demonstrate that proteoglycans do play a previously unknown role in the structure and biophysical properties of basement membranes, and we propose that mutation or degradation of the BM PG would result in biophysical changes in the basement membrane.

Earlier it was demonstrated that changes in the ILM protein structure during development are related to biophysical changes. In chapter 4 we investigated changes in BM properties further along the BM timeline, adult aging. Biologically speaking, changes in various BM have been associated with the pathogenesis of many biological abnormalities. BM thickening has

been associated with degeneration and loss of function in cerebral microvessels, strial vessels of the inner ear, seminiferous tubules of the testes, and in kidney tubules [38-41]. The thickening in these cases was associated to an age-related increase in the associated BM thickness, and in some cases a coinciding increase in collagen IV. By electron microscopy it was apparent that in the adult human ILM there was also an age-related increase in the thickness, as well as a change in the morphology as the ILM became much more irregular, protruding into the retina. While these associated problems may be due to thickening of the basement membranes, there may also be additional factors, such as changes in the elastic properties of the basement membranes with aging. By utilizing AFM techniques we found both an age-related increase in the thickness and elasticity of the ILM in adult human samples. The thickness increased from $\sim 1.7 \mu\text{m}$ in a 44 year old to $\sim 3.5 \mu\text{m}$ for an 88 year-old ILM and was proportional to the increase found in the dehydrated TEM samples. There was also a coinciding increase in the stiffness of the adult human ILM from $\sim 1.5 \text{ MPa}$ in a 44 year old to $\sim 4.0 \text{ MPa}$ in an 88 year old. Both of these phenomena would be explained by a slow accumulation of collagen IV during aging, shifting the protein composition from a laminin dominated to a collagen IV dominated protein structure. There is some evidence to support this idea, as ILM from embryonic chick ILM have been heavily laminin dominant with only $\sim 3\%$ collagen IV, and adult human ILM are approximately 60% collagen IV. The resulting degeneration and loss of function of microvessels and tubules may be related to this previously unknown age-related change in BM biomechanics in addition to the previously known age-related thickening and compositional change. The surrounding BM are both growing thicker and stiffening, which could lead to choking and improper flexibility necessary for proper function. Also the conformational changes could make it harder for nutrients and waste to be transported through the BMs. In addition we repeated the GAG-

removal experiments from chapter 3 on adult human ILM. Again we saw a decrease in the thickness and increase in the elasticity in the adult human ILM. Adult human ILM from 45 and 53 year old donors exhibited a ~50% decrease in thickness and ~ 50-60% increase in relative stiffness after removal of heparan sulfate GAG side chains. From 86 year old adult human ILM there was a 17% decrease in thickness and 19% increase in relative stiffness. The embryonic chick ILM in comparison had a 55% decrease in thickness and 80% increase in relative stiffness. With the slow accumulation of collagen IV during aging, the results may indicate that ILMs as they move towards a 60% collagen IV have less proteoglycans as a percent of total mass. This would result in less drastic changes after removal of water sequestering GAG proteoglycans side chains.

Previously discussed histological data has shown that basement membranes are not properly formed during development in eyes with mutations related to cellular BM surface receptors and laminin interaction sites. Mutations of proteins related to the dystroglycan complex and laminin binding are associated with a variety of muscular dystrophies, and without laminin binding there is improper basement membrane formation. The study in Chapter 5 investigates the malformation of basement membranes with knockouts adversely affecting the laminin binding site of the dystroglycan complex. The mouse knockout models studied were for two glucotransferases responsible for the glycosylation of the dystroglycan complex, POMGnT1 and LARGE. The BM laminin molecules bind to the carbohydrate side chain of dystroglycan, so without glycosylation there is no laminin binding. The biophysical properties of mutant mouse ILM were investigated by AFM on postnatal day two. Visually the ILM was greatly disrupted for both POMGnT1 and LARGE knockout models, while the control, or wild type, ILM were smooth and continuous. These disruptions were locations where ectopic retinal cells broke

through the ILM during embryonic development. We saw a coinciding decrease in the elasticity of the ILM in the knockout models. This may be due to inability of the BM proteins to properly interact due to the lack of cell surface attachment sites. Interestingly there was not a similar large decrease in the thickness of the ILM. The inability of the mutant ILM to form properly is directly associated to the laminin molecule to initially bind to the cell surface via glycosylated dystroglycan, a necessary first step for BM formation. While there are other cell surface receptors, such as integrins, that bind laminin, the dystroglycan complex/laminin interaction may form a tighter or stronger BM/cell layer bond. Without this interaction the ILM forms 'looser' and lacks the structural strength necessary for proper physiological function. This study provides initial insight in to the changes in the biomechanics of the ILM due to improper laminin/cell surface receptor interactions that would have implications into the stability and proper functioning of BMs in a congenital muscular dystrophy like model.

The major findings presented tell a linear story relating the protein composition and biophysical properties of the inner limiting membrane, a model for studying BMs. This timeline begins during embryonic development where the ILM is a laminin dominated BM. During early embryonic development the ILM increases in both thickness and stiffness. In addition, it was demonstrated that for proper formation of ILM during embryonic development that properly functioning laminin/cell surface receptor interaction is necessary. During aging there is a compositional shift that takes place to a collagen IV dominant protein composition. While the ILM thickness increases steadily until around 40-50 years old in adult human samples, there is a coinciding increase in the elasticity of the ILM. Later in aging there is an irregular thickening of the BM associated with a stiffer ILM. The thickening of BMs has been associated with the pathogenesis of a variety of biological complications, and the increase in the stiffness of BM

may also play an important role. In addition to the timeline of ILM development the function of a prominent BM component, BM proteoglycans was demonstrated. The PGs are responsible for ‘swelling’ of BM by sequestering water via GAG side chains. This results in a much thicker and more robust BM than previously thought. These results are the first in depth study of the biophysical properties of a BM under physiological conditions.

6.2 FUTURE DIRECTIONS

This study provided insight into the previously unstudied biophysical properties of basement membranes through the ability to isolate and study the inner limiting membrane. This provided a fundamental understanding of changes that occur in the ILM under a variety of biological circumstance. These provide a baseline for future investigations into other biologically significant perturbations.

Future studies can be grouped into two areas: (1) how can we apply other methods to further reinforce our results and (2) now that we have set a baseline for BM study, what can we apply this to? An example of the first area is a possible method to investigate the thickness of thin delicate membranes, elipsometry. To further investigate the effects of dehydration of on BM properties, measurements could be taken on a BM in solutions of varying level of salt concentrations. This would swell or dehydrate the sample at varying degrees, instead of the massive loss of water thought to occur with total GAG side chain removal. While our technique for studying the biomechanics of BM relies on direct vertical indentation of a flat mount ILM gives an indication of changes due to protein structure and composition, developing a method to study the elastic properties parallel to the fiber mesh would be useful. One possible method

would be to flat mount the BM over a small circular hole and ‘stretch’ the sample using a larger spherical indenter, much like a drum head.

We looked at the ILM after mutations of the cell-surface receptor responsible for laminin binding, but it would be advantageous to look at the biophysical changes related to mutations of the major BM protein components to determine which are most likely to adversely effect the BM, information that could be important to a variety of abnormalities, such as laminin deficient muscular dystrophy. With the baseline and techniques to study BM established, it would be advantageous to attempt to isolate other BMs. Isolating the Bruch’s membrane (Appendix B) for example would be important for studying the pathology of exudative age-related macular degeneration. Also, with a baseline established for BM biophysiology the pathology for BM related forms of diabetes could be studied. By establishing the AFM techniques used for studying such thin structures a variety of possible avenues for future work are possible.

APPENDIX A

DERIVATION OF THE 2-PARAMETER FIT EQUATION USED FOR DETERMINING THE YOUNG'S MODULUS OF ELASTICITY

The Sneddon Model for a conical indenter is applied to calculate the elastic modulus of a sample indented by a sharp AFM tip. The Sneddon Model states that the force is a function of indentation.

$$F = E^* (2 \cdot \tan(\alpha) \delta^2) / \pi$$

Where F represents the force applied to the tissue from the cantilever tip, α is the half angle of the cantilever tip, δ is the indentation of the sample, and E^* is the modulus of elasticity. For the gathered indentation curves known parameters of this method are the applied force and the half angle of the cantilever's tip. We assume that the total deflection of the system is equal to the deflection of the cantilever and the deflection of the tissue. The total deflection (δ) can be found from the following expression:

$$(z - z_0) = \delta + d$$

Where z_0 is the point of indentation and z is the total deflection. By isolating only the sample indentation we now have the sample deflection for an applied force.

it can further be shown that F is related to indentation by a simple approximation of a quadratic equation.

$$F = a * \delta^2$$

Where

$$a = \left(\frac{2 \tan \alpha}{\pi}\right) E^*$$

Also Hooke's law states that:

$$F = kd$$

Where k is the spring constant of the AFM cantilever.

By incorporating Hooke's law and the deflection relation into the Sneddon equation and solving for the Force (F) applied by the AFM cantilever to cause the indentation of the sample we find the following fit equation.

$$F = k * (z - z_0) + \frac{k^2}{2a} - \sqrt{\left(\frac{k^4}{4a^2} + k^3 * \frac{(z - z_0)}{a}\right)} + F_0$$

The initial force (F_0) and point of indentation (z_0) are inputs into the fitting equation and we solve for the 'a' variable. This variable is directly proportional to the apparent Young's modulus of the sample. The 2-parameter fit equation is used for high throughput processing of force curves using IgorPro (Wavemetrics).

APPENDIX B

INVESTIGATION INTO THE BIOMECHANICAL PROPERTIES OF THE BRUCH'S MEMBRANE

B.1 INTRODUCTION

This study provides initial results into investigating the biomechanical properties of the Bruch's membrane (BrM). Fundamental difficulties arose from a difficulty in properly isolating the membrane without altering the biomechanical properties through fixation. Trauma from cryosectioning of unfixed samples produced a broken and disrupted BrM region due to the thickness of surrounding tissues of the eye capsule. The BrM is also not easily from the surrounding extracellular matrix of the choriocapillaris. The following is a summary of results from initial experiments.

Age-related macular degeneration (AMD) is a major cause of vision loss in the developed world; it affects greater than 11 million people in the United States [120, 121]. AMD exists in two distinct forms: dry and wet. While the wet (exudative) form makes up only 15% of AMD cases, it is characterized by a more rapid and severe vision loss. New blood vessels from the choroids breach the Bruch's membrane and grow into the subretinal space causing an accumulation of blood beneath the retinal pigment epithelium (RPE), the detachment of the RPE

and the formation of disciform scars[122, 123]. It is assumed that a structural breach of the Bruch's membrane is a prerequisite for the development of this choroidal neovascularization. Extending from the optic nerve to the ora serrata, Bruch's membrane is located between the choroid/choriocapillaris and the RPE/photoreceptors[124]. The choriocapillaris provides nutrients to the RPE layer. During aging, there is a significant amount of remodeling of the structure and chemical composition of the BM, such as an increase in membrane thickness by 100% or more over a person's lifetime; debris (lipids, cholesterol, drusen) deposition and calcification within the elastic membrane are also common[125-131]. This suggests alterations in extra cellular matrix, such as the elastic fiber network in the Bruch's membrane, could be a major factor in the development of AMD. This is supported by studies in the histology of the Bruch's membrane in patients with AMD. The integrity of the BM elastin layer was much weaker in patients with AMD or active choroidal neovascularization[132]. There is also a link between ruptures in the BM and CNV shown through clinical studies [133, 134].

Critically located between the RPE/photoreceptors and their nutrient source, the choriocapillaris, the Bruch's membrane is composed of 5 distinct layers: (1) the basal lamina of the RPE, (2) the inner collagenous sublayer, (3) the central elastin sublayer, (4) the outer collagenous sublayer, and (5) the basal lamina of the choriocapillaris. Approximately 90% of Bruch's membrane consists of the elastin and inner and outer collagenous layers, and its thickness varies with age and location. Nutrients are continuously transported across Bruch's membrane from the choroidal blood supply to the metabolically active photoreceptors via the RPE. Also the RPE actively transports ions, metabolites, and fluid from the subretinal space to the choriocapillaris via Bruch's membrane [135, 136]. Also for the renewal of photoreceptors, old photoreceptor disk membranes are shed and phagocytized from the RPE, with waste being

transported through the BrM [137]. Structural changes and degeneration of the BrM would have significant impact of traffic related to photoreceptor function.

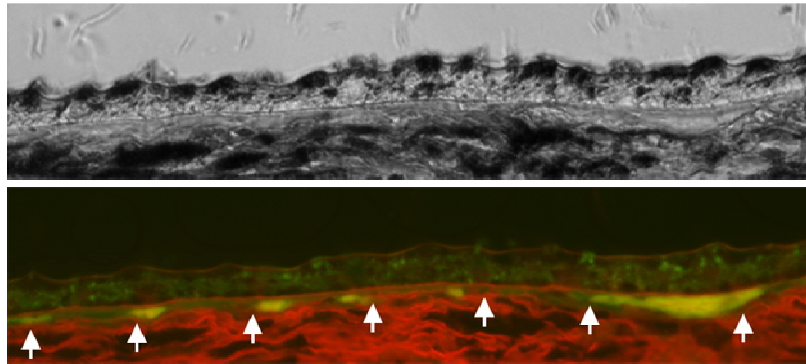
Changes in the ultrastructure of the BrM during aging have been noted: the BrM approximately doubles in thickness over a person's lifespan [125, 126]. In the macular region this thickening initially occurs in the inner layers of the BrM, on the RPE side[128]. Contributing factors to membrane thickening are (1) deposition of materials (mostly cellular waste) within the BrM[130]; and (2) an increase in collagen content in the BrM. Evidence that the BrM also undergoes significant remodeling over time was demonstrated by showing that BrM solubility membrane collagen is reduced by 50% over a 90 year lifespan[138], which is likely due to progressive cross-linking of collagen, reducing the elasticity and increasing the stiffness of the BrM.

The relationship between the structural changes in the Bruch's membrane and the initiation of CNV necessary for AMD is not well defined. For CNV to develop angiogenic twigs and the neovascularization must somehow penetrate the BrM. The mechanical properties of the BrM can have implications for CNV. The elastin layer is the predominant determinant of BrM elasticity, and in addition to increased cross lining of collagen molecules, an increased calcification is seen in the elastin layer [139, 140]. There has also been a strong correlation between the degree of calcification and fragmentation of BrM and development of exudative AMD compared with nonexudative AMD [141].

B.2 PRELIMINARY FINDINGS

Histology of the Bruch's membrane

In our preliminary study we have examined the structure and elasticity of the porcine Bruch's membrane and its sublayers. Porcine eyes were used due to their similar size and structure to human eyes. The thickness of the porcine Bruch's membrane is approximately 2 μm , similar to that of a young person.

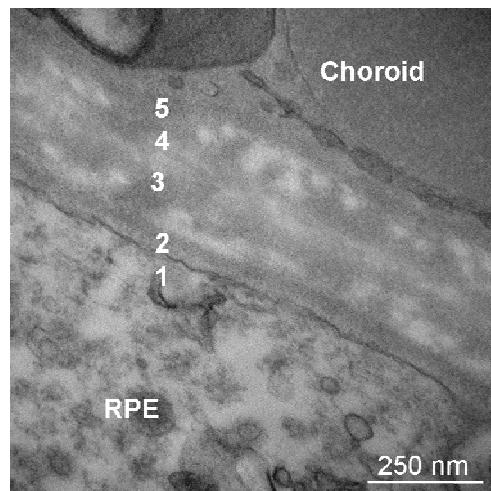


Appendix Figure B-1: Bright field light microscopy (top panel) and fluorescence image of porcine RPE/Bruch's membrane/choroid (bottom panel). Samples were stained with 0.1% Direct Red 80 (Sirius stain) with 1% picric acid (picrosirius). Collagen fibers showed the characteristic fluorescence of red-orange. Elastin fibers showed intrinsic green fluorescence (arrows).

The structure of the Bruch's membrane was analyzed using optical microscopy, along with scanning and transmission electron microscopy (SEM and TEM). Samples were both cryosectioned and paraffin sectioned for optical microscopic analysis. Figure B-1 shows an optical microscopy image of the porcine RPE/BrM/choroidal structures in the posterior region of the eye. For this experiment, 5 μm thick paraffin sections were stained with 0.1% Direct Red 80 dye (Sirius stain) in 1% picric acid (picrosirius). Collagen fibers interact strongly with the Sirius-red dye and show the characteristic red-orange fluorescence. Elastin fibers show strong

green fluorescence (arrows) [142]. A continuous layer of elastin fibers can be seen throughout the BrM in the porcine eye. The distribution of the elastin is not even as there are regions of the BrM that exhibit higher thickness of the elastin fibers. The varied elastin density could be due to the changes in the BM thickness, which varies significantly.

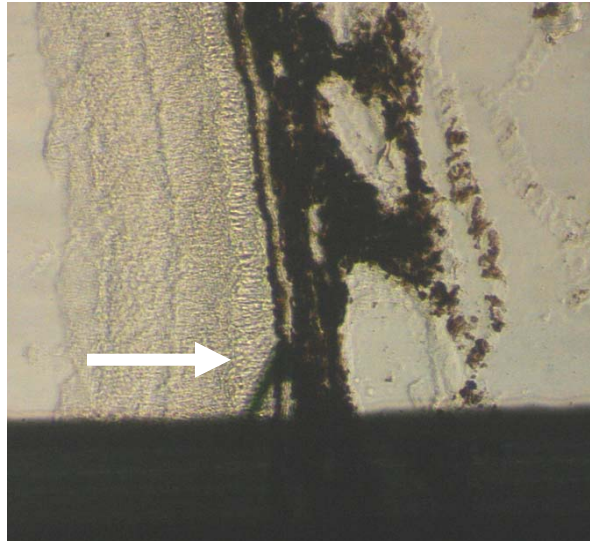
The fine structure of the BrM morphology was also studied at higher resolution using electron microscopy. A TEM image (Figure B-2) of a porcine BrM cross section (1 μ m thick) shows the five sublayers of the Bruch's membrane: basal lamina of the RPE (1), inner collagenous layer (2), elastin layer (3), outer collagenous layer (4), and the basal membrane of the choriocapillaris (5). The elastin and two collagenous layers form the majority of the Bruch's membrane.



Appendix Figure B-2: Transmission electron micrograph (TEM) of porcine Bruch's membrane cross-section. The sublayers of the Bruch's membrane: 1) RPE basal lamina, 2) inner collagenous layer, 3) elastin layer, 4) outer collagenous layer, and 5) basal membrane of the choriocapillaris.

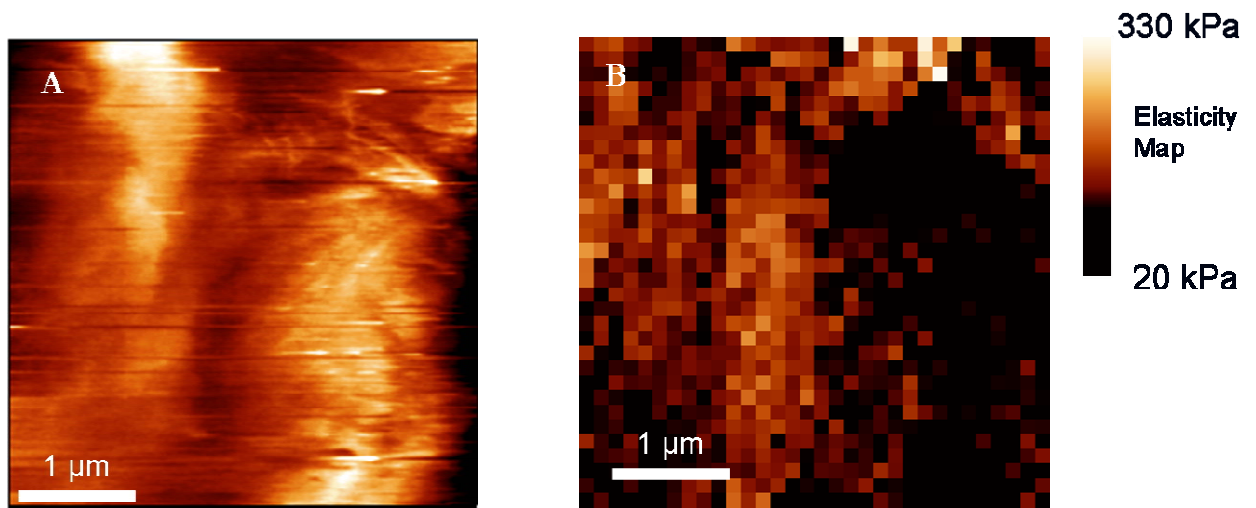
Imaging and Elasticity Measurements of Porcine Bruch's Membrane Using Atomic Force Microscopy:

Atomic force microscopy and light microscopy were used to image unfixed cryosections of porcine Bruch's membrane. The retina/BrM/choroids were cryo-sectioned at 20C and stored at -80C on glass slides. The tissue sections were thawed in PBS at room temperature before testing. The imaging and elasticity measurements were done at room temperature and in PBS. Cryosections were made at thicknesses of 5 μm to 100 μm , with thicknesses of 10-20 μm providing the best results. Figure B-3 shows a bright field image of the RPE/BrM/choroid region underneath the AFM tip. The AFM is mounted on an inverted Olympus IX-71 optical microscope, which allows for us to visually place the AFM tip in the region containing the Bruch's membrane.



Appendix Figure B-3: Optical microscopy image of the porcine retina/Bruch's membrane/choroid tissue section. The retina is on the left side of the image and the choroid is on the right. The AFM tip (arrow), at the apex of the triangular cantilever is positioned near the Bruch's membrane.

AFM images were first taken of the region thought to contain the BrM. Smaller regions were zoomed in on as we located the regions believed to be the BrM. Figure B-4A shows a height image of the BrM with a $4\ \mu\text{m} \times 4\ \mu\text{m}$ window size. Brighter colors represent areas of greater height. The Young's modulus at each point was calculated from an AFM indentation curve taken at that location, and the resulting elasticity map (128×128 points) is shown in Figure B-4B. One caveat to keep in mind is that the topographic image gives the contour of the surface only; artifacts in the sectioning, for example, may make it difficult to visualize the BrM in all cases. The measured Young's modulus of the porcine Bruch's membrane is approximately 200-300kPa. The central elastin layer is once again seen to be significantly softer than the out regions that contain a high density of collagen fibers.



Appendix Figure B-4: Height mode (topography) afm image (A) and elasticity map (B) of the Bruch's membrane. The image sizes are $4\ \mu\text{m} \times 4\ \mu\text{m}$ and the resolution of the elasticity modulus (Young's modulus) measurements is 32×32 pixels. Each pixel in (B) represents an area of $\sim 100\ \text{nm} \times 100\ \text{nm}$.

These experiments demonstrate our ability to map the elastic properties and image the BrM using atomic force microscopy. The resolution of the maps can be improved by taking more sampling points over the same area. We can gather elasticity maps of the BrM with a

spatial resolution of approximately 20 nm by 20 nm per pixel. This study is an example of one of the avenues of investigation available. The biomechanical properties of the Bruch's membrane are directly related to the disease pathogenesis of exudative age related macular degeneration. Once the fundamental difficulty in isolating the BrM is overcome; changes in the biophysical properties may be determined to be a major causation of the disease progression.

BIBLIOGRAPHY

1. Yurchenco, P.D. and J.J. O'Rear, *Basal lamina assembly*. Curr Opin Cell Biol, 1994. **6**(5): p. 674-81.
2. Timpl, R. and J.C. Brown, *Supramolecular assembly of basement membranes*. Bioessays, 1996. **18**(2): p. 123-32.
3. Erickson, A.C. and J.R. Couchman, *Still more complexity in mammalian basement membranes*. J Histochem Cytochem, 2000. **48**(10): p. 1291-306.
4. Halfter, W., M. Willem, and U. Mayer, *Basement membrane-dependent survival of retinal ganglion cells*. Invest Ophthalmol Vis Sci, 2005. **46**(3): p. 1000-9.
5. LeBleu, V.S., B. Macdonald, and R. Kalluri, *Structure and function of basement membranes*. Exp Biol Med (Maywood), 2007. **232**(9): p. 1121-9.
6. Khoshnoodi, J., V. Pedchenko, and B.G. Hudson, *Mammalian collagen IV*. Microsc Res Tech, 2008. **71**(5): p. 357-70.
7. Khoshnoodi, J., et al., *Mechanism of chain selection in the assembly of collagen IV: a prominent role for the alpha2 chain*. J Biol Chem, 2006. **281**(9): p. 6058-69.
8. Tunggal, P., et al., *Laminins: structure and genetic regulation*. Microsc Res Tech, 2000. **51**(3): p. 214-27.
9. Hallmann, R., et al., *Expression and function of laminins in the embryonic and mature vasculature*. Physiol Rev, 2005. **85**(3): p. 979-1000.
10. Miosge, N., T. Sasaki, and R. Timpl, *Evidence of nidogen-2 compensation for nidogen-1 deficiency in transgenic mice*. Matrix Biol, 2002. **21**(7): p. 611-21.
11. Kohfeldt, E., et al., *Nidogen-2: a new basement membrane protein with diverse binding properties*. J Mol Biol, 1998. **282**(1): p. 99-109.
12. Iozzo, R.V., *Basement membrane proteoglycans: from cellar to ceiling*. Nat Rev Mol Cell Biol, 2005. **6**(8): p. 646-56.

13. Poschl, E., et al., *Collagen IV is essential for basement membrane stability but dispensable for initiation of its assembly during early development*. *Development*, 2004. **131**(7): p. 1619-28.
14. Miner, J.H. and P.D. Yurchenco, *Laminin functions in tissue morphogenesis*. *Annu Rev Cell Dev Biol*, 2004. **20**: p. 255-84.
15. Miner, J.H., et al., *Compositional and structural requirements for laminin and basement membranes during mouse embryo implantation and gastrulation*. *Development*, 2004. **131**(10): p. 2247-56.
16. Chung, A.E., et al., *Biological functions of entactin*. *Kidney Int*, 1993. **43**(1): p. 13-9.
17. Kramer, J.M., *Basement membranes*. *WormBook*, 2005: p. 1-15.
18. Kalluri, R., *Basement membranes: structure, assembly and role in tumour angiogenesis*. *Nat Rev Cancer*, 2003. **3**(6): p. 422-33.
19. Miosge, N., et al., *Ultrastructural triple localization of laminin-1, nidogen-1, and collagen type IV helps elucidate basement membrane structure in vivo*. *Anat Rec*, 1999. **254**(3): p. 382-8.
20. Smyth, N., et al., *Absence of basement membranes after targeting the LAMC1 gene results in embryonic lethality due to failure of endoderm differentiation*. *J Cell Biol*, 1999. **144**(1): p. 151-60.
21. Costell, M., et al., *Perlecan maintains the integrity of cartilage and some basement membranes*. *J Cell Biol*, 1999. **147**(5): p. 1109-22.
22. Arikawa-Hirasawa, E., et al., *Perlecan is essential for cartilage and cephalic development*. *Nat Genet*, 1999. **23**(3): p. 354-8.
23. Willem, M., et al., *Specific ablation of the nidogen-binding site in the laminin gamma1 chain interferes with kidney and lung development*. *Development*, 2002. **129**(11): p. 2711-22.
24. Bader, B.L., et al., *Compound genetic ablation of nidogen 1 and 2 causes basement membrane defects and perinatal lethality in mice*. *Mol Cell Biol*, 2005. **25**(15): p. 6846-56.
25. Gautam, M., et al., *Defective neuromuscular synaptogenesis in agrin-deficient mutant mice*. *Cell*, 1996. **85**(4): p. 525-35.
26. Fukai, N., et al., *Lack of collagen XVIII/endostatin results in eye abnormalities*. *EMBO J*, 2002. **21**(7): p. 1535-44.
27. Williams, R.S., et al., *Cerebro-ocular dysgenesis (Walker-Warburg syndrome): neuropathologic and etiologic analysis*. *Neurology*, 1984. **34**(12): p. 1531-41.

28. Nakano, I., et al., *Are breaches in the glia limitans the primary cause of the micropolygyria in Fukuyama-type congenital muscular dystrophy (FCMD)? Pathological study of the cerebral cortex of an FCMD fetus.* Acta Neuropathol, 1996. **91**(3): p. 313-21.
29. Halfter, W., et al., *A critical function of the pial basement membrane in cortical histogenesis.* J Neurosci, 2002. **22**(14): p. 6029-40.
30. Gould, D.B., et al., *Mutations in Col4a1 cause perinatal cerebral hemorrhage and porencephaly.* Science, 2005. **308**(5725): p. 1167-71.
31. Georges-Labouesse, E., et al., *Essential role of alpha 6 integrins in cortical and retinal lamination.* Curr Biol, 1998. **8**(17): p. 983-6.
32. Graus-Porta, D., et al., *Beta1-class integrins regulate the development of laminae and folia in the cerebral and cerebellar cortex.* Neuron, 2001. **31**(3): p. 367-79.
33. Moore, S.A., et al., *Deletion of brain dystroglycan recapitulates aspects of congenital muscular dystrophy.* Nature, 2002. **418**(6896): p. 422-5.
34. Halfter, W., *Disruption of the retinal basal lamina during early embryonic development leads to a retraction of vitreal end feet, an increased number of ganglion cells, and aberrant axonal outgrowth.* J Comp Neurol, 1998. **397**(1): p. 89-104.
35. Halfter, W. and B. Schurer, *Disruption of the pial basal lamina during early avian embryonic development inhibits histogenesis and axonal pathfinding in the optic tectum.* J Comp Neurol, 1998. **397**(1): p. 105-17.
36. Halfter, W., et al., *Temporary disruption of the retinal basal lamina and its effect on retinal histogenesis.* Dev Biol, 2001. **238**(1): p. 79-96.
37. Balasubramani M, C.J., Schreiber E, Balasubramani S, Kurtz J, Halfter W, *Proteomic analysis of basement membranes; a role of proteoglycans for the elasticity of BMs.* Submitted for publication, 2009.
38. Uspenskaia, O., et al., *Aging is associated with increased collagen type IV accumulation in the basal lamina of human cerebral microvessels.* BMC Neurosci, 2004. **5**: p. 37.
39. Thomopoulos, G.N., et al., *Age-related thickening of basement membrane in stria vascularis capillaries.* Hear Res, 1997. **111**(1-2): p. 31-41.
40. Richardson, L.L., H.K. Kleinman, and M. Dym, *The effects of aging on basement membrane in the testis.* J Androl, 1995. **16**(2): p. 118-26.
41. Hasslacher, C. and P. Wahl, *Influence of diabetes control on synthesis of protein and basement membrane collagen in isolated glomeruli of diabetic rats.* Res Exp Med (Berl), 1980. **176**(3): p. 247-53.

42. Wahl, P., D. Deppermann, and C. Hasslacher, *Biochemistry of glomerular basement membrane of the normal and diabetic human*. *Kidney Int*, 1982. **21**(5): p. 744-9.
43. Quist, A.P., et al., *Physiological role of gap-junctional hemichannels. Extracellular calcium-dependent isosmotic volume regulation*. *J Cell Biol*, 2000. **148**(5): p. 1063-74.
44. A-Hassan, E., et al., *Relative microelastic mapping of living cells by atomic force microscopy*. *Biophys J*, 1998. **74**(3): p. 1564-78.
45. Laney, D.E., et al., *Changes in the elastic properties of cholinergic synaptic vesicles as measured by atomic force microscopy*. *Biophys J*, 1997. **72**(2 Pt 1): p. 806-13.
46. Candiello, J., et al., *Biomechanical properties of native basement membranes*. *FEBS J*, 2007. **274**(11): p. 2897-908.
47. Halfter, W., W. Reckhaus, and S. Kroger, *Nondirected axonal growth on basal lamina from avian embryonic neural retina*. *J Neurosci*, 1987. **7**(11): p. 3712-22.
48. Halfter, W., et al., *Composition, synthesis, and assembly of the embryonic chick retinal basal lamina*. *Dev Biol*, 2000. **220**(2): p. 111-28.
49. Halfter, W. and Y. Von Boxberg, *Axonal Growth on Solubilized and Reconstituted Matrix from the Embryonic Chicken Retina Inner Limiting Membrane*. *Eur J Neurosci*, 1992. **4**(9): p. 840-852.
50. Halfter, W., et al., *Distribution and substrate properties of agrin, a heparan sulfate proteoglycan of developing axonal pathways*. *J Comp Neurol*, 1997. **383**(1): p. 1-17.
51. Halfter, W., et al., *Collagen XVIII is a basement membrane heparan sulfate proteoglycan*. *J Biol Chem*, 1998. **273**(39): p. 25404-12.
52. Balasubramani, M., et al., *Perlecan and its immunoglobulin like domain IV are abundant in vitreous and serum of the chick embryo*. *Matrix Biol*, 2004. **23**(3): p. 143-52.
53. Ring, C., J. Hassell, and W. Halfter, *Expression pattern of collagen IX and potential role in the segmentation of the peripheral nervous system*. *Dev Biol*, 1996. **180**(1): p. 41-53.
54. Radmacher, M., M. Fritz, and P.K. Hansma, *Imaging soft samples with the atomic force microscope: gelatin in water and propanol*. *Biophys J*, 1995. **69**(1): p. 264-70.
55. Rhee, S.K., A.P. Quist, and R. Lal, *Amyloid beta protein-(1-42) forms calcium-permeable, Zn²⁺-sensitive channel*. *J Biol Chem*, 1998. **273**(22): p. 13379-82.
56. Sneddon, I., *The relation between load and penetration in the axisymmetric Boussinesq problem for a punch of arbitrary profile*. *Int J Eng Sci*, 1965. **3**: p. 47-57.
57. Fisher, R.F., *The significance of the shape of the lens and capsular energy changes in accommodation*. *J Physiol*, 1969. **201**: p. 1-19.

58. Libby, R.T., et al., *Laminin expression in adult and developing retinae: evidence of two novel CNS laminins*. J Neurosci, 2000. **20**(17): p. 6517-28.
59. Halfter, W., et al., *Embryonic synthesis of the inner limiting membrane and vitreous body*. Invest Ophthalmol Vis Sci, 2005. **46**(6): p. 2202-9.
60. Alberts B, J.A., Lewis J & Raff M, *Molecular Biology of the Cell*. 4th ed. 2002, New York, NY: Garland Science.
61. Jurvelin, J.S., M.D. Buschmann, and E.B. Hunziker, *Optical and mechanical determination of Poisson's ratio of adult bovine humeral articular cartilage*. J Biomech, 1997. **30**(3): p. 235-41.
62. Lee, C.R., et al., *Effects of harvest and selected cartilage repair procedures on the physical and biochemical properties of articular cartilage in the canine knee*. J Orthop Res, 2000. **18**(5): p. 790-9.
63. Gaon, M.D., K.H. Ho, and B.J. Wong, *Measurement of the elastic modulus of porcine septal cartilage specimens following Nd: YAG laser treatment*. Lasers Med Sci, 2003. **18**(3): p. 148-53.
64. Lambert, R.K., et al., *A method for estimating the Young's modulus of complete tracheal cartilage rings*. J Appl Physiol, 1991. **70**(3): p. 1152-9.
65. Stolz, M., et al., *Dynamic elastic modulus of porcine articular cartilage determined at two different levels of tissue organization by indentation-type atomic force microscopy*. Biophys J, 2004. **86**(5): p. 3269-83.
66. Allen, D.M. and J.J. Mao, *Heterogeneous nanostructural and nanoelastic properties of pericellular and interterritorial matrices of chondrocytes by atomic force microscopy*. J Struct Biol, 2004. **145**(3): p. 196-204.
67. Gueta, R., et al., *Measurement of the mechanical properties of isolated tectorial membrane using atomic force microscopy*. Proc Natl Acad Sci U S A, 2006. **103**(40): p. 14790-5.
68. Krag, S. and T.T. Andreassen, *Mechanical properties of the human posterior lens capsule*. Invest Ophthalmol Vis Sci, 2003. **44**(2): p. 691-6.
69. Fisher, R.F. and J. Wakely, *The elastic constants and ultrastructural organization of a basement membrane (lens capsule)*. Proc R Soc Lond B Biol Sci, 1976. **193**(1113): p. 335-58.
70. Fisher, R.F. and B.P. Hayes, *The elastic constants and ultrastructure organization of regenerated basement membrane (lens capsule)*. Q J Exp Physiol, 1982. **67**(2): p. 213-24.
71. Fisher, R.F. and B.P. Hayes, *Macromolecular organization of collagen fibres in natural and tanned basement membrane*. J Mol Biol, 1987. **198**(2): p. 263-79.

72. Krag, S., T. Olsen, and T.T. Andreassen, *Biomechanical characteristics of the human anterior lens capsule in relation to age*. Invest Ophthalmol Vis Sci, 1997. **38**(2): p. 357-63.
73. Candiello AJ, F.A., Elyaderani T, Friberg R & Lin H, *Nano indentation measurements of Bruch's membrane mechanical properties*, in ARVO. 2005, Invest Ophthalmol Vis Sci.
74. Bruel, A., G. Ortoft, and H. Oxlund, *Inhibition of cross-links in collagen is associated with reduced stiffness of the aorta in young rats*. Atherosclerosis, 1998. **140**(1): p. 135-45.
75. Kiviranta, P., et al., *Collagen network primarily controls Poisson's ratio of bovine articular cartilage in compression*. J Orthop Res, 2006. **24**(4): p. 690-9.
76. Saarakkala, S., et al., *Depth-wise progression of osteoarthritis in human articular cartilage: investigation of composition, structure and biomechanics*. Osteoarthritis Cartilage, 2009.
77. Kanwar, Y.S. and M.G. Farquhar, *Isolation of glycosaminoglycans (heparan sulfate) from glomerular basement membranes*. Proc Natl Acad Sci U S A, 1979. **76**(9): p. 4493-7.
78. Iozzo, R.V. and J.D. San Antonio, *Heparan sulfate proteoglycans: heavy hitters in the angiogenesis arena*. J Clin Invest, 2001. **108**(3): p. 349-55.
79. Sertie, A.L., et al., *Collagen XVIII, containing an endogenous inhibitor of angiogenesis and tumor growth, plays a critical role in the maintenance of retinal structure and in neural tube closure (Knobloch syndrome)*. Hum Mol Genet, 2000. **9**(13): p. 2051-8.
80. Rossi, M., et al., *Heparan sulfate chains of perlecan are indispensable in the lens capsule but not in the kidney*. EMBO J, 2003. **22**(2): p. 236-45.
81. Sarthy, P.V. and M. Fu, *Localization of laminin B1 mRNA in retinal ganglion cells by in situ hybridization*. J Cell Biol, 1990. **110**(6): p. 2099-108.
82. Dong, L.J. and A.E. Chung, *The expression of the genes for entactin, laminin A, laminin B1 and laminin B2 in murine lens morphogenesis and eye development*. Differentiation, 1991. **48**(3): p. 157-72.
83. Sarthy, V., *Collagen IV mRNA expression during development of the mouse retina: an in situ hybridization study*. Invest Ophthalmol Vis Sci, 1993. **34**(1): p. 145-52.
84. Dong, S., et al., *Expression of basal lamina protein mRNAs in the early embryonic chick eye*. J Comp Neurol, 2002. **447**(3): p. 261-73.
85. Henry, M.D. and K.P. Campbell, *A role for dystroglycan in basement membrane assembly*. Cell, 1998. **95**(6): p. 859-70.

86. Satz, J.S., et al., *Brain and eye malformations resembling Walker-Warburg syndrome are recapitulated in mice by dystroglycan deletion in the epiblast*. J Neurosci, 2008. **28**(42): p. 10567-75.
87. Semina, E.V., et al., *Mutations in laminin alpha 1 result in complex, lens-independent ocular phenotypes in zebrafish*. Dev Biol, 2006. **299**(1): p. 63-77.
88. Lee, J. and J.M. Gross, *Laminin beta1 and gamma1 containing laminins are essential for basement membrane integrity in the zebrafish eye*. Invest Ophthalmol Vis Sci, 2007. **48**(6): p. 2483-90.
89. Zenker, M., et al., *Human laminin beta2 deficiency causes congenital nephrosis with mesangial sclerosis and distinct eye abnormalities*. Hum Mol Genet, 2004. **13**(21): p. 2625-32.
90. Sebag, J., *Anatomy and pathology of the vitreo-retinal interface*. Eye, 1992. **6** (Pt 6): p. 541-52.
91. Bishop, P.N., *Structural macromolecules and supramolecular organisation of the vitreous gel*. Prog Retin Eye Res, 2000. **19**(3): p. 323-44.
92. Sebag, J., *Anomalous posterior vitreous detachment: a unifying concept in vitreo-retinal disease*. Graefes Arch Clin Exp Ophthalmol, 2004. **242**(8): p. 690-8.
93. Sebag, J., *Vitreous: From biochemistry to clinical relevance*, in *Duan'e Foundation of Clinical Ophthalmology*. 2005, W. Tasman and EA Jaeger: Philadelphia.
94. Cotman, S.L., W. Halfter, and G.J. Cole, *Agrin binds to beta-amyloid (Abeta), accelerates abeta fibril formation, and is localized to Abeta deposits in Alzheimer's disease brain*. Mol Cell Neurosci, 2000. **15**(2): p. 183-98.
95. Hutter JL, B.J., *Calibration of atomic force microscope tips* J Rev Sci Instrum, 1993. **993**(64): p. 1868-1873.
96. Bertazzoli-Filho, R., E.M. Laicine, and A. Haddad, *Synthesis and secretion of transferrin by isolated ciliary epithelium of rabbit*. Biochem Biophys Res Commun, 2003. **305**(4): p. 820-5.
97. Kubota, R., et al., *Identification of ciliary epithelial-specific genes using subtractive libraries and cDNA arrays in the avian eye*. Dev Dyn, 2004. **229**(3): p. 529-40.
98. Meezan, E., J.T. Hjelle, and K. Brendel, *A simple, versatile, nondisruptive method for the isolation of morphologically and chemicaly pure basement membranes from several tissues*. Life Sci, 1975. **17**(11): p. 1721-32.
99. Duhamel, R.C., E. Meezan, and K. Brendel, *Selective solubilization of two populations of polypeptides from bovine retinal basement membranes*. Exp Eye Res, 1983. **36**(2): p. 257-67.

100. Halfter, W., et al., *Origin and turnover of ECM proteins from the inner limiting membrane and vitreous body*. Eye, 2008. **22**(10): p. 1207-13.
101. Binnig, G., C.F. Quate, and C. Gerber, *Atomic force microscope*. Phys Rev Lett, 1986. **56**(9): p. 930-933.
102. Begley MR, M.T., *Spherical indentation of freestanding circular thin films in the membrane regime*. J Mech Phys Solids, 2004. **52**: p. 2005-2023.
103. Fisher, R.F., *Elastic constants of the human lens capsule*. J Physiol, 1969. **201**(1): p. 1-19.
104. Krag, S. and T.T. Andreassen, *Mechanical properties of the human lens capsule*. Prog Retin Eye Res, 2003. **22**(6): p. 749-67.
105. Danysh, B.P. and M.K. Duncan, *The lens capsule*. Exp Eye Res, 2009. **88**(2): p. 151-64.
106. Gartner, J., *Electron microscopic observations on the cilio-zonular border area of the human eye with particular reference to the aging changes*. Z Anat Entwicklungsgesch, 1970. **131**(3): p. 263-73.
107. Foos, R.Y., *Vitreoretinal juncture; topographical variations*. Invest Ophthalmol, 1972. **11**(10): p. 801-8.
108. Matsumoto B, B.J., Ryan SJ, *Topographic variations in the rabbit and primate internal limiting membrane*. Invest Ophthalmol Visc Sci, 1982. **25**: p. 71-82.
109. Bishop PN, H.D., Kadler KE, McLeod D, Bos KJ, *Age-related changes on the surface of vitreous collagen fibrils*. Invest Ophthalmol Vis Sci, 2003. **45**: p. 1041-1046.
110. Maroudas, A., G. Palla, and E. Gilav, *Racemization of aspartic acid in human articular cartilage*. Connect Tissue Res, 1992. **28**(3): p. 161-9.
111. Verzijl, N., et al., *Effect of collagen turnover on the accumulation of advanced glycation end products*. J Biol Chem, 2000. **275**(50): p. 39027-31.
112. Verzijl, N., et al., *Age-related accumulation of the advanced glycation endproduct pentosidine in human articular cartilage aggrecan: the use of pentosidine levels as a quantitative measure of protein turnover*. Matrix Biol, 2001. **20**(7): p. 409-17.
113. Muntoni, F. and T. Voit, *The congenital muscular dystrophies in 2004: a century of exciting progress*. Neuromuscul Disord, 2004. **14**(10): p. 635-49.
114. Emery, A.E., *The muscular dystrophies*. Lancet, 2002. **359**(9307): p. 687-95.
115. Lisi, M.T. and R.D. Cohn, *Congenital muscular dystrophies: new aspects of an expanding group of disorders*. Biochim Biophys Acta, 2007. **1772**(2): p. 159-72.

116. Reed, U.C., *Congenital muscular dystrophy. Part II: a review of pathogenesis and therapeutic perspectives.* Arq Neuropsiquiatr, 2009. **67**(2A): p. 343-62.
117. Cohn, R.D., *Dystroglycan: important player in skeletal muscle and beyond.* Neuromuscul Disord, 2005. **15**(3): p. 207-17.
118. Williamson, R.A., et al., *Dystroglycan is essential for early embryonic development: disruption of Reichert's membrane in Dag1-null mice.* Hum Mol Genet, 1997. **6**(6): p. 831-41.
119. Barresi, R., et al., *LARGE can functionally bypass alpha-dystroglycan glycosylation defects in distinct congenital muscular dystrophies.* Nat Med, 2004. **10**(7): p. 696-703.
120. Ferris, F.L., 3rd, S.L. Fine, and L. Hyman, *Age-related macular degeneration and blindness due to neovascular maculopathy.* Arch Ophthalmol, 1984. **102**(11): p. 1640-2.
121. Allikmets, R., et al., *Mutation of the Stargardt disease gene (ABCR) in age-related macular degeneration.* Science, 1997. **277**(5333): p. 1805-7.
122. Green, W.R. and C. Enger, *Age-related macular degeneration histopathologic studies. The 1992 Lorenz E. Zimmerman Lecture.* Ophthalmology, 1993. **100**(10): p. 1519-35.
123. Green, W.R., *Histopathology of age-related macular degeneration.* Mol Vis, 1999. **5**: p. 27.
124. Marshall J, H.A., Starita C, et al, *Aging and Bruch's Membrane*, in *Retinal Pigment Epithelium: Function and Disease*, M.F.a.W. Marmor, T.J., Editor. 1998, Oxford University Press.
125. Hogan, M.J. and J. Alvarado, *Studies on the human macula. IV. Aging changes in Bruch's membrane.* Arch Ophthalmol, 1967. **77**(3): p. 410-20.
126. Sarks, S.H., *Ageing and degeneration in the macular region: a clinico-pathological study.* Br J Ophthalmol, 1976. **60**(5): p. 324-41.
127. Ramrattan, R.S., et al., *Morphometric analysis of Bruch's membrane, the choriocapillaris, and the choroid in aging.* Invest Ophthalmol Vis Sci, 1994. **35**(6): p. 2857-64.
128. Newsome, D.A., W. Huh, and W.R. Green, *Bruch's membrane age-related changes vary by region.* Curr Eye Res, 1987. **6**(10): p. 1211-21.
129. Holz, F.G., et al., *Analysis of lipid deposits extracted from human macular and peripheral Bruch's membrane.* Arch Ophthalmol, 1994. **112**(3): p. 402-6.
130. Kliffen, M., et al., *Morphologic changes in age-related maculopathy.* Microsc Res Tech, 1997. **36**(2): p. 106-22.

131. Hageman, G.S., et al., *An integrated hypothesis that considers drusen as biomarkers of immune-mediated processes at the RPE-Bruch's membrane interface in aging and age-related macular degeneration*. Prog Retin Eye Res, 2001. **20**(6): p. 705-32.
132. Chong, N.H., et al., *Decreased thickness and integrity of the macular elastic layer of Bruch's membrane correspond to the distribution of lesions associated with age-related macular degeneration*. Am J Pathol, 2005. **166**(1): p. 241-51.
133. Friberg, T.R. and J.W. Luce, *A comparison of the elastic properties of human choroid and sclera*. Exp Eye Res, 1988. **47**(3): p. 429-36.
134. Hu, X., et al., *Pseudoxanthoma elasticum: a clinical, histopathological, and molecular update*. Surv Ophthalmol, 2003. **48**(4): p. 424-38.
135. Tsuboi, S., *Measurement of the volume flow and hydraulic conductivity across the isolated dog retinal pigment epithelium*. Invest Ophthalmol Vis Sci, 1987. **28**(11): p. 1776-82.
136. Hughes, B., R. Gallemore, and S. and Miller, *Transport Mechanisms in the retinal pigment epithelium*, in *Retinal Pigment Epithelium: Function and Disease*, M.F.a.W. Marmor, T.J., Editor. 1998, Oxford University Press.
137. Bok, D., *Retinal photoreceptor-pigment epithelium interactions. Friedenwald lecture*. Invest Ophthalmol Vis Sci, 1985. **26**(12): p. 1659-94.
138. Karwatowski, W.S., et al., *Preparation of Bruch's membrane and analysis of the age-related changes in the structural collagens*. Br J Ophthalmol, 1995. **79**(10): p. 944-52.
139. Feeney-Burns, L. and M.R. Ellersieck, *Age-related changes in the ultrastructure of Bruch's membrane*. Am J Ophthalmol, 1985. **100**(5): p. 686-97.
140. van der Schaft, T.L., et al., *Element analysis of the early stages of age-related macular degeneration*. Arch Ophthalmol, 1992. **110**(3): p. 389-94.
141. Spraul, C.W. and H.E. Grossniklaus, *Characteristics of Drusen and Bruch's membrane in postmortem eyes with age-related macular degeneration*. Arch Ophthalmol, 1997. **115**(2): p. 267-73.
142. Borges, L.F., S.R. Taboga, and P.S. Gutierrez, *Simultaneous observation of collagen and elastin in normal and pathological tissues: analysis of Sirius-red-stained sections by fluorescence microscopy*. Cell Tissue Res, 2005. **320**(3): p. 551-2.